MAGNETO-CALORIC EFFECT OF FE-BASED METALLIC GLASSES AT ROOM TEMPERATURE

GUO DAOQIN

PhD

The Hong Kong Polytechnic University

2018

The Hong Kong Polytechnic University

Department of Industrial and Systems Engineering

Magneto-caloric effect of Fe-based metallic glasses at room temperature

GUO Daoqin

A thesis submitted in partial fulfillment of the requirements
for the degree of Doctor of Philosophy

September 2017

CERTIFICATE OF ORIGINALITY

I hereby declare that this dissertation is my own work and that, to the best of my knowledge and belief, it reproduces no material previously published or written nor material which has been accepted for the award of any other degree or diploma, except where due acknowledgements has been made in the text.

________________________(Signed)

_____GUO Daoqin_______(Name of Student)

Abstract

The magnetocaloric effect (MCE) is the temperature change of magnetic materials corresponding to an external magnetic field change. Specifically, magnetic materials will heat up when they are magnetized and cool down when they are demagnetized. Magnetic refrigeration, based on the MCE, is a new technique which is more energy-saving and environmentally friendly than the conventional cooling method and has already been used in low temperature applications. Over the last decade, many researchers have further explored replacing the conventional gas expansion/compression cooling technique for room temperature applications by magnetic refrigeration. For working refrigerants, the magnetocaloric effect of magnetic materials is critical for the performance of a refrigerator. It has been reported that the refrigeration capacity (RC) of amorphous materials is generally larger than that of crystals. Among various amorphous MCE materials, Gd-based materials have attracted much research interest due to their large magnetocaloric effect. However, their Curie temperature is still too low to be applied for room temperature magnetic refrigeration. On the other hand, the MCE of Fe-based amorphous materials is generally smaller than that of Gd-based materials. The advantages of the Fe-based amorphous materials are easily tunable Curie temperatures and low cost. By adjusting the composition or alloying with some minor additions, the MCE of the Fe-based metallic glasses is able to be enhanced to a great extent.

In this project, the prime aim is to develop the Fe-based metallic glasses with an enhanced magnetocaloric effect. To fulfill this objective, new compositions were tried on the basis of results in the literature. In order to ascertain the amorphous structure of the new materials, adjustment of the composition was carried out. With more Fe content, the magnetic properties are supposed to be better, while the glass forming ability (GFA) is worse. As a result, metallic ribbons were chosen instead of bulk rods in order to lower the critical cooling rate. FeZrB series amorphous materials were chosen as the master alloys in my study due to their excellent MCE among the Fe-based metallic glasses, after the MCE of FeZrB ternary amorphous materials were thoroughly reviewed in the literature. To enhance the MCE of the chosen master alloys, the effect of minor additions of different elements was thoroughly studied, for example Cr, Co, Cu, Sm, Mn and Er. With the addition of these elements, both the Curie temperatures and the peak magnetic entropy changes were affected. The results provided a feasible method to enhance the MCE and maintain the Curie temperatures around room temperature.

To verify the experimental results as well as predict the MCE of new magnetic materials, Monte Carlo simulations were used in this project. The simulation was based on the importance sampling method. Since little work was done on the simulation of the MCE of amorphous materials, the simulation work in this project

started from the binary Gd-based amorphous materials in order to simplify the codes and calculations. Then the simulation was used to calculate the MCE of Fe-based amorphous materials. For materials consisting of all magnetic elements, the results of the Curie temperatures obtained from the simulation fitted well with data from experiments, and the magnetic entropy changes were predicted. For materials consisting of magnetic and non-magnetic materials, the simulation still needs to be improved. The findings of the present study not only provide a better understanding of the MCE of the amorphous materials, but also form a strong foundation for further improvement of the simulation work.

Publications Arising from the Research

1. D. GUO, K.C. CHAN and L. XIA, Influence of minor addition of Cr on the magnetocaloric effect in Fe-based metallic ribbons, Mater. Trans., 57 (2016) 9-14.

2. D. GUO, K.C. CHAN, L. XIA and P. YU, Magneto-caloric effect of $Fe_xZr_yB_{100-x-y}$ metallic ribbons for room temperature magnetic refrigeration, J. Magn. Magn. Mater., 423 (2017) 379-385.

3. B. Tang, D. Guo, D. Ding, L. Xia, and K.C. Chan, Large adiabatic temperature rise above the ice point of a minor Fe substituted $Gd_{50}Co_{50}$ amorphous alloy, J. Non-Cryst. Solids, 464 (2017) 30-33.

4. B. Tang, D. Guo, L. Xia, D. Ding and K.C. Chan, Magnetoelastic and magnetocaloric properties of $Tb_{62.5}Co_{37.5}$ amorphous alloy, J. Alloy Compd., 728 (2017) 747-751.

5. D. GUO, Y. Yuan and K.C. CHAN, The effect of different minor additions on the magneto-caloric effect of FeZrB metallic glass ribbons, J. Magn. Magn. Mater., 446 (2018) 12-17.

6. D. GUO, K.C. CHAN and L. Xia, Investigation on the Curie temperature of Gd-based binary amorphous ribbons by Monte Carlo simulation, in preparation.

Acknowledgments

First, I would like to sincerely thank Prof. K.C. Chan, my chief supervisor, for the guidance and support in fulfilling my project. Prof. Chan was always patient with me to find the way to do the research: not only how to find a valuable topic, analyze the data and construct a research paper, but more importantly, to learn the attitude required for a career as a researcher/professor. I also want to thank Prof. L. Xia (Shanghai University), for the helpful guidance in preparing the specimens, carrying out the experiments and providing suggestions and discussions throughout the Ph.D student study.

I gratefully acknowledge the experimental help, kind suggestions and fruitful discussions on my work from Dr. S.H. Chen, Dr. J. MA, Mr L. Zhao, Mr. S. Guan, Dr. S.D. Feng, Mr. C. Wu and Mr. Y.D. Yuan for the experimental assistance and friendship during my study. Special thanks go to Mr S.Y. Lau for the experimental guidance.

I am thankful for the Research Committee of the Hong Kong Polytechnic University for the financial support of my research in this work.

Finally, I would like to express my most sincere thanks to my parents and all my family members for their love and continuous support on my graduate journey in Hong Kong. Thank you to all my friends and the support from the teachers/staffs in my previous and present institutions.

Contents

List of Figures and Tables

Chapter 1 Introduction

1.1 Motivation and background

With the continuing development of society, more and more resources are needed, especially those that are non-renewable. In addition, environment problems are always a big concern and not enough attention is generally paid on them. It is also true that oil and coal, which are the core energy sources for our society, are running out and the environment we live in is under great threat from pollution. As a consequence, there is a need to find new technologies which are expected to be energy-saving and environmentally-friendly. One of the technologies that affects almost everyone’s life is the refrigeration. For the moment, the common principles used in refrigeration are based on the expansion/compression of gas which has a lot to do with ozone depletion and the greenhouse effect. Magnetic refrigeration emerges as a revolutionary method to achieve cooling without usage of that kind of gas. For now, one of the greatest challenges to realize the room temperature application of the magnetic refrigeration is to find the most appropriate working materials.

During last few decades, thanks to the highly developed technology, numerous new materials have been fabricated. Metallic glasses, for example, have successfully attracted our attention due to their outstanding properties and performance when compared with conventional materials, and their potential for magnetic refrigeration. Metallic glasses were not known until Duwez and his co-workers first discovered an Si-Au alloy with an amorphous structure in 1960 [1]. Before that, metallic materials were commonly considered as crystalline materials with atoms well arranged in a periodic way. Duwez discovered metallic glasses with the help of a rapid solidification processing (RSP) method during which the cooling rate was about 10^5-10^6 K/s. To achieve such a high rate, the ribbon sample had to be extremely thin, the thickness being no more than 0.1mm at the beginning. As more research on metallic glasses was done, researchers were able to fabricate metallic glasses under relatively low cooling rates. The lower the cooling rate, the larger the specimen size of the metallic glass, and with larger sizes, metallic glasses can have more and wider applications. In 1984, Kui et al made a metallic glass $Pd_{40}Ni_{40}P_{20}$ with a minimum dimension over 6 mm under a cooling rate of only 1 K/s [2]. Such materials with any dimensional size over 1mm are referred as bulk metallic glasses [3]. Till now, the largest diameter of a bulk metallic glass rod of $Pd_{40}Cu_{30}Ni_{10}P_{20}$ is 72 mm [4]. However, Pd is too expensive for wide applications even though Pd-based BMGs possess non-comparable glass forming ability. In the late 1980s, a $La_{55}Al_{25}Ni_{20}$ BMG of 1.2 mm in diameter was produced by Inoue and Masumoto. It was remarkable not just because of its size but that its composition lacked noble metals [5], which is of great importance for the application of BMGs. In recent decades, many other BMGs without noble metals have been successfully produced, such as Gd-based BMGs [6], Fe-based BMGs [7] and so on. Based on numerous experiments, scientists determined the criterion for the glass forming ability of different materials which enabled prediction of new metallic glasses [8-13].

Metallic glasses have been proven to have superior properties over conventional materials due to their special structures, for example mechanical properties and magnetic properties. Recently, more and more investigations have been focused on the magnetic applications of metallic glasses and some impressive progress has been made. Metallic glasses with magnetic properties have already been used in various applications, like transformers, magnetic heads, etc. Nowadays, scientists would like to replace current refrigeration working materials with magnetic metallic glasses for the purpose of reducing pollution, saving energy and improving efficiency, by means of magnetic refrigeration (MR). Nevertheless, there are still several issues before metallic glasses can be used for cooling, especially at room temperature.

1.2 Key issues and objectives

Magnetic refrigeration technology is based on the magnetocaloric effect (MCE) which was discovered by William Thomson in 1860 [14] and was firstly reported by Warburg in 1881 [15]. The temperature of iron was found to change as the magnetic field changed. Specifically, the temperature increased when iron was magnetized and decreased when iron was demagnetized. This technology has attracted significant attention because of its great advantages, such as environmental safety and high efficiency compared with the traditional gas compression refrigeration [16]. However, the real interest in the magnetic refrigeration for room temperature was ignited after the discovery of the giant MCE in $Gd_5Si_2Ge_2$ which undergoes a first order magnetic-phase transition (FOMT) [17]. There are still some limitations in applying those materials with FOMT because the working temperature range is too small to cover the room temperature range. Materials with a second order magnetic-phase transition (SOMT), on the other hand, have a much wider working temperature range, which makes them more promising in room temperature magnetic refrigeration applications. With more and more research being carried out on this topic, two categories of potential materials with SOMT have been recognized for application. One is Gd-based and the other is Fe-based, with their own features. Gd-based materials have large entropy change and excellent glass forming ability, however, the working temperature range is narrow and the Curie temperature is relatively low. Besides, Gd is too expensive [18-22]. Fe-based materials have a wide temperature range as well as an appropriate Curie temperature. What’s more, Fe is very cheap and abundant. The disadvantages of Fe-based materials are the very small entropy change and the poor glass forming ability [18-51].

In this project, after comprehensively considering the performance of these two materials, Fe-based metallic glasses were chosen as working materials for room temperature refrigeration. There are two key issues in this research, corresponding to the previous disadvantages of Fe-based materials. To solve these problems, some possible methods have been proposed and tried, for example, to fabricate metallic glasses ribbons instead of rods. The prime aim of this project is to discover a new kind of Fe-based metallic glass which not only has a suitable working temperature but also possesses relatively high cooling efficiency. The specific objectives are as follows:

1. To develop new Fe-based metallic glasses by examining different compositions;

2. To study the effect of different elements addition on the magnetocaloric effect;

3. To characterize the microstructure and magnetocaloric effect of the newly-made metallic glasses;

4. To theoretically study and understand the magnetocaloric effect of metallic glasses.

1.3 Organization of this thesis

This report is organized as follows. In first chapter, which is presented above, the background information on this study was introduced, with a review of the relevant literature to try to identify the research gap in chapter two. In chapter three, the methodology applied in this study is explained. Following this, results are presented in chapters four, five-A and five-B. The simulation results are shown in chapter six. The conclusions are given in chapter seven.

Chapter 2 Literature Review

2.1 Introduction

In this chapter, according to the objectives mentioned in section 1.2 of chapter 1, the relevant literature has been reviewed. Figure 2. 1 shows three areas that were the focus of the literature review.

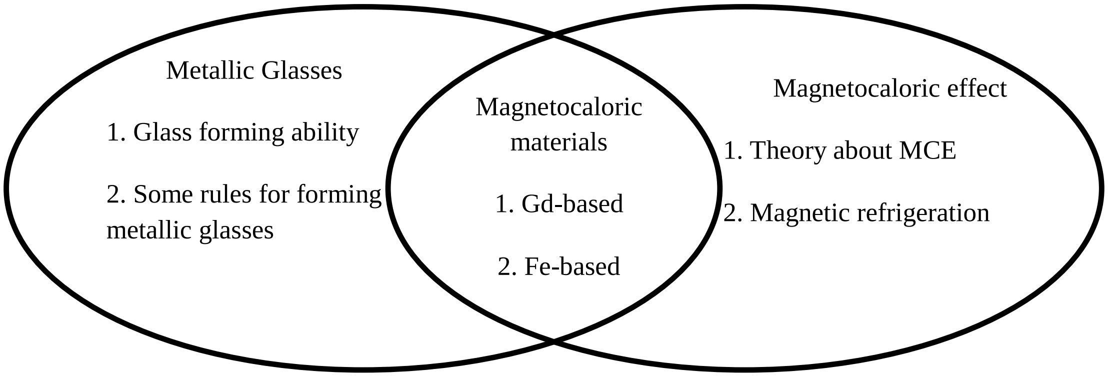

Figure 2. 1 Content of this literature review

The areas above are designed not to reflect that the contents are equal in scope but demonstrate the inter-relations involved. In the first section, the literature on metallic glasses is reviewed, which helps identify new MCE materials for the present study. Following this, the magnetocaloric effect (MCE) is introduced to clarify the principles of magnetic refrigeration, with the main attention paid to two promising magnetocaloric materials (MCMs), Fe-based and Gd-based amorphous alloys.

2.2 Metallic glasses

2.2.1 Glass forming ability

Duwez and his coworkers made it possible to synthesize alloys into amorphous states by rapid solidification processing (RSP), rather than a crystalline state [1]. In fact, the amazing result of their experiments was by accident [3]. It is of great importance to understand the principles of the glass forming ability (GFA) of alloys if we want to develop metallic glasses with enhanced properties. Glass formation can be accomplished only when a critical cooling rate R_c, which is regarded as an indicator of GFA, is achieved. It has been proven that the critical cooling rate relies

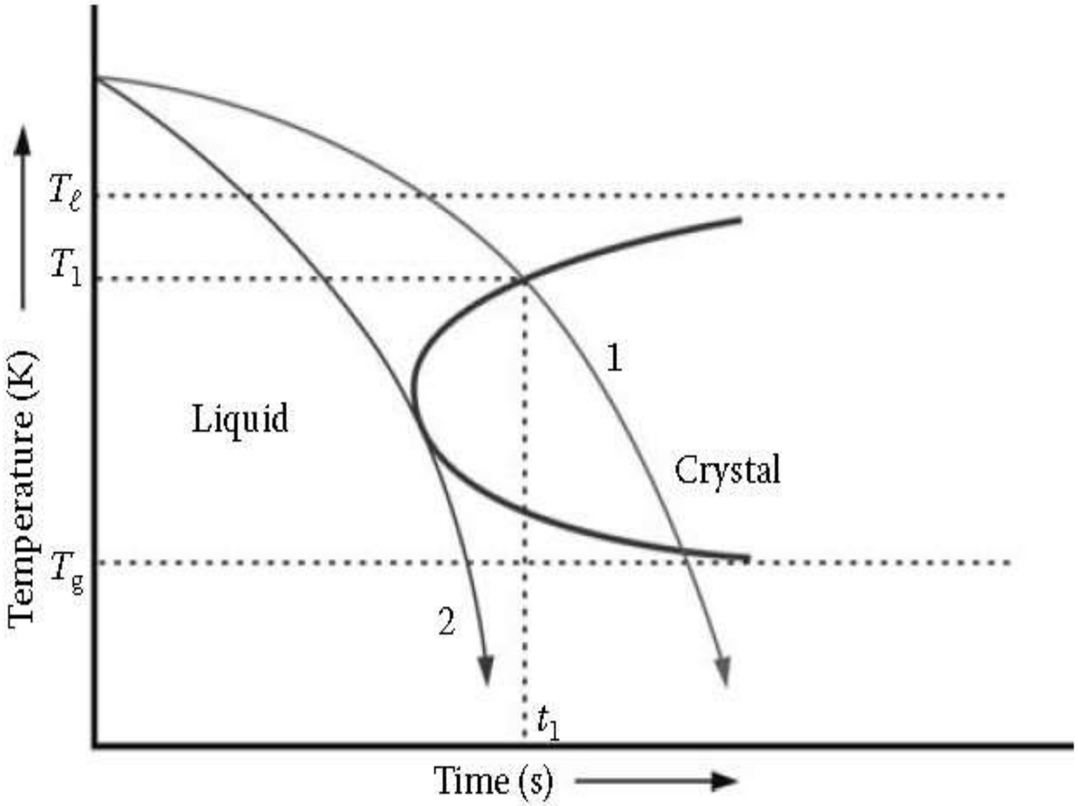

Figure 2. 2 A general T-T-T diagram [3]

on the composition of the alloys. Since the interaction of atoms is extremely complicated, the best way forward to obtain R_C is to build a T-T-T (time-temperature-transformation) diagram, as shown in Figure 2.2 [3]. From this diagram, it is readily recognized that curve 2 represents the critical cooling rate for this alloy. When the alloy liquid cools down as curve 1, it will become crystal. If the cooling rate is at least as fast as curve 2, the alloy will become amorphous. With this approach, in 1981, Barandiarán and Colmenero successfully deduced how to calculate R_C for glass formation, as follows [52]:

$$\ln R = A - \frac{B}{\left(T_l - T_{xc}\right)^2} \qquad (2.1).$$

In this equation, R represents the cooling rate with two constants A and B, liquid temperature T_l and the temperature at the beginning of solidification T_{xc}. From the diagram, it can be seen that $(T_l - T_{xc})$ changes as the cooling rate R changes. According to their theory, the critical cooling rate, R_C, can be obtained when $(T_l - T_{xc})$ becomes sufficiently large. Then, equation 2.1 can be approximately written as:

$$\ln R_c = A \qquad (2.2).$$

Later, Men and Kim applied the equation for calculating R_C of Mg-Cu-Gd bulk metallic glass and proved its applicability [53].

Another method to estimate the critical cooling rate was proposed by Lin and Johnson in 1995 [54]. They discovered that R_C could be calculated from the equation:

$$R_c = \frac{10}{d^2} \quad (2.3).$$

In equation 2.3, d stands for the size of the specimen thickness or diameter in cm units.

It is somewhat difficult to measure R_C very precisely. Moreover, R_C cannot indicate the potential to form a metallic glass structure. A more reliable gauge of GFA is needed. It was observed that the heating rate has little impact on the temperature where the glass phase transition occurs, and the reduced glass transition temperature T_{rg} was proposed [55]:

$$T_{rg} = \frac{T_g}{T_l} \quad (2.4).$$

T_g is the glass transition temperature, T_l is still the liquid temperature. In general, T_g has a negligible dependence on the concentration while T_l on the other hand often has a strong negative correlation with the concentration. As the alloy becomes more concentrated, T_g nearly remains unchanged and T_l becomes much lower. The interval between T_g and T_l therefore decreases, resulting in the increase of T_{rg}. The possibility of cooling from T_g to T_l without crystallization is increased, which means enhancement of the GFA [56].

However, in some rare earth transition metal (RE-TM) based BMGs, no glass transition temperatures could be observed before crystallization, for example $Nd_{60}Fe_{30}Al_{10}$ and $Nd_{70}Co_{20}Al_{10}$ alloys, which have already been prepared into amorphous state in rods, 12 mm in diameter [9, 57]. To quantify the GFA of these materials, the reduced crystallization temperature (T_{rx}) was proposed by Inoue [9]:

$$T_{rx} = \frac{T_x}{T_l} \qquad (2.5)$$

where T_x represents the crystallization temperature. Besides, another parameter was proposed to evaluate the GFA, which was obtained as $T_x/(T_g+T_l)$ [13].

2.2.2 Some rules for forming metallic glasses

It has been found that the C-shape curve in the T-T-T diagram is extremely sensitive to the elements mixed in the alloys. A curve moving to the right results in lowering the critical cooling rate, R_C. Therefore, more metallic glasses, especially bulk metallic glasses, are able to be synthesized [58]. Apart from R_C, there also have been some empirical rules for predicting the glass formation by the rapid solidification processing method.

Based on the analysis of numerous metallic glasses, especially binary ones, researchers found that the size ratios of the compositions affect the glass formation significantly. According to Egami's theory, mixing elements make crystallization difficult which inversely helps glass to form easily [59]. In 1984, Egami and Waseda proposed that for binary metallic glasses obtained from RSP methods, a minimum solute concentration is necessary [60]. They also summarized a relationship between the solute concentration and the atomic volume as:

$$\left|\frac{(V_A - V_B)}{V_A}\right| C_B^{\min} = 0.1 \qquad (2.6),$$

where V_A stands for the atomic volume of the solvent and V_B for the solute.

For the formation of bulk metallic glasses, Inoue drew a conclusion, now known as the three empirical rules [61, 62]. Since then, a series of BMGs have been fabricated under the guidance of Inoue's rules. The criteria can be explained as:

1. The composition must include at least three kinds of elements.

2. The atomic size mismatch between each main component should exceed 12%.

3. Negative mixing enthalpy is also a precondition.

Even though the above criteria have been verified in many BMGs, exceptions still can't be avoided. Binary BMGs have also been fabricated, such as Cu-Zr [63], Pd-Si [64] and Ni-Nb [65] systems. In addition, the enthalpy change of alloying is found to be unnecessary for the formation of some BMGs, for example Cu-Zr [66] systems. In summary, there is still a need to find more reliable and measureable criteria to quantify the GFA of metallic glasses.

2.2.3 Properties and applications of amorphous alloys

Because of the limitations in equipment and technology, cooling rates were rather small in the early stages of metallic glass development. As a result, the materials could not become amorphous unless they were synthesized in ribbon or wire shapes. Consequently, such metallic ribbons or wires are more suitable for the magnetic applications. For example, the materials used in recording heads and the electric-magnetic cores are generally Fe-based metallic glasses [67-69].

Thanks to the die casting method, different shapes of bulk metallic glasses can be formed, and BMGs can therefore be used in wider applications. Nowadays, the heads of the golf clubs are made of BMGs. Compared to a conventional Ti driver, the BMG-made heads exhibit twice the hardness and four times the elasticity. Only 70% of the impact energy can be transferred from a Ti driver head to the golf ball; however, the energy efficiency becomes almost 99% when it comes to a BMG-made head. What is more, the BMG-made heads can vary in both shapes and sizes due to the high strength-weight ratio. Similarly, the BMGs have also been applied in other sporting goods demanding high energy transfer efficiency, for example, tennis rackets, baseball bats and hunting bows. In addition, applications of BMGs in edged tools have as well been explored, such as axes [70].

Since BMGs can be fabricated into a net shape on thin plates, applications in electronic devices can be realized. With personal electronic devices being more portable, the cases of the devices need to be thinner. In the meantime, good mechanical strength of the cases is also desired. Obviously, the BMGs perform better than conventional materials such as polymers or alloys, and applications have already been found in niche mobile phones and digital cameras [71].

Other than the daily-life applications, the metallic glasses have also been adopted for military use, for instance, anti-tank penetrators. In conventional circumstances, anti-tank penetrators made of crystalline materials will flatten after impaction, while those made of amorphous alloys will sharpen after impaction. Besides, the use of radiation hazards uranium can be avoided in penetrators made of metallic glasses [71].

As regards the biomedical area, BMGs have some outstanding properties that make BMGs have an advantage over conventional materials, especially in orthopedic applications. The properties include: (1) excellent bio-compatibility (2) high strength-weight ratio (3) high wear resistance (4) easy production of desired surface morphologies There are already some products, for example, spinal implants, fractured fixations, reconstructive devices and instrumentations [71], available in the market.

More interestingly, the fine jewelry companies are paying increasing attention to BMGs due to the fact that stunning surface finishes can be accomplished by BMGs[71].

In order to make the best of BMGs, more efforts are being made to further develop wider potential applications suitable for BMGs [71]. To sum up, some possible/potential applications of the BMGs are listed in Table 2.1.

Table 2. 1 Possible/potential applications and corresponding properties of the BMGs [70-73]

Application areas	Major properties
Sporting goods materials	High elastic energy
Machinery structural materials	High strength
Corrosion resistance materials	High corrosion resistance
Cutting materials	High hardness

Optical precision materials	High reflection ratio
Die materials	High fracture toughness
Writing appliance materials	High viscous flowability
Tool materials	High impact fracture energy
Electrode materials	Efficient electrode
Soft magnetic materials	Excellent soft magnetism
Hard magnetic materials	Excellent hard magnetism

2.2.4 Conclusions

Knowledge of glass forming ability is of great importance for predicting the possibility of the synthesis of new bulk metallic glasses. For now, some parameters have been proposed to identify GFA. Since there are still exceptions, as mentioned before, new attempts to optimize the principles for indicating the GFA of alloys continue.

2.3 Magnetocaloric effect (MCE)

2.3.1 The theory of MCE

The paper on the MCE in 1881 by Warburg [15] evoked a large number of investigations on MCE. After in-depth research, the MCE has been proven to be intrinsic to any magnetic material. In addition, the entropy change caused by the magnetic field variation is mainly responsible for the MCE. Therefore, the entropy change plays an important role in characterizing the MCE [72]. According to Tishin [73], the total entropy of a magnetic material, S, is generally determined in three parts, when the pressure is assumed to be constant. These are the magnetic entropy S_M, the lattice entropy S_{lat} and the electron entropy S_{el}, as in the equation below:

$$S(H,T) = S_M(H,T) + S_{lat}(H,T) + S_{el}(H,T) \quad (2.7).$$

where H and T are the magnetic field and temperature respectively. Gopal proposed that S_{lat} and S_{el} can be regarded as only related to the temperature [74]. Thus, equation 2.7 can be written as:

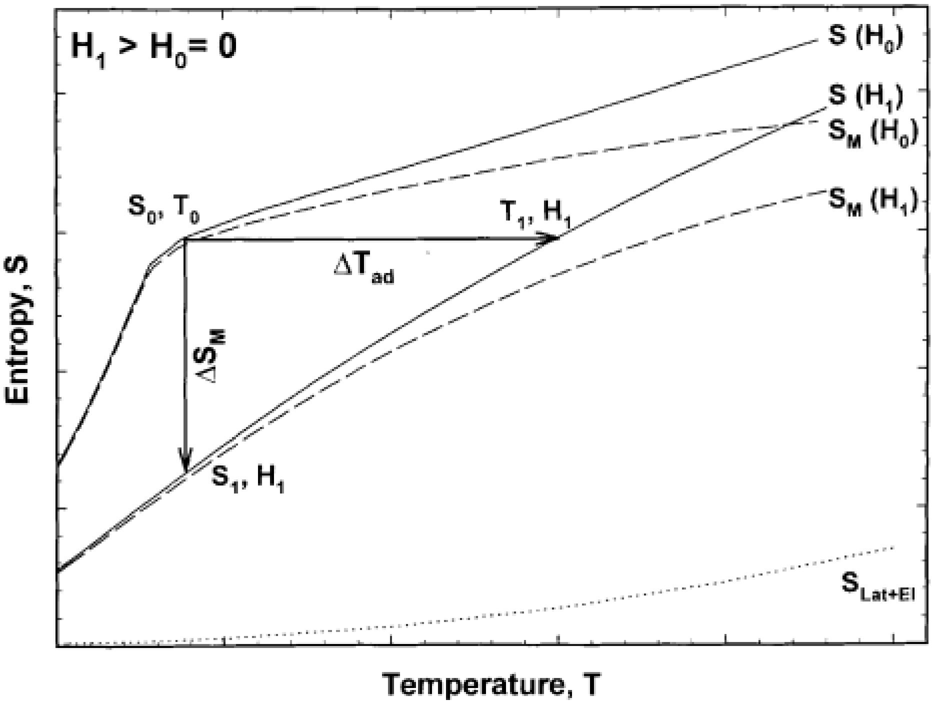

Figure 2. 3 The entropy-temperature diagram for illustrating the MCE [51]

$$S(H,T) = S_M(H,T) + S_{lat}(T) + S_{el}(T) \tag{2.8}$$

Figure 2.3 gives a general illustration for the MCE [51]. H_0 stands for a zero magnetic field and H_1 for a non-zero magnetic field. From the diagram, S_{lat} and S_{el} seem to be negligible when compared with S_M. The MCE can be achieved through the following procedures. When a magnetic field is isothermally applied to the material, the entropy will decrease from S_0 to S_1, because the application of a magnetic field will result in a regular arrangement of the spins. Thus, the entropy change, $\Delta S_M = S_1 - S_0$, which corresponds to the change of the magnetic field, is suitable to characterize the MCE. There is also another way to express the MCE. When the magnetic field is isoentropically applied, the temperature will increase from T_0 to T_1, with the entropy unchanged. Similarly, the temperature change, $\Delta T_{ad}=T_1-T_0$, which also corresponds to the change of the magnetic field, can be used as the indicator of the MCE.

To calculate the exact values of ΔS_M and ΔT_{ad}, one of the Maxwell's relations [75] is needed

$$\left(\frac{\partial S}{\partial H}\right)_{T,p} = \left(\frac{\partial M}{\partial T}\right)_{H,p} \tag{2.9}$$

Here, M represents the magnetization and the pressure, p, is considered constant.

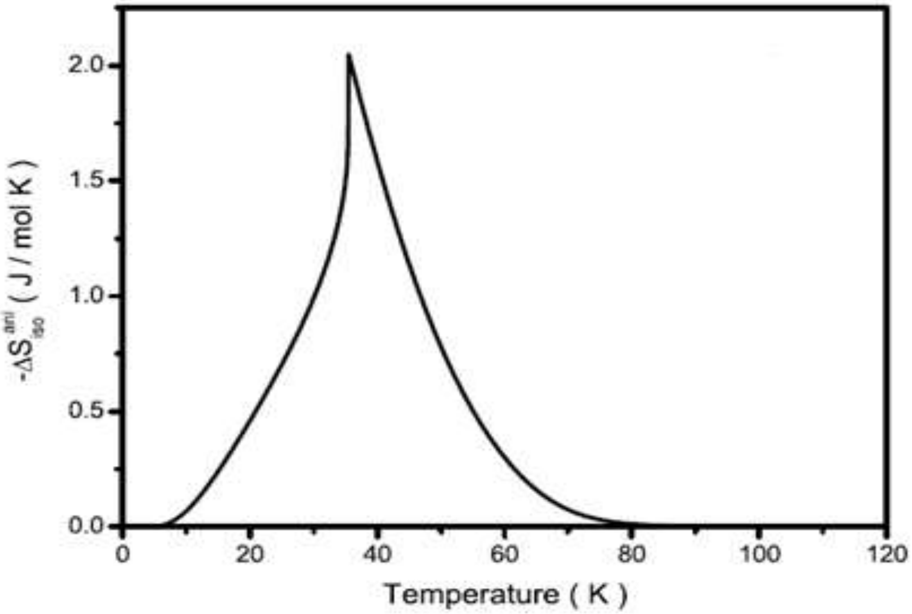

Figure 2. 4 An example of magnetic entropy change versus temperature diagram

Then, ΔS_M can be obtained by integrating the magnetic fields from H_0 to H_1:

$$\Delta S_M(T,\Delta H)=\int_{H_0}^{H_1}\left(\frac{\partial M(T,H)}{\partial T}\right)_H dH \qquad (2.10).$$

After a series of magnetization curves, under different temperatures, are measured, the temperature dependence of the magnetic entropy change curve can be established, as Figure 2.4 shows.

With the above equation, ΔT_{ad} can be calculated by using the relationship $CdT = dQ$ and $dQ = -TdS$. Further, ΔT_{ad} can be expressed as:

$$\Delta T_{ad}(T,\Delta H) = -\int_{H_0}^{H_1} \left(\frac{T}{C(T,H)} \right)_H \left(\frac{\partial M(T,H)}{\partial T} \right)_H dH \qquad (2.11).$$

Here, C represents the heat capacity.

Eqs. 2.9 to 2.11 revealed some characteristics of the MCE in magnetic materials:

(i) In a ferromagnetic material, $|(\partial M/\partial T)_H|$ reaches its maximum value at the Curie temperature (T_C), which therefore means that $|\Delta S_M(T,\Delta H)|$ should peak at T_C. This also provides an approach for determining T_C (in Fig. 2.4, T_C is around 38 K).

(ii) According to Eq. 2.10, when $\Delta H \to 0$, ΔT_{ad} of a ferromagnetic material also peaks near T_C [76]. ΔT_{ad} and $|\Delta S_M(T,\Delta H)|$ should follow a similar behavior in that they will be reduced as the temperature moves away from T_C.

(iii) According to Eq. 2.10, when the value of the $|\Delta S_M(T,\Delta H)|$ is unchanged, ΔT_{ad} will become larger at higher temperatures or with smaller total heat capacity. Moreover, at high temperatures, significant ΔT_{ad} cannot be observed until $|(\partial M/\partial T)_H|$ becomes sufficiently large, due to the large total heat capacity.

2.3.2 Magnetic refrigeration

On the basis of the MCE, magnetic refrigeration (MR) can be realized. As a new technology for cooling, MR has attracted much attention due to its outstanding features, energy-saving and environmentally-friendliness [16, 72, 77].

It is well known that modern refrigerators accomplish cooling via the compression and expansion of gases in a fixed cycle. The working medium in conventional refrigerators usually contains dichlorodifluoromethane (also known as CFC) which are sources of ozone depletion and the greenhouse effect. According to the Montreal Protocol on Substances that Deplete the Ozone Layer, CFCs are scheduled to be totally replaced. More information is given in Appendix I. In addition, the efficiency is somewhat too low.

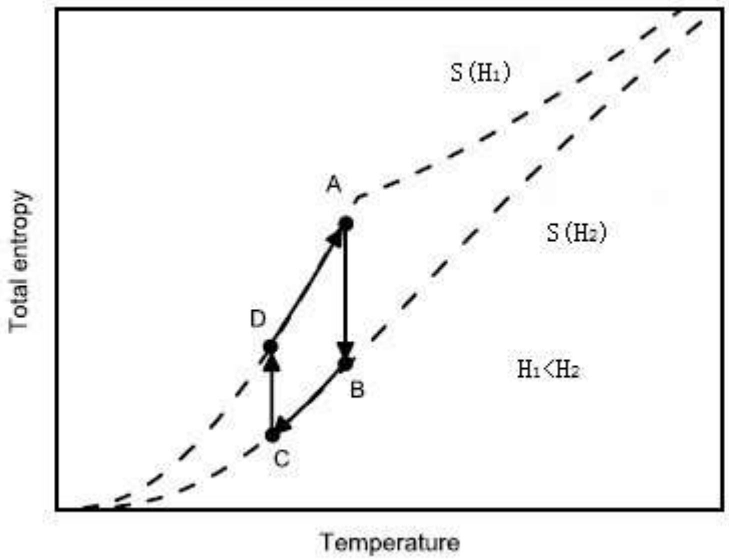

Figure 2. 5 A schematic diagram for the Ericsson cycle [49]

In magnetic refrigerators, however, the working fluid is simply water which is harmless, and the working materials are magnetic materials and magnets. To get a better understanding of magnetic refrigeration, the basic principles need to be known. Just like the conventional cooling method, magnetic refrigeration works in a given cycle. Till now, there have been three main cycles: the Carnot, Ericsson and Brayton cycles [43, 51, 78-80]. For refrigeration, a hot source and a cold source are needed to absorb and transfer heat. Take the Ericsson cycle for example, in which Figure 2.5 gives a general illustration of the steps ABCD [49]. As the diagram shows, a complete Ericsson cycle consists of two isothermal processes (AB and CD) and two isofield processes (BC and DA). From A to B, the working material is isothermally magnetized. After that, the working material is linked to a hot source with the field being unchanged. Heat will be transferred from the working material to the hot source, as BC shows. Demagnetization will then be applied isothermally, which is

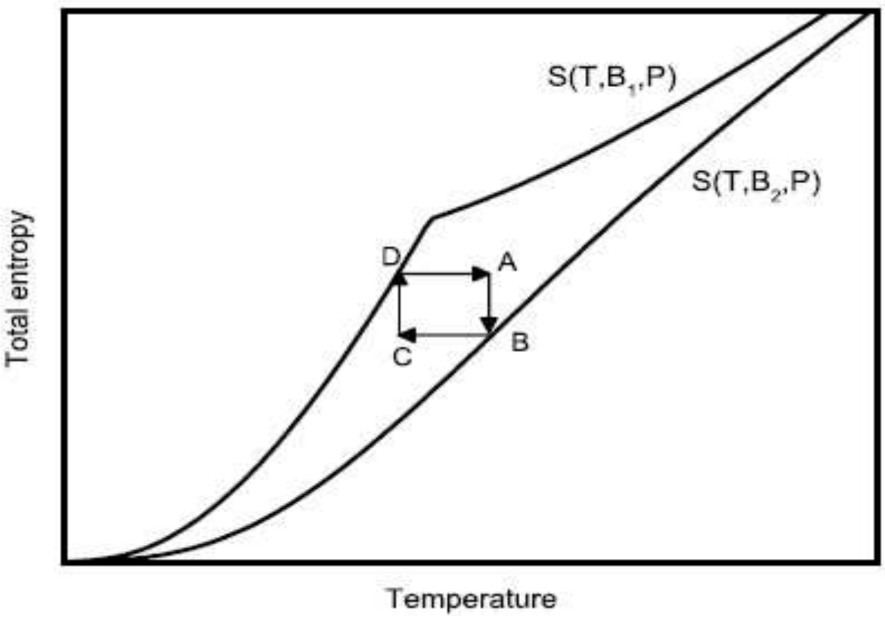

Figure 2. 6 A schematic diagram for the Carnot cycle [49]

represented by CD. By the end of demagnetization, a cold source will be attached to the working material to make the temperature rise while the magnetic field is constant. In this way, the heat is transferred from a cold source to hot source through the working material and refrigeration is realized [81-83].

Similar to the Ericsson cycle, the schematic description for the Carnot cycle and Brayton cycle are shown in Figure 2.6 and 2.7, respectively.

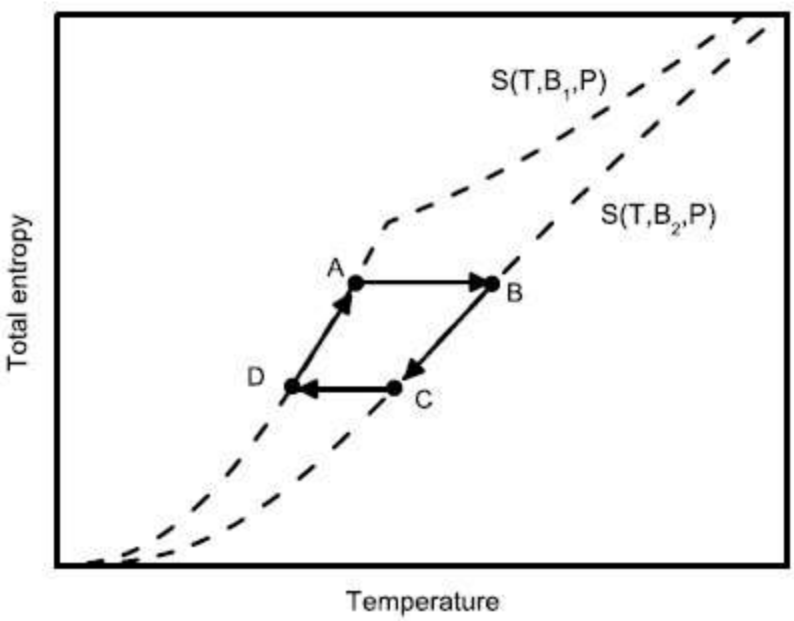

Figure 2. 7 A schematic diagram for the Brayton cycle [49]

From the figures above, differences between the Carnot, Brayton and Ericsson cycles can be found. In the Carnot cycle, the working cycle consists of two isothermal (AB and CD) and two adiabatic (DA and BC) processes. The Brayton cycle is made up of two adiabatic (AB and CD) and two isofield (BC and DA) processes. With regard to the working principles of these two cycles, they are much like those of the Ericsson cycle.

To quantify the ability of materials to realize magnetic refrigeration, the refrigeration capacity (*RC*) is introduced. According to the principles of MCE, *RC* can be defined as:

$$RC(\delta T, H_{\max}) = \int_{T_{cold}}^{T_{hot}} |\Delta S_M(T, \Delta H)| dT \qquad (2.12).$$

In equation 2.12, $\Delta H = H_1 - H_0$ and δT is the temperature range (T_{hot}-T_{cold}) for the refrigeration cycle [84]. On the basis of the theory of Gschneidner, the refrigeration capacity can also be approximately expressed by the peak entropy change, $|\Delta S_M^{peak}|$, multiplied by the temperature range, δT_{FWHM}, which stands for the full width at the half maximum of the ΔS-T curve [85]. Therefore, equation 2.12 can be changed into [32]:

$$RC(\delta T, H_{\max}) = |\Delta S_M^{peak}| \times \delta T_{FWHM} \qquad (2.13).$$

2.3.3 Conclusions

Magnetic refrigeration, based on the magnetocaloric effect, has promising applications with its competitive advantages compared to traditional techniques. In addition, a criterion for determining the refrigeration capacity has been proposed. The challenge now is to find the most appropriate working material for magnetic cooling.

2.4 Magnetocaloric materials (MCMs)

Since the MCE was discovered in 1881 [15], numerous investigations have been carried out to discover materials with excellent MCE. Till now, there are two categories of materials which are considered to be promising in the utilization of magnetic refrigeration; Gd-based and Fe-based materials. According to the above discussion, it is clear that the MCE is significant around T_C. Therefore, the first important step in the design of an MR system is to find an appropriate magnetic material which exhibits a T_C around room temperature with a sufficiently large MCE. Although materials that undergo first order magnetic transition show relatively large MCE, the transition temperature range is too small to be used for the MR at room temperature. The desired refrigerant system should exhibit a significant MCE over a span of temperature around room temperature. This makes materials that undergo second order magnetic transition preferred.

2.4.1 MCMs with a first order magnetic-phase transition (FOMT)

There are three major characteristics in materials that undergo a FOMT. Firstly, their entropy change is discontinuous. During the phase transition, there is the latent heat which is also known as the isofield enthalpy, ΔE_H. Secondly, couplings to secondary fields are required during the transition. As a result, magnetoelastic or magnetostructral transitions occur during the phase transition. Thirdly, the hysteresis in these materials is obvious, which makes the phase transition irreversible in a finite region.

As discussed before, the discovery of $Gd_5Si_2Ge_2$ with the giant magnetocaloric effect (GMCE) ignited new interest in magnetic refrigeration at room temperature [17]. Subsequently, investigations on GMCE increased at great speed. In the following years, other families of materials were also found to possess a giant magnetocaloric effect. They include $Tb_5Si_2Ge_2$, $La(Fe_{1-x}Si_x)_{13}$, $MnFeP_xAs_{1-x}$ and $MnAs_{1-x}Sb_x$ [16, 72, 85-88]. The GMCE, however, arises from the first order transformation, which results in some potential problems when these materials are applied in magnetic refrigeration. There are three main problems, summarized by previous researchers, namely, a great change in volume, significant magnetic hysteresis and a finite time to maximize the ΔT_{ad} [16, 89-93].

2.4.2 MCMs with a second order magnetic-phase transition (SOMT)

Materials undergo a SOMT also have three characteristics corresponding to those with FOMT. Firstly, the entropy change is continuous. Besides, as the temperature varies, the fluctuation of the entropy change is smaller than that in materials with FOMT. Secondly, during the transition, the volume remains unchanged. Thirdly, there is nearly zero magnetic hysteresis.

2.4.2.1 Gd-based materials

Magnetic refrigeration with Gd-based materials has already been used to obtain low temperatures below 1 K [94]. However, the application of Gd for room temperature refrigeration is still being researched. Although Gd has been proven to provide a large MCE [16], the high cost of Gd limits its application.

Combining the technology of metallic glasses, certain metallic glasses have been successfully synthesized, with a comparable MCE to Gd. In 2010, Schwarz fabricated $Gd_{60}Co_{30}Al_{10}$ metallic ribbons, which had a large MCE as well [95]. Gd-B series metallic ribbons were also prepared and characterized in 2010. The results showed that the largest RC value of this system was about 430 J/kg [96]. Zhong and his coworkers studied the Gd-Ni metallic glasses and obtained a RC value over 700 J/kg with a magnetic field of 5 T [97]. In 2011, a $Gd_{55}Al_{20}Co_{25}$ amorphous rod 2 mm in diameter was made [19]. Under a maximum field of 5 T, the RC value reached as high as 800 J/kg. In addition, $Gd_{55}Ni_{22}Mn_{3}Al_{20}$ was also made into bulk metallic glass, with an RC value of over 800 J/kg under a magnetic field of 5T [18]. Recently, Zheng's group synthesized Gd-Al-Fe metallic glass, with RC values around 700 J/kg, in a 5 T magnetic field [21].

Recently, a new form of magnetic materials was developed by Bingham and his colleagues [98]. In that work, melt-extracted Gd-based amorphous microwires ($Gd_{53}Al_{24}Co_{20}Zr_3$) were fabricated and arranged in parallel. Large magnetic entropy change (10.3 J/kgK at 95 K) and refrigeration capacity (733.4 J/kg) were obtained in a maximum magnetic field of 5 T for an array of forty microwires. The RC value of this microwire array is nearly twice as large as that of Gd (410 J/kg). Compared to the RC value of the bulk metallic glass state of $Gd_{53}Al_{24}Co_{20}Zr_3$ (590 J/kg), the enhancement of microwires was significant [99]. This study developed another approach to enhance the refrigeration capacity of magnetic materials by designing new mechanical structures, other than by simply adjusting the compositions.

2.4.2.2 Fe-based materials

Unlike the Gd-based metallic glasses which can be easily made into a bulk state, Fe-based amorphous alloys are normally in the form of ribbons due to their poor glass forming ability. Interest in Fe-based materials arises mainly because of two reasons. One is that Fe is abundant world-wide and cheap in cost, and the other is that the Curie temperature, T_C, of Fe-based alloys is higher than that of Gd-based alloys, and T_C can be easily tuned to be around room temperature for better performance.

In 1967, the first Fe-based amorphous alloy, Fe-P-C, was fabricated by Duwez [24], and was proven to be ferromagnetic. After that, a large number of investigations on Fe-based metallic glasses have been under taken. Fe-based amorphous materials have shown their extraordinary features in application, for example high saturation magnetization, low coercivity and negligible hysteresis [46].

Compared to Gd-based alloys, the peak value of the entropy change of Fe-based metallic glasses is relatively small. The Curie temperature of Fe-based materials, however, can be tuned to around room temperature, and these materials have a fast response to the external field due to the lack of hysteresis [41].

$Fe_{64}Mn_{15-x}Co_xSi_{10}B_{11}$ amorphous alloys were studied thoroughly by Lee[40], with a peak entropy change of about 0.82 J/kgK at 309 K. What was very important in his work is that he proved that the MCE of this kind of Fe-based metallic glasses is sensitive to the Co content in the alloy.

Among the Fe-based metallic glasses, two systems have shown impressive performances. One is Fe-B-Cr based and the other is Fe-B-Zr based. In Fe-Cr-B alloys, Franco studied $Fe_{80}Cr_{8}B_{12}$ and $Fe_{77}Cr_{8}B_{15}$ and came to the conclusion that both the peak entropy change and Curie temperature have a positive relationship with the B content [41]. Subsequently, the effect of adding a small amount of other elements on the magnetocaloric effect was studied. Law and Franco investigated the influence of some rare earth elements added to Fe-B-Cr based amorphous alloys [32]. They discovered that the Curie temperature, $T_{C,}$ can be easily changed by varying the amount of rare-earth elements while the magnetic entropy change, ΔS, remains constant. Surprisingly, $Fe_{79}La_{1}B_{12}Cr_{8}$ was proven to have a larger RC value than the well-known magnetocaloric material $Gd_{5}Si_{2}Ge_{1.9}Fe_{0.1}$ [92]. Fe-Zr-B alloys were investigated by Álvarez in 2009 [37], and Fang revealed that the MCE of Fe-Zr-B ribbons is enlarged with a small addition of B. Moreover, the alloying of Mn, Cr or Co had some interesting results. The Curie temperature was changed while the refrigeration capacity varied relatively insignificantly. Furthermore, Wang and Bi searched for the relationship between the content of Zr and B and the MCE of the Fe-Zr-B metallic glasses [48]. In their study, they found that it was the total amount of Zr and B that influenced the MCE rather than the individual amounts. A new method was adopted by Álvarez [28], in which a composite was fabricated with two amorphous alloys, and the result showed that the refrigeration capacity could be enhanced.

A new category of alloy which combined Gd and Fe was fabricated. Zheng and his colleagues prepared a series of $Gd_{75-55}Al_{25-5}Fe_{0-40}$ alloys and obtained *RC* values in the range of about 532-780 J/kg in a maximum field of 5 T [21].

It has also been proven that the magnetic properties are enhanced if there is more Fe in the alloys [29].

Table 2.2 shows the performance of some existing Gd-based and Fe-based magnetocaloric materials, where "A" represents an amorphous alloy and "C" represents a crystal alloy.

Table 2. 2 The magnetocaloric effect of some existing Gd-based and Fe-based materials

	T_c(K)	Structure	H(T)	$(-\Delta S_M)_{max}$(J $kg^{-1}K^{-1}$)	RC(J kg^{-1})	Refs.
$Gd_{55}Ni_{22}Mn_3Al_{20}$	90	A	5	7.54	815	[18]
$Gd_{55}Co_{15}Al_{30}$	96	A	5	9.4	910	[20]
$Gd_{55}Co_{15}Al_{28}Si_2$	98	A	5	9.1	890	[22]
$Gd_{75}Al_{25}$	104	A	5	6.02	683	[100]
$Gd_{71}Fe_3Al_{26}$	117.5	A	5	7.4	750	[101]
$Gd_{68}Ni_{32}$	124	A	5	8.0	583	[97]
$Gd_{70}Al_{20}Fe_{10}$	149	A	5	7.14	780	[100]

$Gd_{55}Al_5Fe_{40}$	222	A	5	2.7	532	[100]
$Gd_{60}Fe_{20}Co_{10}Al_{10}$	222	A	5	4.4	736	[102]
$Fe_{79}B_{12}Cr_8Ce_2$	325	A	1.1	0.84	72	[32]
$Fe_{79}B_{12}Cr_8La_1$	355	A	1.1	0.88	88	[32]
$Fe_{79}B_{12}Cr_8Gd_1$	355	A	1.1	1.11	107	[103]
$Fe_{64}Mn_{14}Co_1Si_{10}B_{11}$	457	A	0.8	0.51	67	[40]
Gd	294	C	5	10.2	556	[101]
$Gd_5Ge_2Si_2$	275	C	5	20.0	305	[92]
$Gd_5Ge_{1.9}Si_2Fe_{0.1}$	305	C	5	7.0	360	[92]
GdFeAl	265	C	5	3.7	420	[101]
$LaFe_{11.4}Si_{1.6}$	202.5	C	5	25	439	[104]

This table lists the MCE of some existing Gd-based materials and Fe-based materials. A represents amorphous and C represents crystal. It can be seen that for Gd-based materials, amorphous ones have larger *RC* values and lower Curie temperatures than crystal ones. Compared with Gd-based materials, Fe-based amorphous materials usually have smaller *RC* values but higher Curie temperatures. From this table, it can be also inferred that the working temperature range of Fe-based materials is much wider than that of Gd-based materials.

2.4.3 Ideal magnetic refrigerants

From the literature review on Gd-based and Fe-based alloys above, they both exhibit their own advantages and disadvantages during applications. To decide which one is better suited for the use of magnetic refrigeration at room temperature, we need to balance various factors. To ascertain if magnetic refrigerators will work well, there are several basic requirements for magnetic materials which act as the core of magnetic refrigeration. The requirements are generally agreed in the literature as follows [43, 105]:

1. A large magnetocaloric effect is obviously needed for high refrigeration efficiency

2. A suitable Curie temperature in the working temperature range is needed to make sure that the magnetic materials can work at their maximum efficiency;

3. Negligible magnetic hysteresis to reduce the energy loss;

4. Large electric resistance to lessen the energy loss caused by eddy currents;

5. Small specific heat and good thermal conductivity to make sure that the temperature change is significant and the heat exchange is fast;

6. Low cost of raw materials, preparation and fabrication to make large scale production easier;

7. Good corrosion resistance and no harm to the environment or health.

For Gd-based alloys, the peak magnetic entropy change is relatively large but the Curie temperature is too low to be applied for room temperature magnetic refrigeration. On the other hand, for Fe-based alloys, the Curie temperature can be easily tuned to be perfect for room temperature applications but the peak magnetic entropy change is somewhat low. From the cost aspect, Fe is much cheaper than Gd.

2.5 Theoretical study of the MCE

Since it is time-consuming to adjust the composition by the trial and error approach to achieve enhanced magnetocaloric effect, a theoretical approach to predict the MCE is most desirable. In addition, there may be errors during experimentation which can’t be avoided. With the help of theoretical calculations or predictions, one can check and verify the results obtained from experiments.

2.5.1 Theoretical study based on experimental results

In 2008, Franco and his coworkers tested the magnetic properties of $Fe_{92-x}Cr_8B_x$ (x=12, 15) amorphous ribbons [41]. Firstly, they carried out experiments on the ribbons to determine their magnetic entropy change. Subsequently, Franco proposed a theoretical way to illustrate the relation between the magnetic entropy changes and the external fields. The Arrot-Noakes equation of state was used for analysis, leading to the following equation:

$$H^{1/\gamma} = a(T - T_C)M^{1/\gamma} + bM^{1/\beta+1/\gamma} \qquad (2.14).$$

In the above equation, H is the magnetic field, M is the magnetization, T_C is the Curie temperature, T is temperature, a and b are parameters related to the composition and β and γ are the critical exponents. After the parameters in this equation are obtained, one can calculate the magnetic entropy change at different temperatures, according to equation 2.10. In Franco's work, the parameters for two Fe-based metallic glasses were obtained. Figure 2.8 shows the results from both the experiments and theoretical calculations. B12 stands for $Fe_{80}Cr_8B_{12}$ and B15 stands for $Fe_{77}Cr_8B_{15}$. VSM and SQUID are the two methods for the investigation of the magnetic properties. AN means the analytical calculation. From the curves and dots in Figure 2.8, the prediction or theoretical calculation fits well with the experimental results.

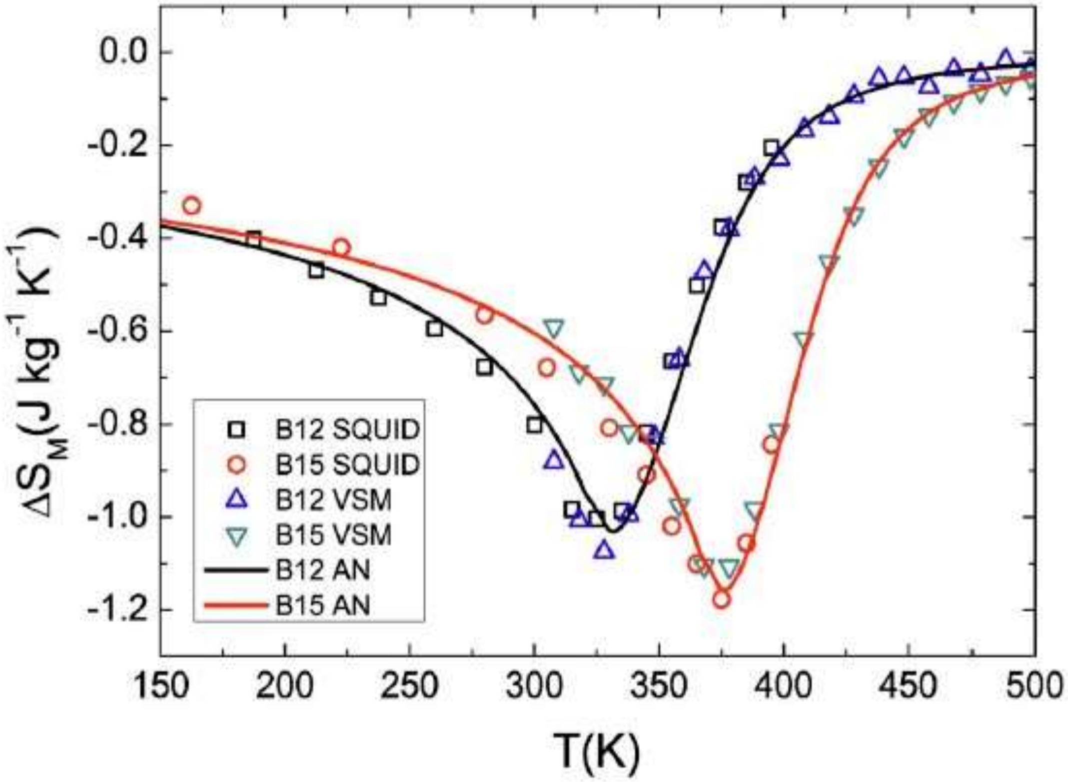

Figure 2. 8 The results from both experiments and theoretical calculations

It is recognized that the maximum magnetic field will influence the magnetocaloric effect of magnetic materials. However, relevant research had a breakthrough when Franco proposed a relationship between the magnetic entropy change and the magnetic field in 2006 [31]. The $Fe_{83}Zr_6B_{10}Cu_1$ amorphous alloy was examined. According to the Arrot-Noakes equation of state, mentioned before, the magnetic entropy change can be expressed as:

$$\Delta S_M \Big|_{T=T_C} = \frac{-a\beta\gamma}{b^{(\beta+\gamma\beta)}(2\beta+\gamma-1)} H^{[(\beta-1)/(\beta+\gamma)]+1} \qquad (2.15).$$

A relationship between the magnetic entropy change and the magnetic field can be obtained from the above equation. To simplify the expression, a parameter n was introduced:

$$n = 1 + \frac{\beta - 1}{\beta + \gamma} \tag{2.16}$$

As a result, the relation between the magnetic entropy change and magnetic field can be expressed as:

$$\Delta S_M \propto H^n \tag{2.17}$$

To obtain the value of *n*, experiments were carried out to measure the magnetization

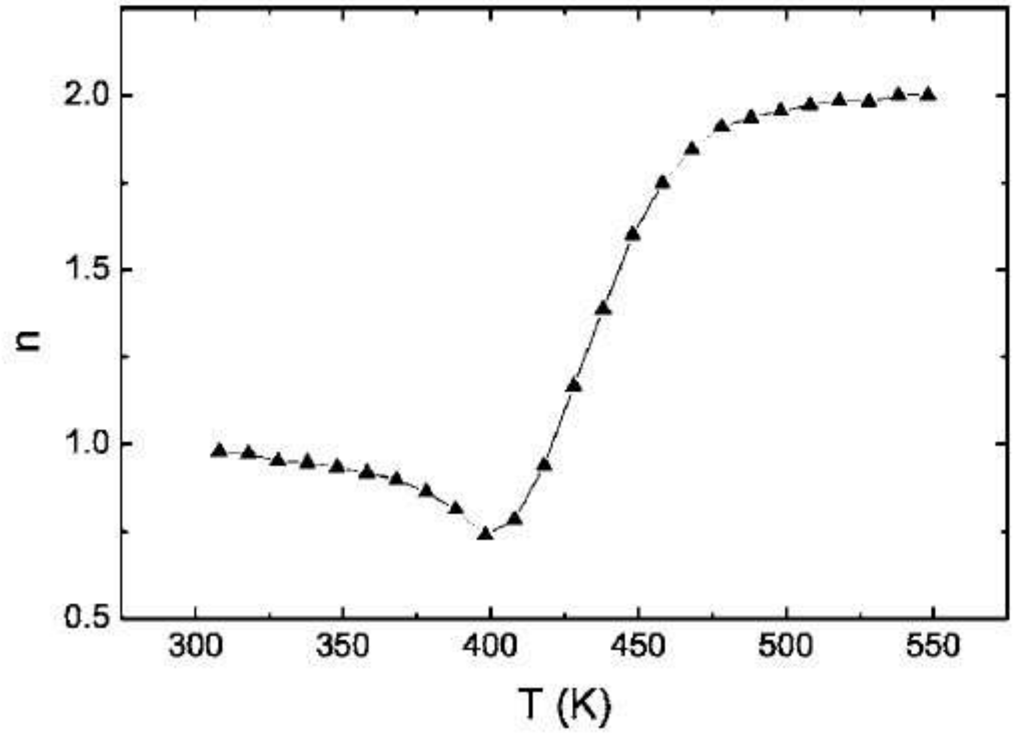

Figure 2. 9 The temperature dependence of n for $Fe_{83}Zr_6B_{10}Cu_1$

curves of $Fe_{83}Zr_6B_{10}Cu_1$, and according to equation 2.14, the values of n at different temperatures were calculated. Thus, an n versus temperature diagram can be built, as in Figure 2.9. From the diagram, it is found that for this alloy, $n \approx 0.75$ at temperatures near the Curie temperature, $n = 1$ for temperatures well below the Curie temperature and $n = 2$ for temperatures well above the Curie temperature [31]. With the n exponent, the results obtained under different magnetic fields can be compared.

Meanwhile, a master curve behavior for the magnetic field dependence of magnetic entropy change was proposed by Franco [31]. Tests on the magnetic

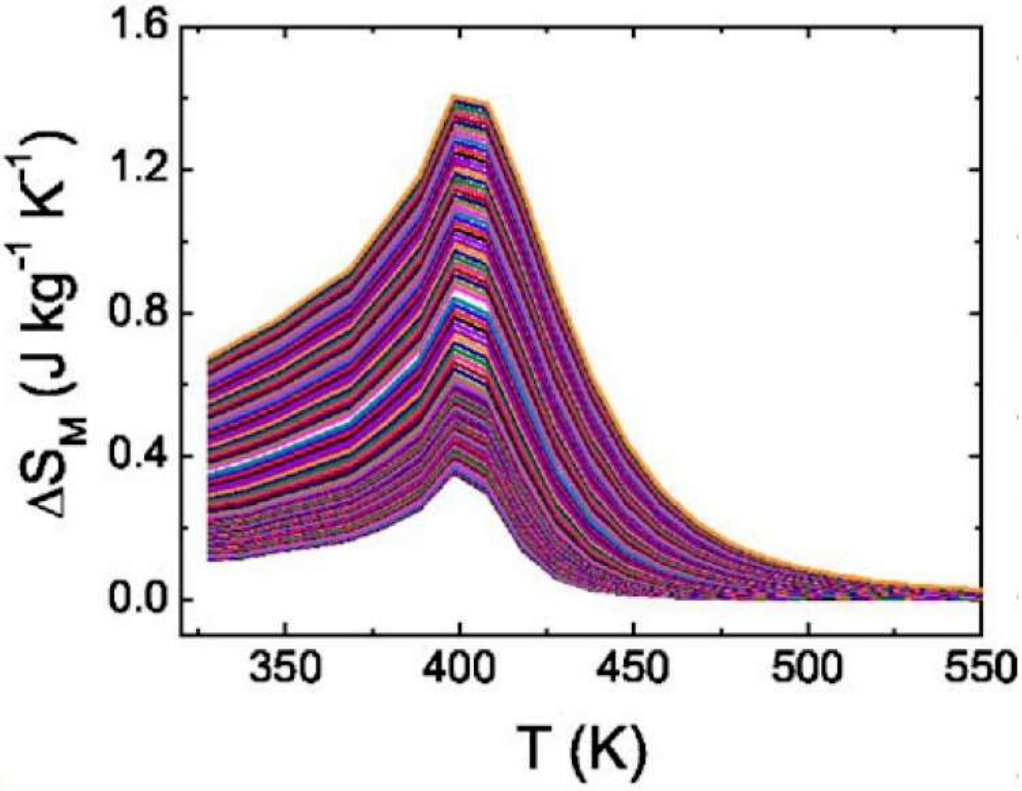

Figure 2. 10 The magnetic entropy change versus temperature diagram under different magnetic fields

properties of $Fe_{83}Zr_6B_{10}Cu_1$ were carried out under a maximum magnetic field of 0.25 T to 1.5 T. The magnetic entropy change versus temperature diagram is shown in Figure 2.10. The master curve can be obtained by changing the units of the X axis and Y axis. For the Y axis, normalization was used, and the magnetic entropy change was converted to

$$\Delta S'(T, H_{\max}) = \Delta S_M(T, H_{\max}) / \Delta S_M^{peak}(H_{\max}) \qquad (2.18).$$

For the X axis, a new parameter, θ was introduced to replace temperature, and the relationship can be expressed as:

$$\theta = \begin{cases} -(T - T_C)/(T_{r1} - T_C), T \le T_C \\ (T - T_C)/(T_{r2} - T_C), T > T_C \end{cases} \qquad (2.19).$$

In the above equation, T_{r1} and T_{r2} are the temperatures corresponding to half of the

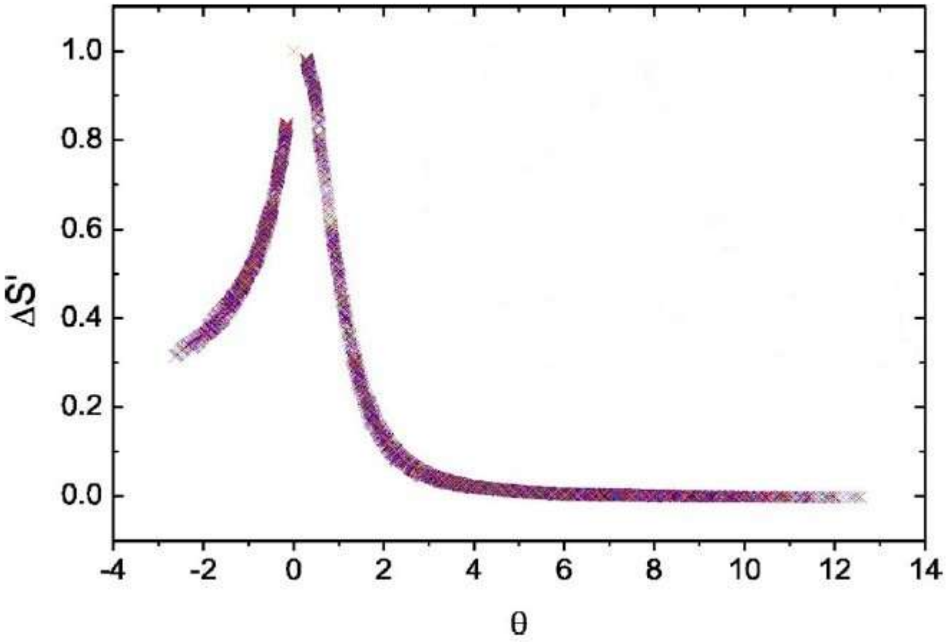

Figure 2. 11 The master curve of $Fe_{83}Zr_6B_{10}Cu_1$

peak of the magnetic entropy change. Therefore, the master curve can be obtained, as in Figure 2.11.

Franco and his team also studied the field dependence of the *RC* [106]. Basically, there are two methods to calculate the *RC*, as described in Eqs. 2.12 and 2.13. One is the area under the $|\Delta S_M| - T$ curve between T_{cold} and T_{hot} which are applied as the integration limits and the other is the product of the $\left|\Delta S_M^{peak}\right|$ and T_{FWHM}. Regardless of the calculation method, the *RC* has a correlation with the magnetic field as follows:

$$RC \propto H^{1+1/\delta} \qquad (2.20).$$

The critical exponent δ can be obtained from the Arrott-Noakes equation of state at T_C [107]:

$$H^{1/\gamma} = bM^{(1/\beta)+(1/\gamma)} \qquad (2.21)$$

where b is a constant, β and γ are critical exponents. The relations between the exponents were given in [23, 106] as $\Delta = \beta + \gamma$ and $1/\Delta + (1-\alpha)/\Delta = 1 + 1/\delta$. Eq. 2.21 can be therefore changed into:

$$M(T = T_C) \propto H^{1/\delta} \qquad (2.22).$$

By fitting the magnetization curve at T_C, the related critical exponents can be calculated and the field dependence of *RC* can also be obtained.

2.5.2 Theoretical study based on Monte-Carlo simulation

In section 2.5.1, theoretical study was performed on the basis of experimental results. Predictions could not be made about the magnetic properties of new materials without taking time to do experiments according section 2.5.1. Simulation work, therefore, is necessary and desirable. The algorithm was based on the Monte-Carlo method and was designed for crystalline alloys.

In 1949, a general description of Monte Carlo simulation was presented by Metroplios and Ulam [108]. In Monte Carlo simulation, models change with time in a stochastic way on the basis of random numbers generated by the simulation [109]. The method provides a solution to the integro-differential equations used in various nature sciences, which is perfectly suited to the area of magnetism. Based on a Monte Carlo algorithm, a computer program named MCMAG was developed with Fortran language in order to simulate magnetic structures in 1987 [110]. The main purpose of the program was to determine the ground state of a system with n spins. The orientation of each spin is marked as S_i (i = 1, 2, …, n). The energy of the whole system, therefore, can be obtained as:

$$E = f(S_1, \dots, S_i, \dots, S_n) \qquad (2.23).$$

With the function f, the determination of the ground state can be realized by minimizing the energy through changing the orientations of the spins.

As mentioned in Chapter 2.3.1, the total entropy is the sum of three parts: $S = S_M + S_{el} + S_{lat}$. In the simulation, each part was calculated as follows:

$$S_M(T,H) = \int_0^T \frac{C_M(T,H)}{T} dT \qquad (2.24)$$

$$S_{el} = \gamma T \qquad (2.25)$$

$$S_{lat}(T) = N_i \left[-3R\ln\left(1 - e^{-(\theta_D/T)}\right) + 12R\left(\frac{T}{\theta_D}\right)^3 \int_0^{\theta_D/T} \frac{x^3}{e^x-1} dx \right] \qquad (2.26)$$

where $C_M(T,H)$ is the magnetic part of the heat capacity and can be obtained from:

$$C_M(T,H) = \frac{\langle E^2 \rangle - \langle E \rangle^2}{k_B T^2} \qquad (2.27).$$

γ is the Sommerfeld coefficient, N_i is the average number of ions in one formula unit, R is the gas constant, θ_D is the Debye temperature, k_B is the Boltzmann constant. $\langle E^2 \rangle$ and $\langle E \rangle$ are the mean square energy and the mean energy calculated in the simulation.

Simulation work on the MCE has been carried out in crystalline alloys. In a general study on the MCE of individual spins and spin clusters on simple cubic, body center cubic and face center cubic lattices, Bennett [111] reported that the lattice exhibiting the lowest T_C had the largest $\left|\Delta S_M^{peak}\right|$. Nóbrega studied the MCE of different crystalline alloys by Monte Carlo calculations [112-115]. The simulated $|\Delta S_M|$ and ΔT_{ad} were in good agreement with the experimental results.

2.6 Development of the Magnetic Refrigeration

Weiss and Piccard also reported the MCE in 1917 [116]. In the next ten years, major advances were made due to the proposal independently brought out by Debye [117] and Giauque [118] that cooling could be realized by adiabatic demagnetization. In 1933, Giauque and MacDougall successfully reached 0.25 K in experiments [119]. A milestone was achieved in 1997 by Gschneidner at the Ames Laboratory in that the first prototype of a magnetic refrigerator working near room temperature was demonstrated [120]. Since then, interest has been attracted from both researchers and companies all over the world in order to develop new kinds of materials and prototypes for a room temperature MR. In 2002, an important breakthrough was made in that the giant magnetocaloric effect (GMCE) was found in MnFe(P,As) alloys by the University of Amsterdam [121]. Differing from $Gd_5Si_2Ge_2$, which also exhibits the GMCE, MnFe(P,As) alloys can be made from materials abundant found on earth. Table 2.3 shows the research outcomes in recent years concerning the room temperature magnetic refrigerators.

Table 2. 3 Magnetic refrigerators for room temperature applications

Facility	Announcement date	Maximum cooling power (W)	ΔT_{ad}^{max}(K)	Applied Magentic field (T)	Working material	Reference
Ames Laboratory/Astronautics	1997	600	10	5	Gd Spheres	[120]
Mater. Science Institute Barcelona	2000	N/A	5	0.95	Gd foil	[122]
Chubu Electric/Toshiba	2000	100	21	4	Gd Spheres	[123]
University of Victoria	2001	2	14	2	Gd & $Gd_{1-x}Tb_x$	[124]
US Astronautics	2001	95	25	1.5	Gd Spheres	[125]
Sichuan Inst. Tech./Nanjing University	2002	N/A	23	1.4	Gd spheres and $Gd_5Si_{1.985}Ge_{1.985}Ga_{0.03}$ powder	[126]
Chubu Electric/Toshiba	2002	40	27	0.6	$Gd_{1-x}Dy_x$	[127]
Chubu Electric/Toshiba	2003	60	10	0.76	$Gd_{1-x}Dy_x$	[127]
Lab. d'Electrotechnique Grenoble	2003	8.8	4	0.8	Gd foil	[128]

George Washington University	2004	N/A	5	2	Gd foil	[129]
US Astronautics	2004	95	25	1.5	Gd and GdEr spheres	[125]
University of Victoria	2006	15	50	2	Gd, $Gd_{0.74}Tb_{0.26}$ and $Gd_{0.85}Er_{0.15}$ pucks	[130]
University of Salerno	2016	250	12	1.2	Gd 0.600 mm spherical particles	[131]

Apart from the researchers at universities, a number of companies are in competition for MR at room temperature. Cooltech Applications commercialize its magnetic refrigerator in 2014. Two year later, this company successfully launched its first commercial magnetic refrigeration system (MRS) as shown in Figure 2. 12

Figure 2. 12 The Magnetic Refrigeration System (MRS) developed by Cooltech Applications [132]

[132]. Due to the small size and flexible design, the MRS could be integrated in many refrigeration systems, for example, a medical refrigerator and a wine cellar. Figure 2. 13 provides a general illustration of the integration of the MRS into a refrigerated cabinet [132]. Moreover, Haier, Astronautics Corporation of America and BASF worked together to exhibit their first magnetic refrigerator in the Consumer Electronics Show in Las Vegas in 2015.

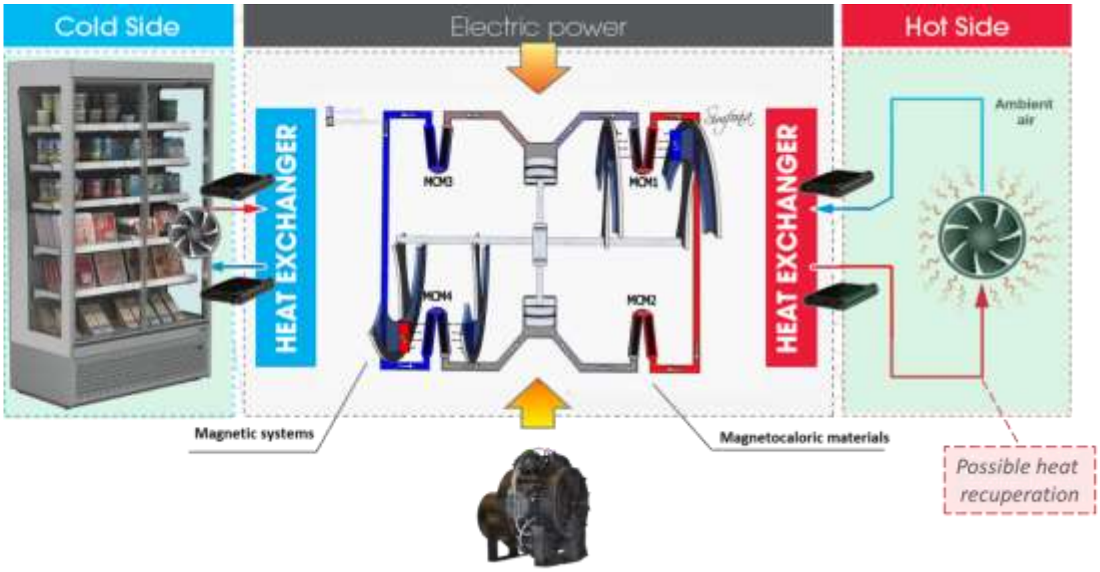

Figure 2. 13 A general illustration of the integration of the MRS into a refrigerated cabinet [132]

The advantages of magnetic refrigeration over the conventional cooling technology can be seen from the following five aspects:

1. Energy saving: Compared with the conventional cooling methods, the magnetic refrigerators can save about 30% energy;

2. Zero hazardous gas emission: In magnetic refrigerators, no refrigerant gas is needed to transfer heat. It will not only help preserve the environment but also avoid violating policies on greenhouse gas emissions;

3. Cost reduction: Due to the low level of maintenance, the operation cos for users will be lower;

4. User safety: Due to the absence of a refrigerant gas, the operation system will function in a low pressure condition, which is safer for the users. Besides, it also avoids the hazardous leaks;

5. Noise and vibration reduction: Magnetic refrigerators usually have low level noise and vibration.

For the moment, the greatest challenge in the commercialization of the magnetic refrigeration is to achieve the most appropriate working materials with sufficient large MCE, good corrosion resistance and small hysteresis loss, around room temperature.

2.7 Conclusions to Chapter Two

In this chapter, the literature on magnetic refrigeration was reviewed and is closely related to the objectives mentioned in chapter one. Particularly, the focus was on five parts:

1. Properties and the current applications of metallic glasses;

2. The mechanism and the application of the magnetocaloric effect;

3. Gd-based and Fe-based materials for magnetic refrigeration;

4. Some theoretical studies of the magnetocaloric effect;

5. Development of the MR.

After comparing Gd and Fe from several aspects, Fe-based amorphous alloys were chosen for experimentation, and Gd-based amorphous alloys were chosen for simulation. In the next chapter, the methodology applied in this study is introduced.

Chapter 3 Methodology

3.1 Selection and preparation of appropriate metallic glass ribbons for the MR

3.1.1 Selection of appropriate composition

To decide on the composition of the specimens, the magnetocaloric effect of some existing materials was studied in order to understand the influence of various elements on the MCE so as to develop new compositions with enhanced performance.

To be a suitable material for magnetic refrigeration, some basic characteristics are required. First of all, a large magnetocaloric effect is needed, and, to make the material perform well near room temperature, the Curie temperature is expected to be just around the room temperature. With regard to the efficiency, the material should exhibit nearly zero magnetic hysteresis. Moreover, to prevent the appearance of an eddy current, a large electric resistance is a must. Materials with small specific heat and large thermal conductivity usually lead to a significant and rapid change of temperature. The cost of the materials should be low and the process of fabrication straightforward [43].

For Fe-based metallic glasses, what is most challenging is their poor glass forming ability. With more Fe content in the alloys, although the magnetic properties will be enhanced, the GFA will be worse. Therefore, it is important to find a balance point and make a reasonable compromise between them. After thorough consideration and trials, Fe-based alloys were fabricated into amorphous ribbons instead of bulk metallic glasses in order to get a larger magnetocaloric effect with a higher Fe content.

After comparing the performance of existing Fe-based magnetic materials, the Fe-Zr-B alloy was chosen as the master alloy. The influence of different minor additions on the MCE was also thoroughly investigated.

3.1.2 Preparation of the ribbon specimens

The raw materials with purities above 99.9% were pre-processed and the ingots of the specimens were prepared using arc-melting technology in a WK-Ⅱ vacuum arc melter. The ingots were melted at least six times to ensure homogeneity. The ribbon samples with 0.02 mm in thickness and 1.5 mm in width were fabricated by a spinning copper roller machine with a single roller under an argon atmosphere.

3.2 Characterization of the metallic glass ribbon samples

3.2.1 Characterization of the microstructure of the ribbon specimens

Since this project aims at metallic glasses, it is necessary to confirm whether the as-cast samples are amorphous or not. The characteration was carried out by X-ray diffraction (XRD) analysis with Cu-K_α radiation. For metallic glasses, there is a typical broad wave package in the XRD pattern with no sharp peaks which are a sign of cystallinity.

3.2.2 Characterization of the magnetic properties of the ribbon specimens

The magnetic property related experiments were performed on a Quantum Design vibrating sample magnetometer (VSM). The magnetic hysteresis loops under different temperatures were measured to check the soft magnetic property. The measurements were carried out in a magnetic field changing between 0.7 T and -0.7 T, with 0.007 T changeper step. The magnetization investigations were performed under temperatures from 150 K to 400 K with 10 K change per step. The investigations were carried out in a changing magnetic field increasing from 0 to 1.5 T with 0.005 T change per step. The magnetocaloric effect (MCE) of the as-spun ribbons was obtained by calculating the working temperature range (ΔT) and the peak magnetic entropy change (ΔS_M^{peak}). The magnetic entropy change (ΔS_M) was calculated from Eq. 2.9. To make the calculation simple and consistent with the results reported in the literature, the *RC* was obtained from Eq. 2.12.

3.3 Theoretical study of the magnetocaloric effect

Since it would take too much time to investigate every possible single specimen, a theoretical way to calculate or predict the magnetocaloric effect is necessary, thereby saving a lot of time as well as providing a reliable method to verify the experimental results.

The measurements of magnetic properties are usually carried out in different maximum magnetic fields, so it is difficult to compare the results between different studies if the experimental conditions are not the same. Thus, the magnetic field dependence of the MCE is meaningful. The correlation between the MCE and the magnetic fields can be obtained by Eqs. 2.16 and 2.19. With this approach, it only compares the results obtained under different experimental conditions but also saves energy by applying a small magnetic field during the measurements.

The simulation study on the MCE based on the Monte Carlo method can verify the experimental results and predict the results of new materials.

Chapter 4 Investigations on the optimization of the MCE of the FeZrB amorphous alloy systems

4.1 Introduction

The most challenging topic in the field of MCE is to search for new materials with their MCE sufficiently large for MR applications. Materials exhibiting second order phase transition which display a ΔS_M^{peak} over a wide temperature range, are preferred, because these working materials are more effective under different temperature conditions. Since Duwez [24] first synthesized Fe-based metallic glass in 1967, much attention has been paid to their superior properties [25, 30, 32, 37, 38, 41, 50, 133-135]. These materials have lower cost than rare-earth based materials, excellent soft magnetic properties without hysteresis losses which make it possible to work in high frequencies with fast response, and tunable Curie temperatures (T_C) which can be easily realized by adjusting the composition [37]. Most of the Fe-based materials have Curie temperatures far above room temperature, which means that the MCE of these materials cannot reach their maximum values under a typical room temperature range, and are therefore not ideal for MR applications at room temperature. Among various Fe-based metallic glasses, FeZrB metallic glasses are better candidates because their T_C is closer to room temperature.

In this chapter, investigations on the MCE of the Fe-Zr-B ternary amorphous ribbons are discussed. The study is focused on the optimization of the MCE in FeZrB systems. The investigation is important for understanding the mechanism of the MCE in FeZrB systems and is also the foundation of further study on the enhancement of the MCE.

4.2 Results and discussion

Ingots with nominal composition $Fe_{94-x}Zr_6B_x$ (x=5, 6, 8 and 10), $Fe_{91-y}Zr_9B_y$ (y=3, 4, 5, 6, 8 and 10) and $Fe_{89-z}Zr_{11}B_z$ (z=3, 4, 5, 6, 8 and 10) were melted repeatedly in a vacuum arc melter machine under an argon atmosphere. Ribbons of 0.02 mm in thickness and 1.5 mm width were obtained in a spinning copper roller machine with a single roller under an argon atmosphere. X-ray diffraction (XRD) investigations were performed using a Rigaku diffractometer with Cu-*Kα* radiation in order to confirm the amorphous state of the specimens. The soft magnetic properties of these ribbons were investigated by carrying out magnetic hysteresis tests. The measurement was performed on a Lakeshore 7407 vibrating sample magnetometer (VSM). The magnetic hysteresis loops were tested in conditions where the magnetic field decreased from 0.7 T to -0.7 T, and then increased back to 0.7 T, in 0.007 T steps. The hysteresis loops for each ribbon sample were tested both below and above its Curie temperature. The magnetization of the ribbons was also characterized on the

VSM. The temperature range for the magnetization test was from 250 K to 400 K, in 10 K steps. At each temperature point, the magnetization curve of each ribbon was obtained under a field increasing from 0 to 1.5 T in 0.005 T steps. The MCE of the ribbons was characterized by calculating the working temperature range (ΔT) and the peak magnetic entropy change (ΔS_M^{peak}). According to one of the fundamental Maxwell's relations [51], the ΔS_M can be obtained as follows:

$$\left(\partial S(T,H)/\partial H\right)_T = \left(\partial M(T,H)/\partial T\right)_H \tag{4.1}$$

where T represents for the temperature, H the magnetic field and M the magnetization. Integrating Eq. (1), under isothermal conditions, gives:

$$\Delta S(T,\Delta H) = \int_{H_1}^{H_2} \left(\partial M(T,H)/\partial T\right)_H dH \cdot \tag{4.2}$$

In a magnetic solid, the total entropy is contributed by three parts:

$$S(T,H) = S_M(T,H) + S_{Lat}(T) + S_{El}(T) \tag{4.3}$$

where S_M represents for the magnetic entropy, S_{Lat} the lattice entropy and S_{El} the electronic entropy. In an isothermal process at a fixed temperature T ,

$$\Delta S_M(T,\Delta H) = \Delta S(T,\Delta H) = \int_{H_1}^{H_2} \left(\partial M(T,H)/\partial T\right)_H dH \tag{4.4}$$

To calculate the refrigerant capacity (RC), the following equation was used:

$$RC(\Delta H) = \int_{T_{cold}}^{T_{hot}} \left|\Delta S_M(T,\Delta H)\right| dT \cdot \tag{4.5}$$

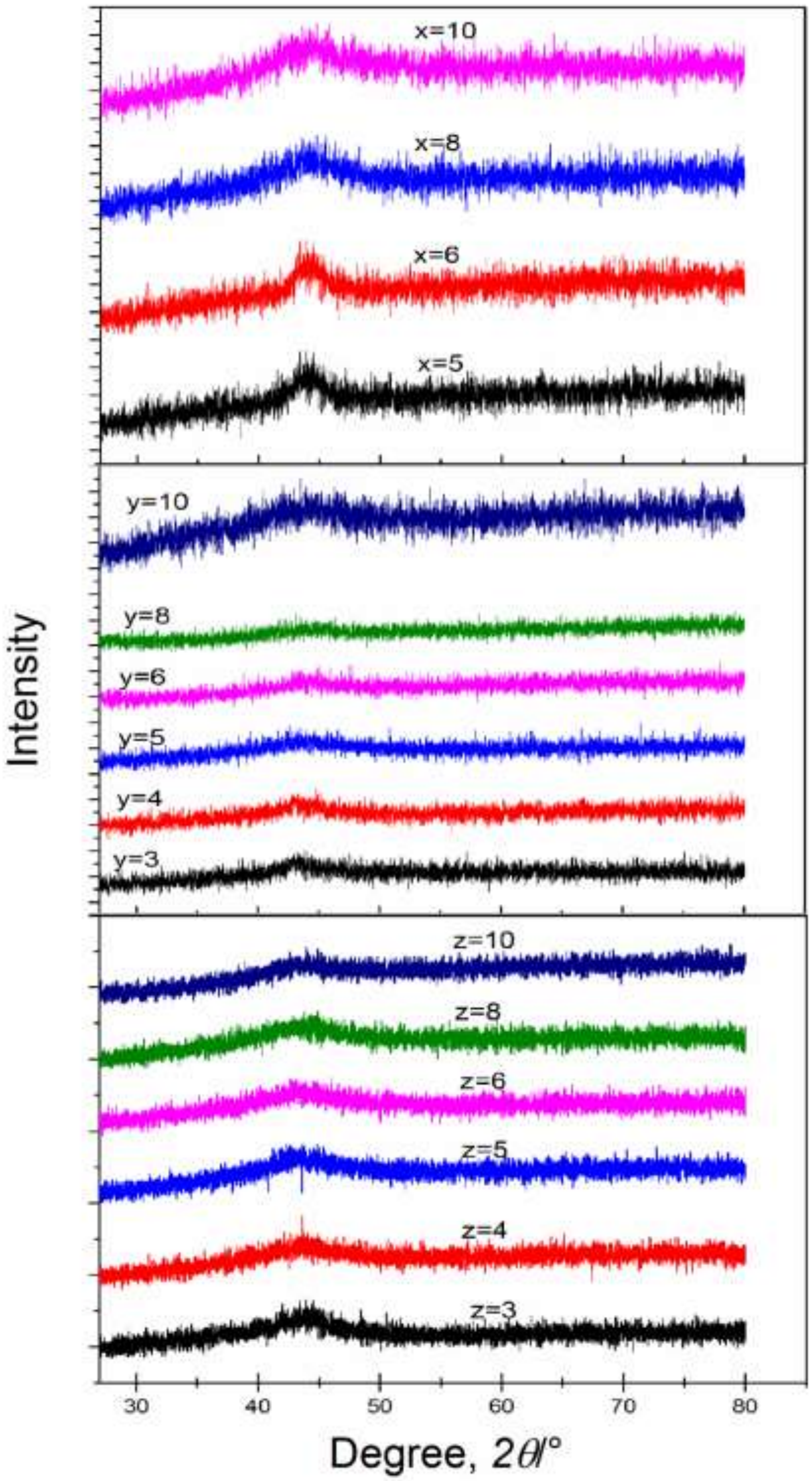

Figure 4. 1 XRD results of $Fe_{94-x}Zr_6B_x$ (x=5, 6, 8 and 10), $Fe_{91-y}Zr_9B_y$ (y=3, 4, 5, 6, 8 and 10) and $Fe_{89-z}Zr_{11}B_z$ (z=3, 4, 5, 6, 8 and 10) ribbons

To simplify the calculations and allow comparison with the results in the literature, RC can also be obtained by:

$$RC(\Delta H) = \left|\Delta S_M^{peak}\right| \times \delta T_{FWHM} . \qquad (4.6)$$

where δT_{FWHM} is the full width at the half maximum of ΔS_M .

The X-ray diffraction tests were carried out and the result of each specimen is presented in Fig. 4.1. Every one of the XRD patterns shows a broad hump around where $2\theta = 45°$ and no sharp crystalline peak. Based on these XRD results, all the specimens are considered to be amorphous. In order to calculate the MCE of the ribbons, magnetization curves were obtained over a wide temperature range. The magnetization curves in Fig. 4.2a, 1b and 1c are the results for three typical ribbons representing $Fe_{94-x}Zr_6B_x$ (x=5, 6, 8 and 10), $Fe_{91-y}Zr_9B_y$ (y=3, 4, 5, 6, 8 and 10) and $Fe_{89-z}Zr_{11}B_z$ (z=3, 4, 5, 6, 8 and 10), respectively. All three figures show that the saturation magnetization increases as the temperature decreases. In addition, the temperature dependence of the magnetization curve shape indicates that all these ribbon samples undergo a second order magnetic transition (SOMT). The magnetic hysteresis loops are shown in Fig. 4.3. The magnetic hysteresis

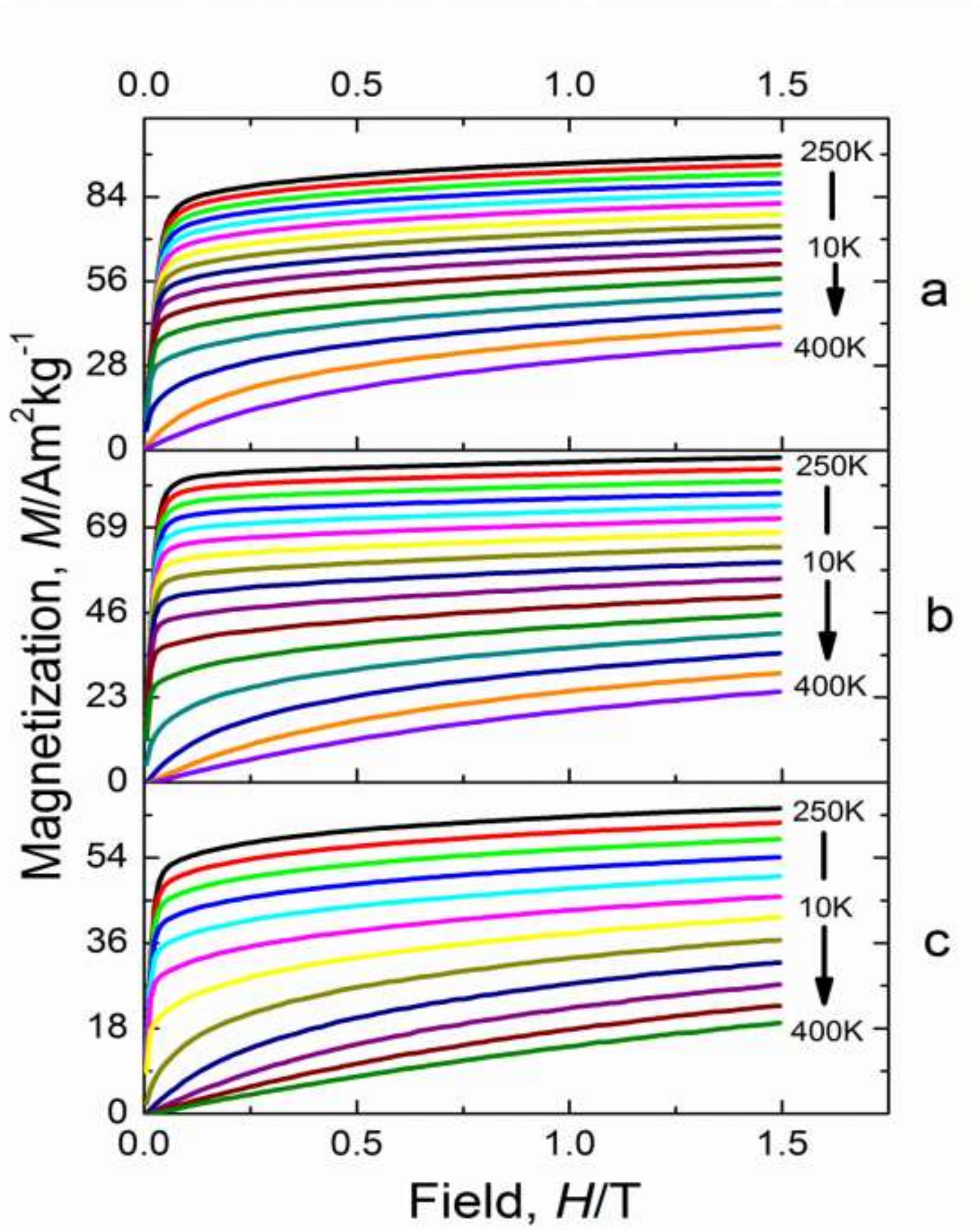

Figure 4. 2 Magnetization curves of three representative samples (a) Fe86Zr6B8, (b) Fe83Zr9B8 and (c) Fe81Zr11B8.

loops were obtained under a magnetic field varying from -0.7 T to +0.7 T in steps of 0.007 T. All the amorphous ribbons exhibited excellent soft magnetic properties since very small hysteresis and nearly zero coercivity were found in each hysteresis loop. Based on the results of the magnetization curves, the temperature dependence of $\left|\Delta S_M\right|$ was calculated according to Eq.(4.2) and the curves are shown in Fig. 4.4, with a maximum value corresponding to the largest entropy change. The broad caret-like shape in each curve also illustrates that the specimens underwent a second order magnetic transition. On the basis of the curves in Fig. 4.4, the peak magnetic entropy

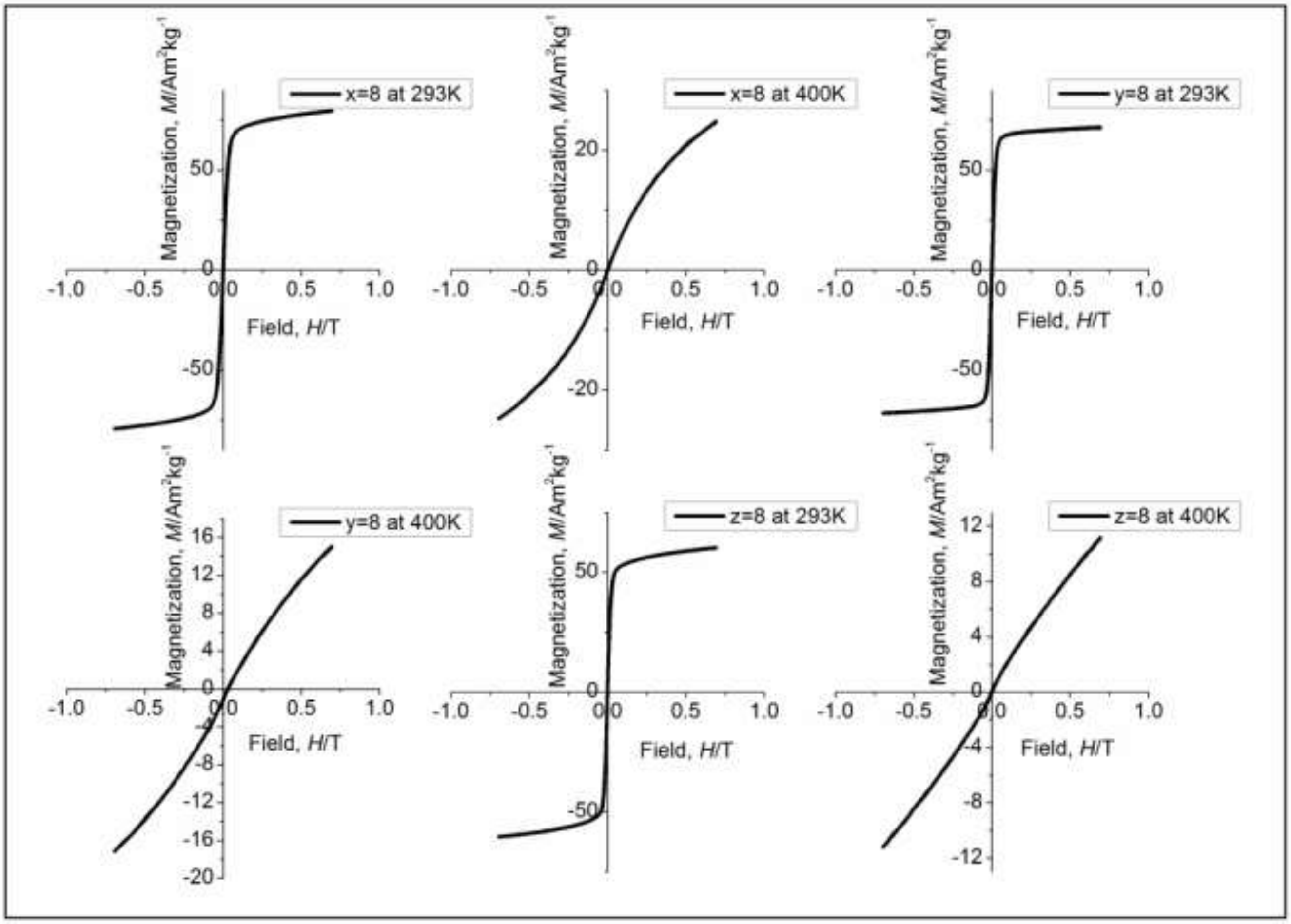

Figure 4. 3 Hysteresis loops of samples (a) Fe86Zr6B8, (b) Fe83Zr9B8 and (c) Fe81Zr11B8 under different temperatures.

change ($\left|\Delta S_M^{peak}\right|$) of each sample can be readily obtained. For comparison, the boron

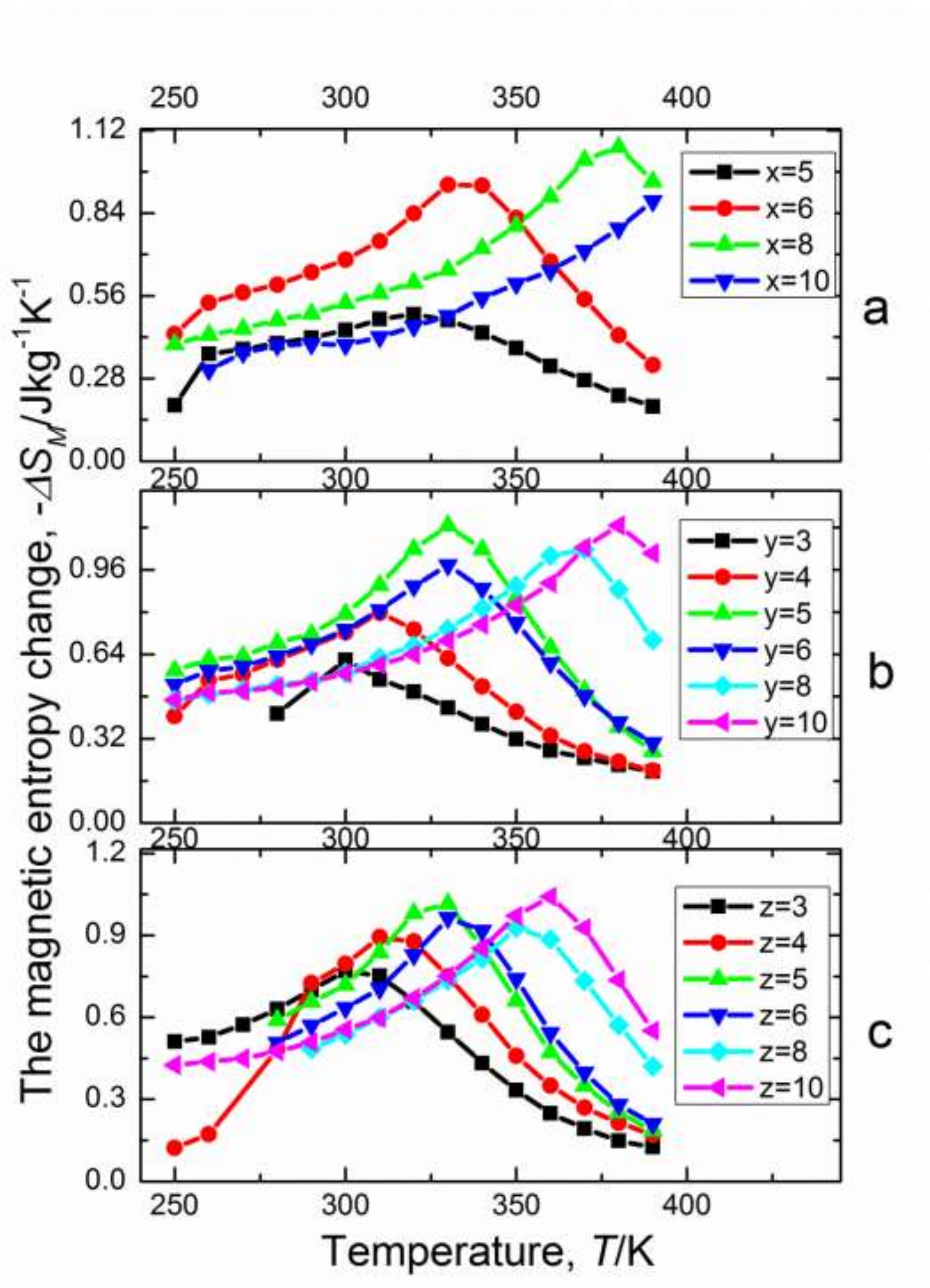

Figure 4. 4 The magnetic entropy change vs. temperature curves of the ribbon samples (a) Fe86Zr6B8, (b) Fe83Zr9B8 and (c) Fe81Zr11B8.

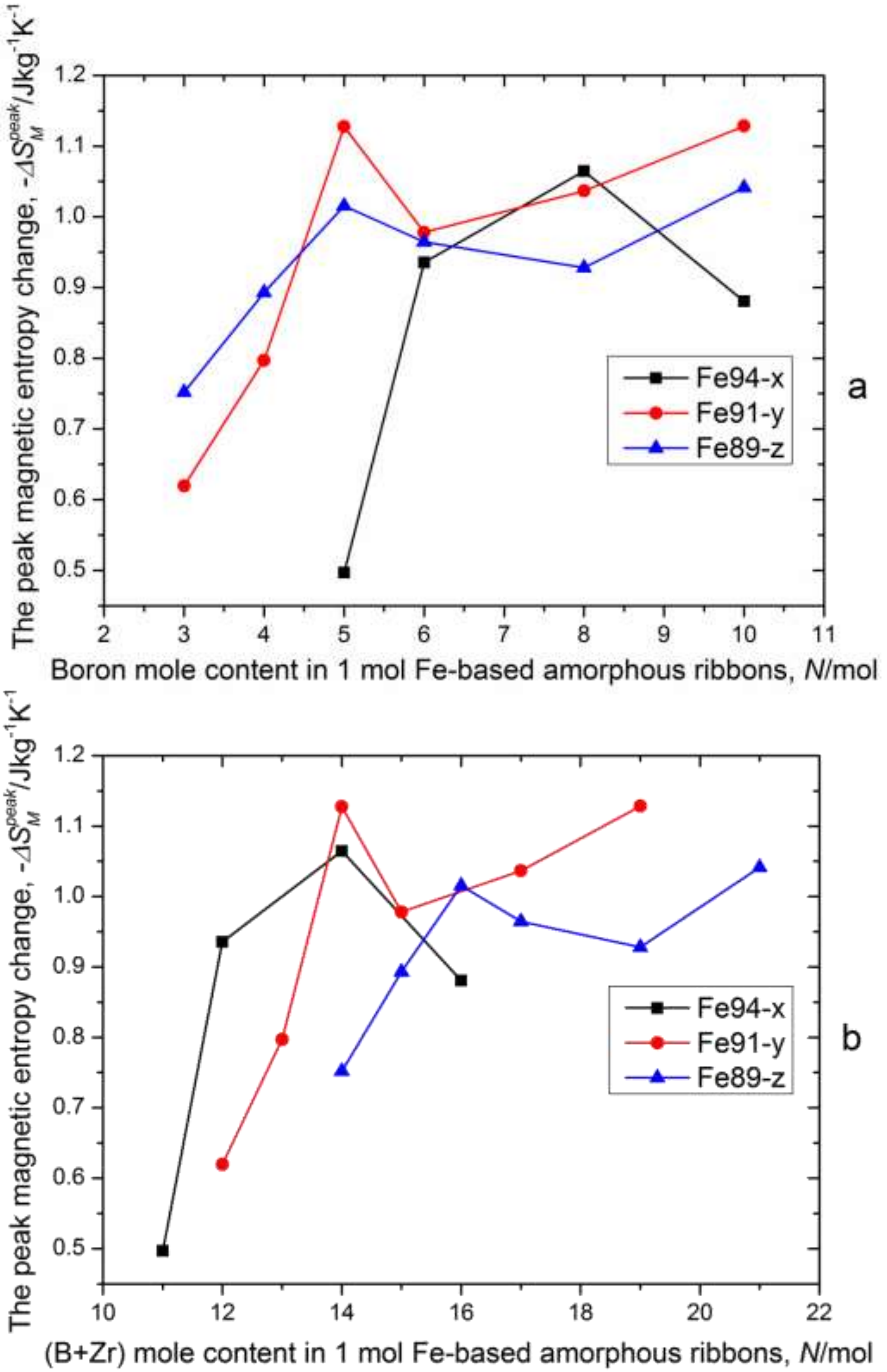

Figure 4. 5 The peak magnetic entropy change vs. the (a) boron and (b) boron + zirconium mole content in 1 mol Fe-based amorphous ribbons curve.

$\left|\Delta S_M^{peak}\right|$ tends to increase as the content of boron increases in all three series

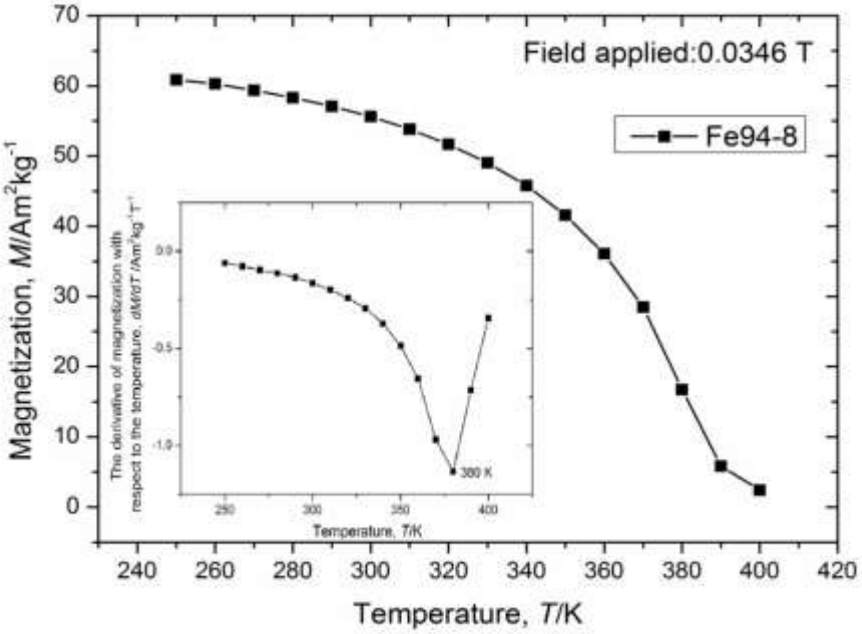
Field applied:0.0346 T
Fe94-8
Magnetization, M/Am²kg⁻¹
Temperature, T/K
70
60
50
40
30
20
10
0
240
260
280
300
320
340
360
380
400
420
The derivative of magnetization with respect to the temperature, dM/dT /Am²kg⁻¹T⁻¹
0.0
-0.5
-1.0
250
300
350
400
Temperature, T/K
380 K

a

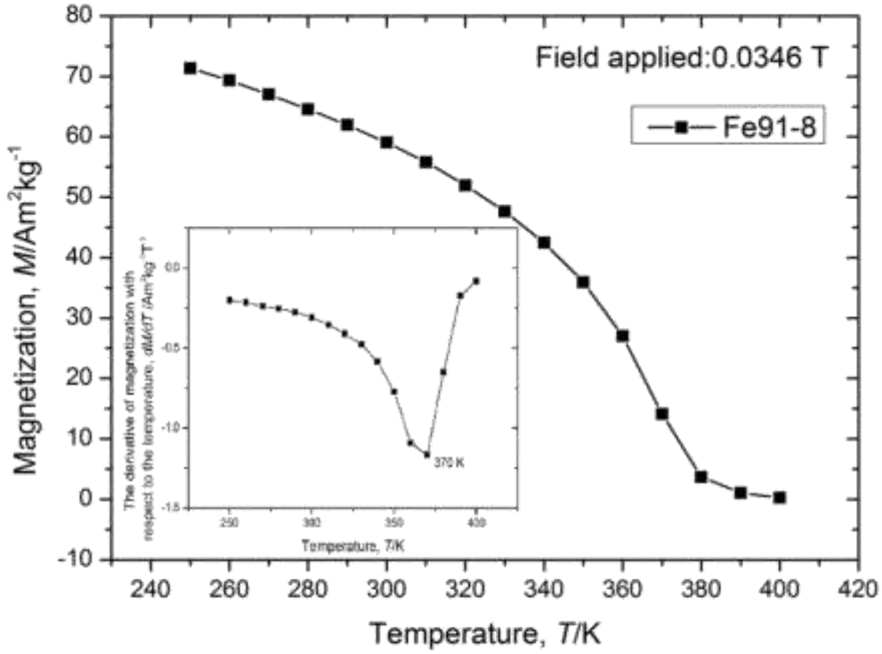
Field applied:0.0346 T
Fe91-8
Magnetization, M/Am²kg⁻¹
Temperature, T/K
80
70
60
50
40
30
20
10
0
-10
240
260
280
300
320
340
360
380
400
420
The derivative of magnetization with respect to the temperature, dM/dT /Am²kg⁻¹T⁻¹
0.0
-0.5
-1.0
-1.5
250
300
350
400
Temperature, T/K
370 K

b

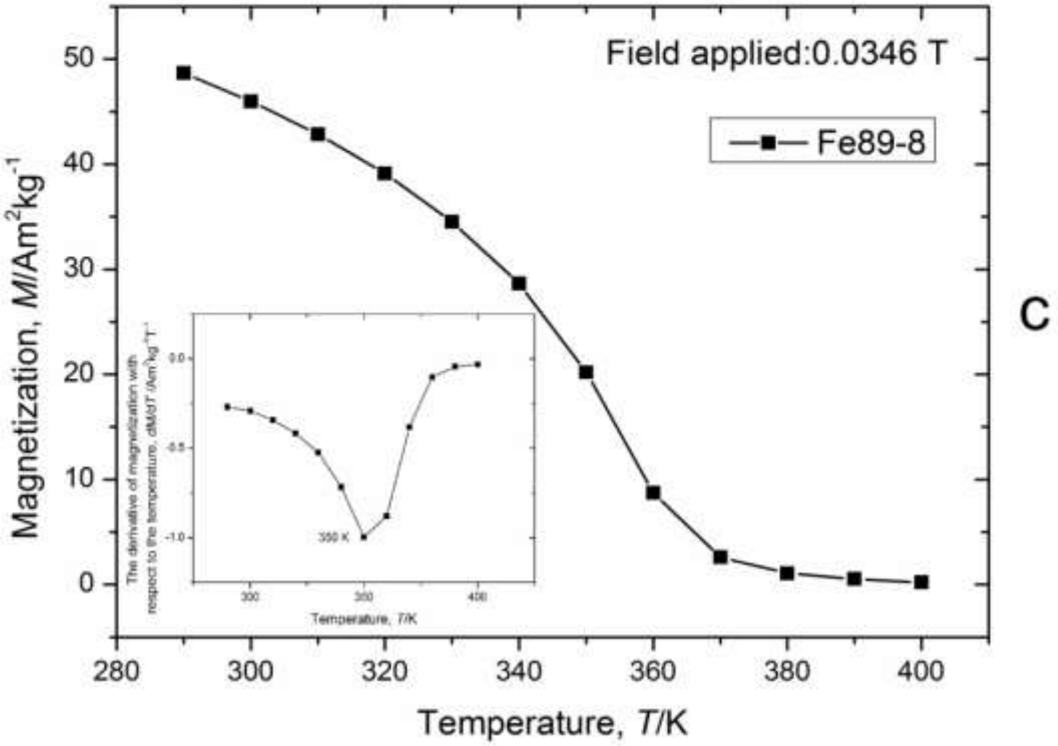

Figure 4. 6 Temperature dependence of magnetization curves of (a) Fe86Zr6B8, (b) Fe83Zr9B8 and (c) Fe81Zr11B8 under the cooling process from 400 K to 250 K at a field of 0.0346 T.

of ribbons. Fig. 4.5b shows the (B + Zr) content dependence of the $\left|\Delta S_M^{peak}\right|$. The $\left|\Delta S_M^{peak}\right|$ of all three series of the Fe-based ribbons occurred for a (B + Zr) content of around 15 at%. To obtain the Curie temperature of each ribbon sample, their temperature-dependent magnetization values were measured in a fixed magnetic field of 0.0346 T with the temperature changing from 400 K to 250 K. For illustration purpose, Fig. 4.6a to Fig. 4.6c shows only three samples, each corresponding to one of the three series. The inset of each figure is the temperature dependence of the derivative of the magnetization with respect to the temperature (*dM/dT*) curve calculated from Fig. 4.6. The temperature where *dM/dT* reaches its minimum value in each inset corresponds to the Curie temperature. Similar to the $\left|\Delta S_M^{peak}\right|$, the boron content dependence of the T_C curves were plotted as solid lines with dots, in Fig. 4.7 for comparison. The dash lines are the results of the linear

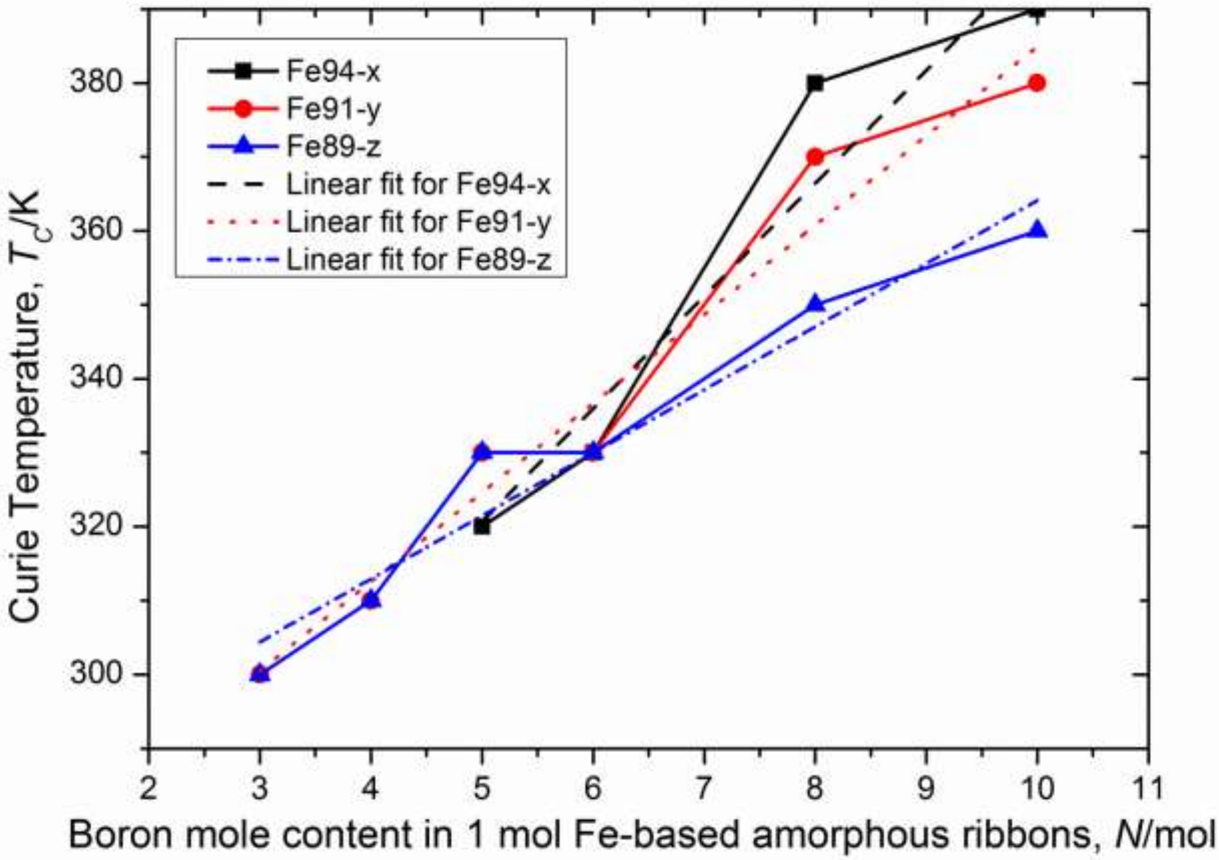

Figure 4. 7 The Curie temperature vs. the boron mole content in 1 mol Fe-based amorphous ribbons curve.

regression. The fitting results for $Fe_{94-x}Zr_6B_x$, $Fe_{91-y}Zr_9B_y$ and $Fe_{89-z}Zr_{11}B_z$ are $T_C = [244 + 15 * (B) \pm 16]K$, $T_C = [264 + 12 * (B) \pm 10]K$ and $T_C = [278 + 8.5 * (B) \pm 4]K$, respectively, where B is the boron mole content in 1 mol alloys. The change of the Curie temperature can be explained by molecular field theory [136]:

$$T_C = J(r) Z_T S(S+1) / 3k_B \tag{4.7}$$

where $J(r)$ represents for the distance-dependence of the inter-atomic exchange integral, Z_T, for coordination about the T site, S is the atomic spin quantum number and k_B is Boltzmann's constant. With increasing addition of boron and a decreasing amount of iron, the distance between the Fe atoms increases, which leads to an increase of $J(r)$. Therefore, T_C increases on the basis of Eq.(4.7). On the other hand, with the substitution of boron for iron, the number of surrounding boron atoms for each iron atom site increases, which leads to an increase of Z_T. As a result, T_C also tends to increase on the basis of Eq.(4.7).

The refrigerant capacity of the amorphous ribbons can be calculated either from Eq. (4.5) or (4.6). The difference between Eq.(4.5) and Eq.(4.6) is that the result of Eq.(4.5) is less and closer to the intrinsic magnetic property of the materials than that of Eq.(4.6). In order to better compare the results, however, the method used for calculating the RC in this work needs to be consistent with that in the literature. In this work, Eq.(4.6) was used for calculation. Comparing the magnetocaloric behavior of the present material with other FeZrB metallic ribbons [37], $\left|\Delta S_M^{peak}\right|$ of $Fe_{91}Zr_7B_2$ is found to be about 90% of that of the present material, $Fe_{86}Zr_9B_5$. Whereas, $\left|\Delta S_M^{peak}\right|$ of $Fe_{88}Zr_8B_4$ is only 78% of that of $Fe_{86}Zr_9B_5$ although T_C of the former (295 K) is slightly closer to room temperature. When comparing with the magnetocaloric behavior of the $Fe_{92-x}Zr_7B_xCu_1$ amorphous ribbons studied before [137], the refrigerant capacities of the present material are higher. For those $Fe_{92-x}Zr_7B_xCu_1$ amorphous ribbons with Curie temperatures lower than 350 K, their refrigerant capacities are less than 48 J/kg under 1.5 T. Whereas, the maximum RC value of the present material under the same condition can be 135.6 J/kg, almost three times as large as 48 J/kg. The magnetocaloric behavior, including the RC results of the as-spun amorphous ribbons, are summarized in Table 4.1, together with the results of some other Gd-based and Fe-based materials reported in the literature, for comparison.

Table 4. 1 The magnetocaloric effect of the magnetic materials studied in this work and reported in the literature

Nominal composition	Structure	Magnetic Field (T)	T_C (K) from the experimental results	T_C (K) from the linear results	δT_{FWHM} (K)	$\left|\Delta S_M^{peak}\right|$ (J kg^{-1}K^{-1})	RC (J kg^{-1})	Ref.
$Fe_{89}Zr_6B_5$	Amorphous	1.5	320	319	110	0.50	55	This work
$Fe_{88}Zr_6B_6$	Amorphous	1.5	330	334	110	0.94	103	This work
$Fe_{86}Zr_6B_8$	Amorphous	1.5	380	364	110	1.06	116.6	This work

$Fe_{84}Zr_6B_{10}$	Amorphous	1.5	390	394	110	0.88	96.8	This work
$Fe_{88}Zr_9B_3$	Amorphous	1.5	300	300	80	0.62	49.6	This work
$Fe_{87}Zr_9B_4$	Amorphous	1.5	310	312	100	0.80	80	This work
$Fe_{86}Zr_9B_5$	Amorphous	1.5	330	324	120	1.13	135.6	This work
$Fe_{85}Zr_9B_6$	Amorphous	1.5	330	336	120	0.98	117.6	This work
$Fe_{83}Zr_9B_8$	Amorphous	1.5	370	360	120	1.04	124.8	This work
$Fe_{81}Zr_9B_{10}$	Amorphous	1.5	380	384	100	1.13	113	This work
$Fe_{86}Zr_{11}B_3$	Amorphous	1.5	300	303.5	100	0.77	77	This work
$Fe_{85}Zr_{11}B_4$	Amorphous	1.5	310	312	80	0.89	71.2	This work
$Fe_{84}Zr_{11}B_5$	Amorphous	1.5	330	320.5	90	1.02	91.8	This work
$Fe_{83}Zr_{11}B_6$	Amorphous	1.5	330	329	90	0.97	87.3	This work
$Fe_{81}Zr_{11}B_8$	Amorphous	1.5	350	346	110	0.93	102.3	This work
$Fe_{79}Zr_{11}B_{10}$	Amorphous	1.5	360	363	110	1.04	114.4	This work
$Fe_{91}Zr_7B_2$	Amorphous	1.5	250	N/A	N/A	1.04	N/A	[37]
$Fe_{88}Zr_8B_4$	Amorphous	1.5	295	N/A	N/A	0.88	N/A	[37]
$Fe_{92-x}Zr_7B_xCu_1$(x<7)	Amorphous	1.5	250~350	N/A	N/A	<1.35	<48	[138]
$Fe_{92-x}Zr_7B_xCu_1$(6<x<24)	Amorphous	1.5	350~530	N/A	N/A	1.35~1.7	48~90	[138]

$Fe_{80}Cr_4B_{10}Zr_5Gd_1$	Amorphous	1.5	360	N/A	120	0.91	110	[139]
$Fe_{75}Nb_{10}B_{15}$	Amorphous	1.5	250	N/A	190	0.60	115	[140]
$Fe_{79}Nb_7B_{14}$	Amorphous	1.5	372	N/A	N/A	1.07	N/A	[141]
$(Fe_{70}Ni_{30})_{89}Zr_7B_4$	Amorphous	1.5	342	N/A	N/A	0.70	N/A	[134]
$Fe_{64}Mn_{14}CoSi_{10}B_{11}$	Amorphous	1.5	457	N/A	N/A	0.83	N/A	[40]
$Fe_{72}Ni_{28}$	Amorphous	1.5	333	N/A	149	0.49	73	[142]
$(Fe_{85}Co_{15})_{75}Nb_{10}B_{15}$	Amorphous	1.5	440	N/A	124	0.82	102	[143]
$Gd_{55}Al_5Fe_{40}$	Amorphous	5.0	222	N/A	197	2.7	532	[100]
$Gd_{60}Fe_{20}Co_{10}Al_{10}$	Amorphous	5.0	222	N/A	167	4.4	736	[102]
$Gd_5Si_2Ge_2$	Crystalline	5.0	276	N/A	16.5	18.5	305	[17]

Clearly, the magnetocaloric effect has a lot to do with the maximum applied magnetic field. As a result, to make the comparison of the MCE between different materials meaningful and accurate, the comparison should be carried out in the same conditions. In such a case, the following relation:

$$|\Delta S_M(T,H)| = \mathrm{c}(T)H^n \tag{4.8}$$

is applied [23, 135], where *n* is an exponent which is a reflection of the material's intrinsic property. According to Eq.(4.8), the value of *n* can be calculated by

$$n = d\ln|\Delta S_M| / d\ln H \quad . \tag{4.9}$$

The curves in Fig. 4.8 show the temperature dependence of the *n* value of the $Fe_{86}Zr_9B_5$ sample under magnetic fields of 1.0 T and 1.5 T respectively. It can be seen that the *n* value is about 0.75 at the Curie temperature (330 K). On the basis of the *n* value and Eq.(4.8), the magnetic entropy change of $Fe_{86}Zr_9B_5$ under different magnetic fields can be readily calculated. When the maximum field reaches 5 T, the peak magnetic entropy change of $Fe_{86}Zr_9B_5$ increases to 2.76 J/kgK which is larger than those of $Fe_{77}Gd_3Cr_8B_{12}$ (2.31 J/kgK) and $Fe_{75}Gd_5Cr_8B_{12}$ (2.34 J/kgK) under 5 T

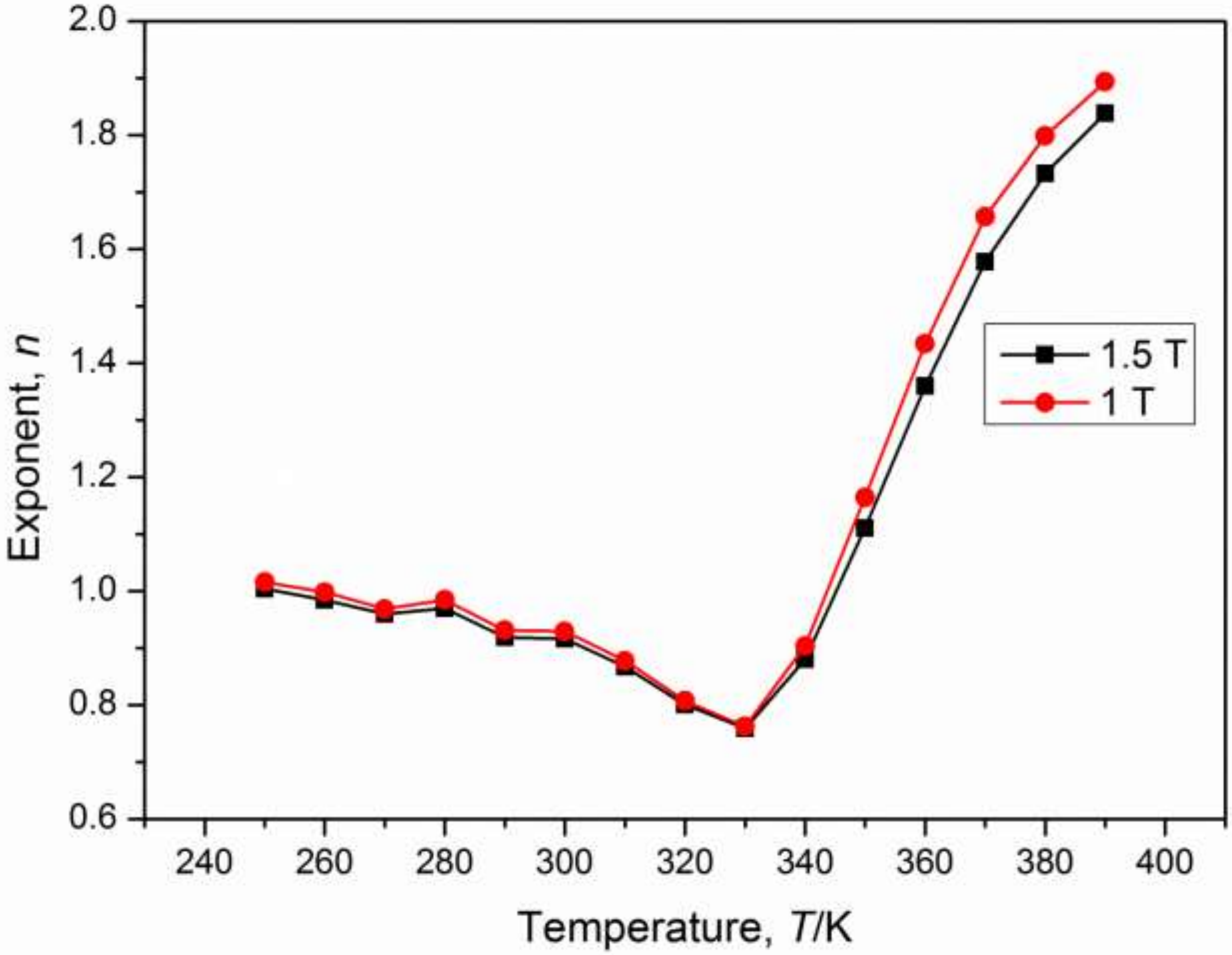

Figure 4. 8 Temperature dependence of the exponent n for ribbon sample Fe86Zr9B5 at two different maximum applied magnetic fields.

[103]. Based on this $\left|\Delta S_M^{peak}\right|$ value, the RC of $Fe_{86}Zr_9B_5$ becomes 331 J/kg on the assumption that δT_{FWHM} remains the same as that under 1.5 T. The reality is, however, with the increase of the maximum applied magnetic field, δT_{FWHM} will be larger. According to the results of Franco [106], the field dependence of RC value can be summarized as:

$$RC \propto H^{1+1/\delta}\,. \tag{4.10}$$

where δ can be obtained from the field dependence of the magnetization at the Curie temperature [106]:

$$M \propto H^{1/\delta}\,. \tag{4.11}$$

On the basis of the magnetization curves of the $Fe_{86}Zr_9B_5$ amorphous ribbon, the value of δ can be obtained by fitting the M-H curve, as below:

$$M = 44.1298 \times H^{0.2101}, \tag{4.12}$$

where the δ value is 4.760. According to Eq.(4.10), RC value of $Fe_{86}Zr_9B_5$ is therefore obtained is 582.10 J/kg when $H_{\max}$ changes from 1.5 T to 5 T. The result makes sense since $Gd_5Si_2Ge_2$, a well-known magnetic material, exhibits a RC value of just 305 J/kg under 5 T, which is only about half value of that of $Fe_{86}Zr_9B_5$, as listed in Table 4.1 [17]. In general, the $\left|\Delta S_M^{peak}\right|$ of the Fe-based magnetic materials is smaller than that of Gd-based magnetic materials, as can be seen in Table 4.1, however, the rather lower fabrication cost of Fe-based materials than those of Gd-based ones plays an important role in industrialization. In addition, due to the compensation of the large δT_{FWHM} , the RC values of the Fe-based and the Gd-based magnetic materials are comparable. In addition, with the Curie temperatures being closer to room temperature, the Fe-based materials have more potential for room temperature applications.

4.3 Conclusions

In this chapter, three new Fe-based series of glassy ribbons were designed and successfully fabricated. The magnetocaloric effect of those Fe-based amorphous ribbons was extensively studied. The results indicate that a small replacement of boron with iron could obviously change both the Curie temperature and the peak magnetic entropy change. By increasing the amount of boron, all specimens in the three series of ribbons tend to exhibit larger peak magnetic entropy changes as well as Curie temperatures. In order to apply this kind of material into room temperature refrigeration, not only the peak magnetic entropy change and the refrigerant capacity but also the Curie temperature should be taken into consideration. In this work, $Fe_{86}Zr_9B_5$ exhibits a $\left|\Delta S_M^{peak}\right|$ value of 1.13 J/kgK at 330 K and a RC value of 135.6 J/kg. Although its $\left|\Delta S_M^{peak}\right|$ is not the largest among all the specimens, it is the most appropriate candidate for room temperature applications due to the fact that both its

$\left|\Delta S_M^{peak}\right|$ and RC are relatively larger than those of other materials and its T_C is relatively closer to room temperature.

Chapter 5 Investigations on the influence of the minor additions on the MCE of the FeZrB amorphous alloy systems

5.1 The effect of Cr Minor Addition on the MCE of FeZrB amorphous alloys

5.1.1 Introduction

In chapter 4, a thorough study of the MCE of FeZrB ternary amorphous ribbons is reported. It can be seen that there is still much space for improvement before the realization of the magnetic refrigeration at room temperature with the Fe-based amorphous materials used as the magnetic refrigerants. In this chapter, research has been carried out to enhance the MCE of a Fe-based metallic glass by the addition of Cr.

5.1.2 Results and discussion

Ingots of nominal composition $Fe_{84-x}Cr_xB_{10}Zr_5Gd_1$ (x=0, 2, 4, 6, 8) were prepared in a copper mold casting machine. Ribbons, 0.05 mm thick and 1.5 mm wide, were fabricated by means of a melt spinning machine. The amorphous state of the as-quenched ribbons was characterized by X-ray diffraction (XRD) with Cu-Kα radiation. The magnetic hysteresis loops were measured to confirm the soft magnetic properties of the ribbon samples. The measurements were carried out using a Lakeshore 7407 vibrating sample magnetometer (VSM) under a magnetic field from -0.7 T to +0.7 T with 0.007T per steps, both below and above the Curie temperature

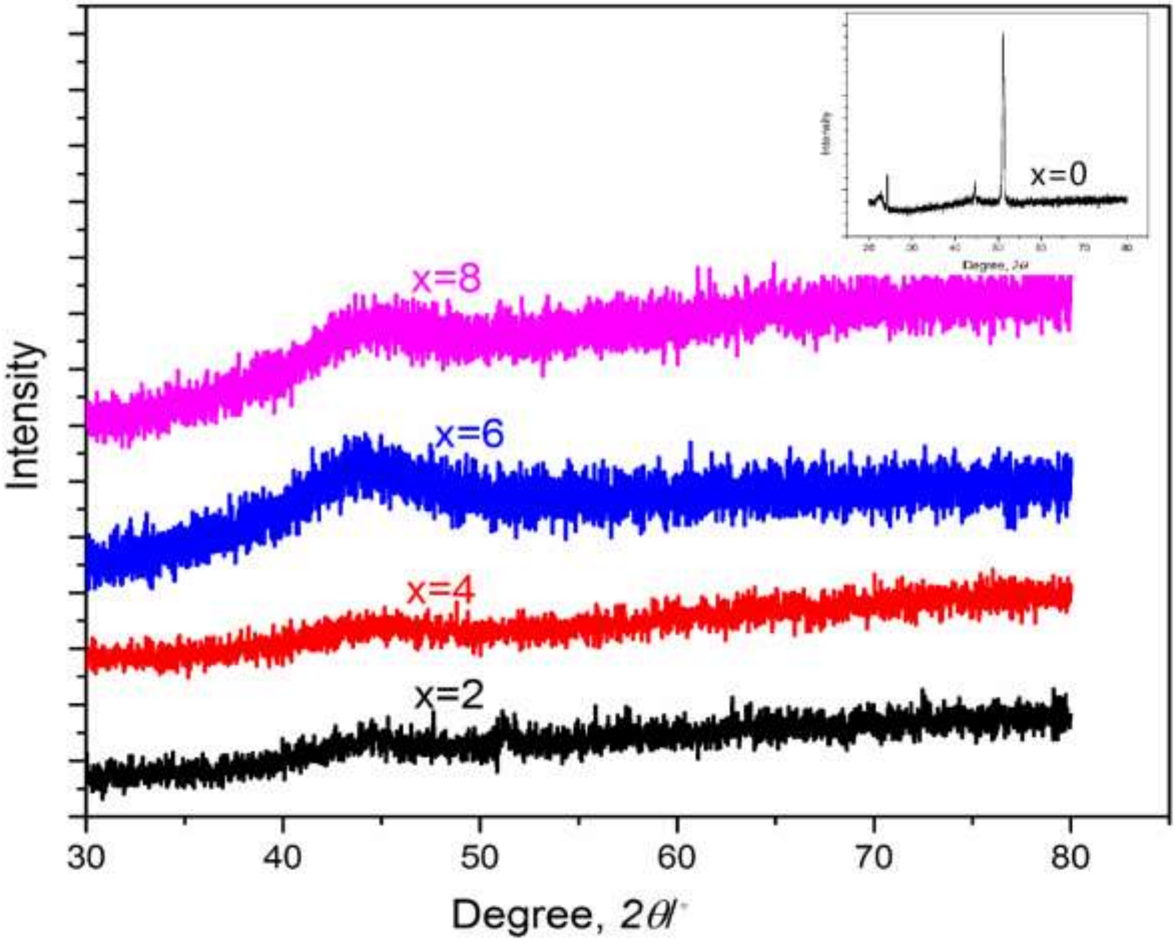

Figure 5. 1 The XRD results of $Fe_{84-x}Cr_xB_{10}Zr_5Gd_1$ (x = 0, 2, 4, 6, 8)

of the ribbon samples. The magnetocaloric effect of the amorphous ribbons was measured with VSM under a maximum applied magnetic field of 1.5 T with 0.005 T per steps at each constant temperature from 290 K to 430 K with 10 K per steps. The calculation methods were similar with those in Chapter 4.

The XRD patterns of $Fe_{84-x}Cr_xB_{10}Zr_5Gd_1$ (x=0, 2, 4, 6, 8) ribbons are shown in Fig. 5.1.

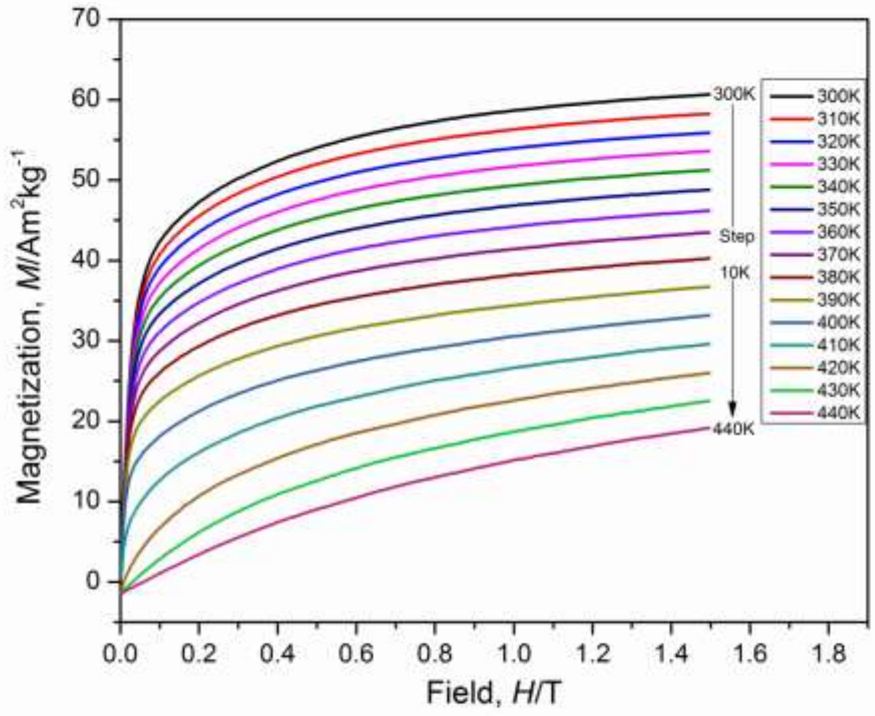

Figure 5. 2 Magnetization curves of sample $Fe_{82}Cr_2B_{10}Zr_5Gd_1$ from 300K to 440 K.

As shown in the insert of Fig. 5.1, there are obvious sharp peaks in the XRD pattern of the $Fe_{84}B_{10}Zr_5Gd_1$ (x=0) ribbon, suggesting that the structure of the sample is crystalline. For the XRD patterns of the x=2, 4, 6 and 8 ribbons, a broad wave pack exists around $2\theta = 45^\circ$ in each curve, which confirms the amorphous state of the ribbons. The microstructural difference between the x=0 sample and the rest is in good agreement with the basic empirical rules of Inoue for the formation of amorphous alloys [3]: with the addition of Cr in the system, the number of components increases. Consequently, the glass forming ability (GFA) of those metallic ribbons increases which makes the amorphous alloy formation easier. The

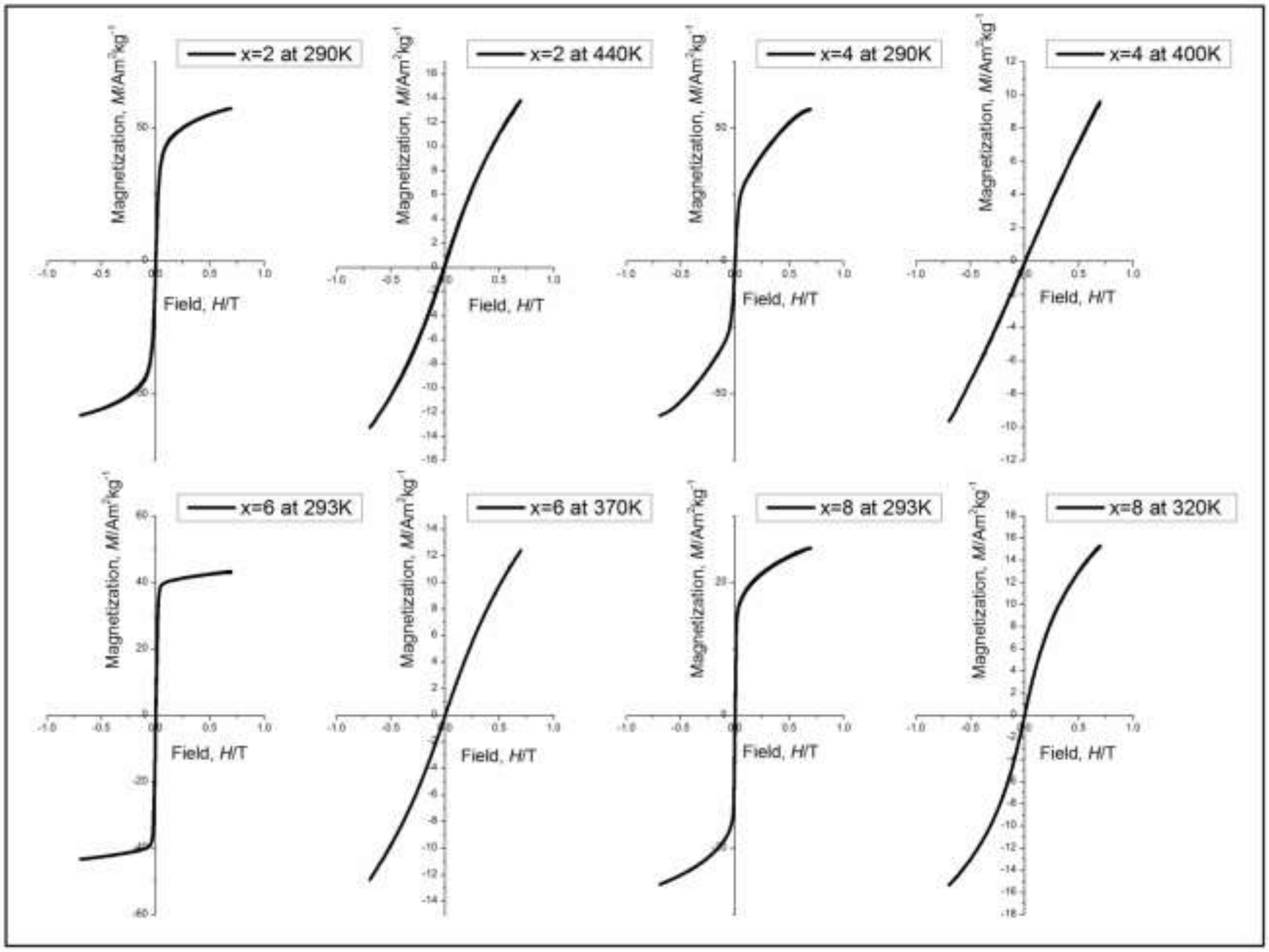

Figure 5. 3 Hysteresis loops of samples $Fe_{84-x}Cr_xB_{10}Zr_5Gd_1$ (x = 2, 4, 6 and 8) under different temperatures

magnetic properties of the ribbon samples with x=2, 4, 6, 8 were characterized. For each ribbon sample, magnetization curves were measured from low temperature to high temperature for further calculation of their MCE. For illustration purposes, the typical magnetization curves of the x=2 sample is shown in Fig. 5.2. It shows that the saturation magnetization decreases with increase of temperature. In addition, the shape of the curves changes as temperature changes, which indicates the phase transition of all the ribbon samples are second order. Fig. 5.3 shows the magnetic hysteresis loops of the ribbons at different temperatures. The magnetic hysteresis tests were carried out under a magnetic field ranging from -0.7 T to +0.7 T, in 0.007T steps. For each sample, the magnetic hysteresis loops were investigated at

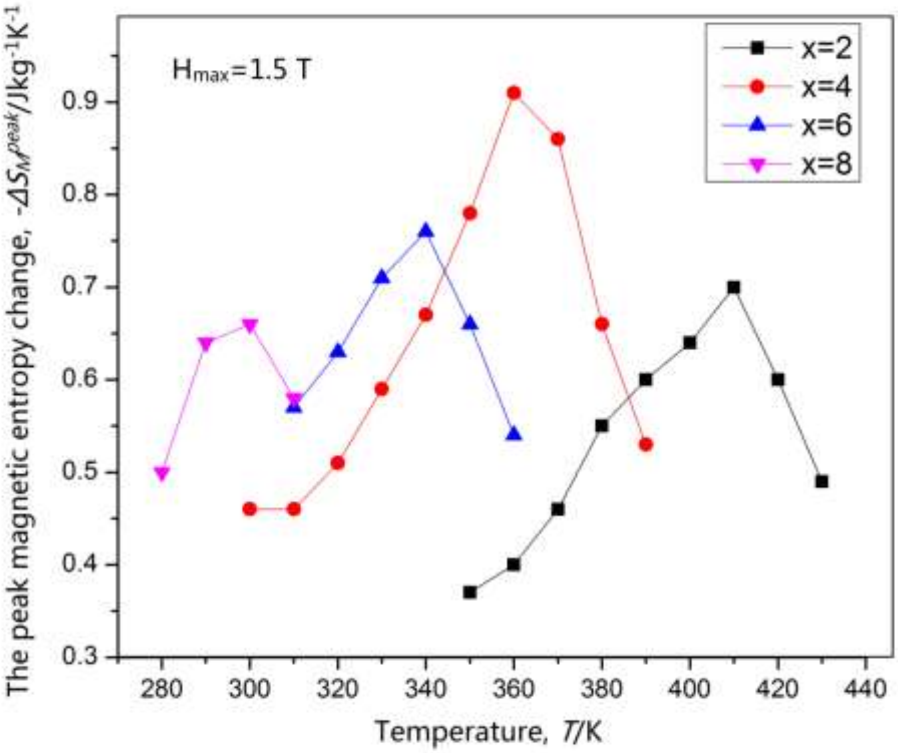

Figure 5. 4 The magnetic entropy change vs. temperature curves of the ribbon samples $Fe_{84-x}Cr_xB_{10}Zr_5Gd_1$ (x = 2, 4, 6 and 8)

temperatures both before and after the phase transition temperature, as can be seen in Fig. 5.2. All the hysteresis loops in Fig. 5.3 show small hysteresis and nearly zero coercivity, which indicates the excellent soft magnetic properties of the amorphous ribbons during their working temperature ranges. Additionally, the saturation magnetization around room temperature has a peak value when the Cr content is 4 mol in 1 mol Fe-based amorphous ribbons. On the basis of the experimental magnetization curves and Eq.(4.2), the $|\Delta S_M|$ vs. T curves were constructed as shown in Fig. 5.4. Each of the curves is shown to have a broad caret-like shape,

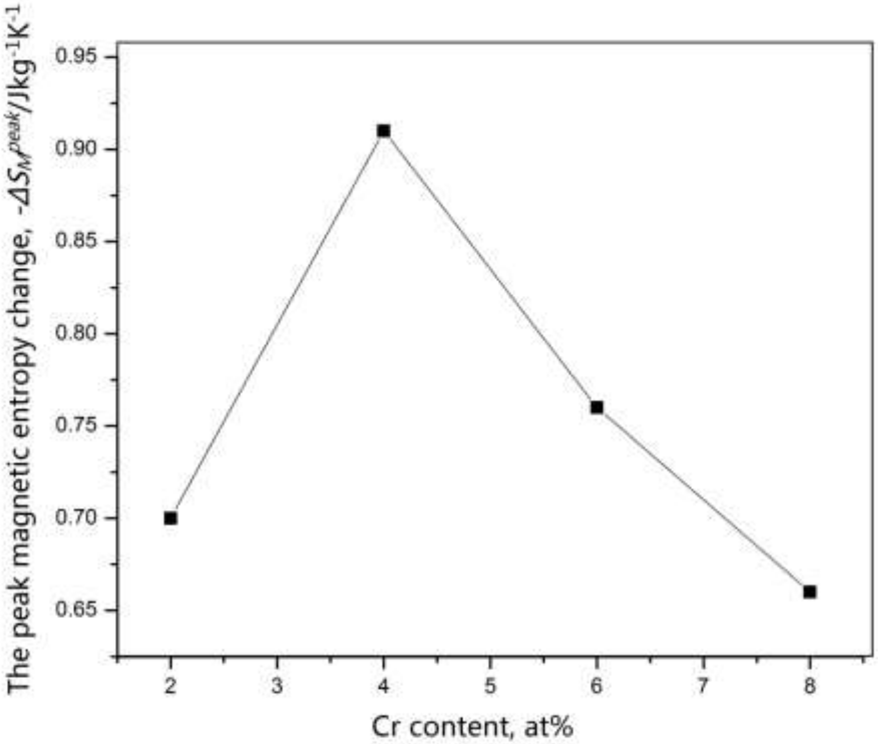

Figure 5. 5 The peak magnetic entropy change vs. the Cr mole content (from 2 mol to 8 mol) in 1 mol Fe-based amorphous ribbons curve

illustrating the second order phase transition. The peak magnetic entropy change ($\left|\Delta S_M^{peak}\right|$) of each sample can also be readily obtained from the curves in Fig. 5.4. To compare the $\left|\Delta S_M^{peak}\right|$ of different metallic ribbons, a compositional dependence (which is actually the mole content of Cr) of the $\left|\Delta S_M^{peak}\right|$ curve was plotted as shown in Fig. 5.5. It reveals that the $\left|\Delta S_M^{peak}\right|$ value first increases and then decreases, when the Cr content increase from 2 mol to 8 mol. The peak value of $\left|\Delta S_M^{peak}\right|$ appears when

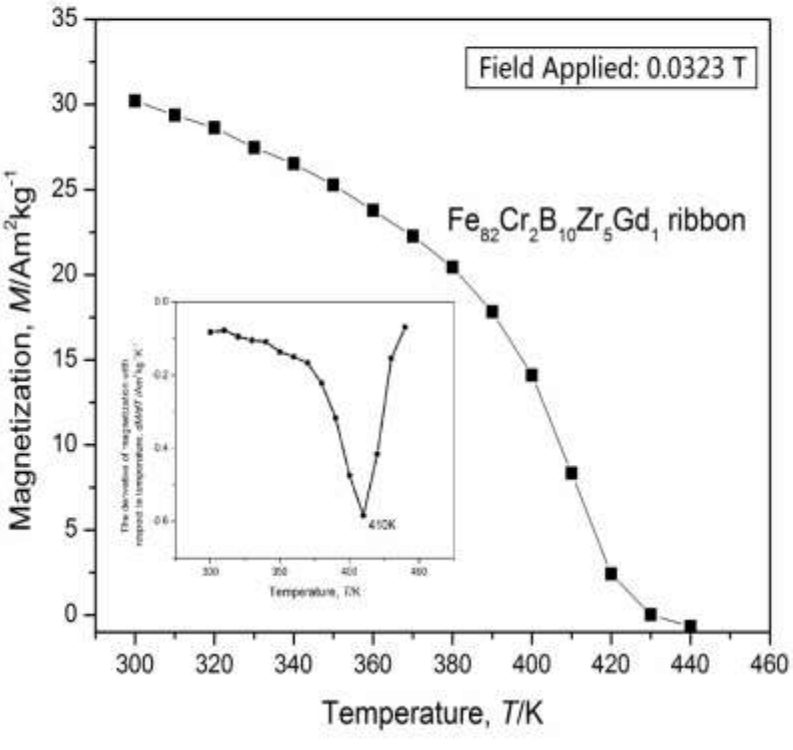

Figure 5. 6 Temperature dependence of magnetization curve of $Fe_{82}Cr_2B_{10}Zr_5Gd_1$ under the cooling process from 440K to 300K at a field of 0.0323 T

the Cr content is 4 mol ($\left|\Delta S_M^{peak}\right|$=0.91 J/kgK). The change of $\left|\Delta S_M^{peak}\right|$ is very similar to the result reported by Caballero-Flores [135]. In his work, the influence of Co and Ni addition on the $Fe_{88-2x}Co_xNi_xZr_7B_4Cu_1$ was studied. The simultaneous addition of Co and Ni makes $\left|\Delta S_M^{peak}\right|$ firstly increase and then decrease as x increases from 0 to 11, in steps of 2.75. Since the magnetic entropy change always peaks around the Curie temperature, the Curie temperature of each ribbon sample can be roughly obtained from Fig. 5.4. To obtain the Curie temperature more precisely, temperature dependence of the magnetization curves were obtained during a cooling process and

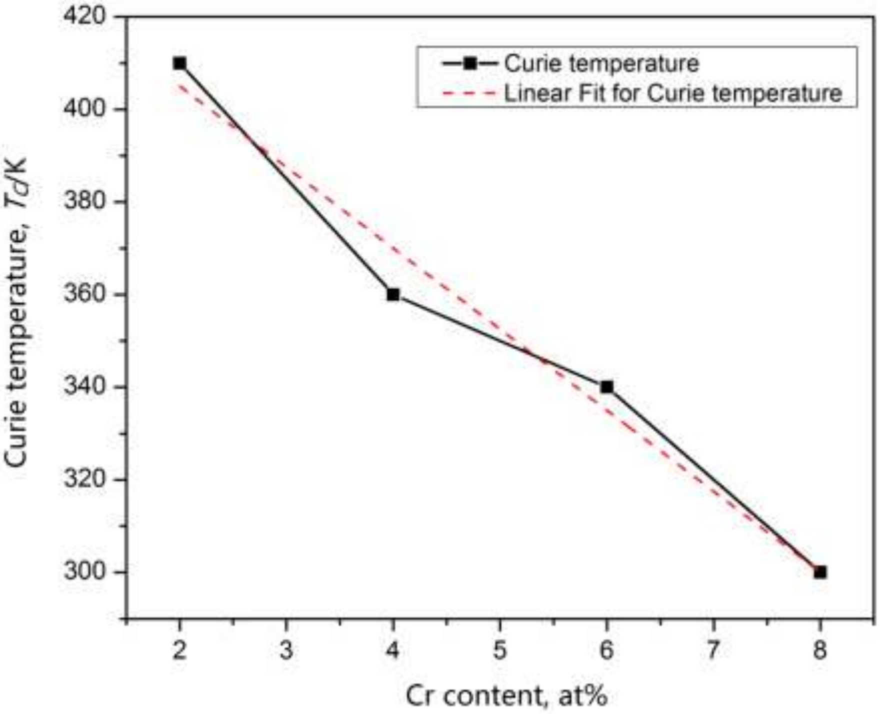

Figure 5. 7 The Curie temperature vs. the Cr mole content (from 2 mol to 8 mol) in 1 mol Fe-based amorphous ribbons curve

a typical curve for $Fe_{72}Cr_2B_{10}Zr_5Gd_1$ was plotted as shown in Fig. 5.6 for illustration purpose. Fig. 5.6 was obtained under the cooling process from 440 K to 300 K at a field of 0.0323 T. The inset is the temperature dependence of the derivative of the magnetization with respect to temperature (dM/dT) curve calculated from Fig. 5.6. The Curie temperature corresponds to the temperature where the value of dM/dT was minimum, which is 410K. Fig. 5.7 shows the experimental T_C vs. the mole content of Cr in 1 mol Fe-based amorphous ribbons curve indicated by the dark line with square dots. Differing from the change of $\left|\Delta S_M^{peak}\right|$, it can be seen that T_C decreases nearly linearly when the Cr content increases from 2 mol to 8 mol (from 410 K to 300 K). The red dash line is the linear regression line with a slope of -17.5 K per Cr content ($T_C = [440 - 17.5 * (Cr) \pm 10]K$, where Cr represents for the Cr mole content in 1 mol Fe-based amorphous ribbons). This behavior can be explained by the negative exchange coupling between the Fe atoms with the newly introduced Cr atoms, which may be similar to the occurrence in some FeCr-based crystals [144]. The addition of Cr atoms brings a decrease in the distance between the Fe atoms, which

Table 5.1 The magnetocaloric effect of the magnetic materials studied in this work and reported in the literature

Nominal composition	Structure	Magnetic Field (T)	T_C (K) from the experimental results	T_C (K) from the linear results	δT_{FWHM} (K)	$\left\|\Delta S_M^{peak}\right\|$ ($J\ kg^{-1}K^{-1}$)	RC ($J\ kg^{-1}$)	Ref.

$Fe_{82}Cr_2B_{10}Zr_5Gd_1$	Amorphous	1.5	410	405	120	0.70	84	This work
$Fe_{80}Cr_4B_{10}Zr_5Gd_1$	Amorphous	1.5	360	370	120	0.91	110	This work
$Fe_{78}Cr_6B_{10}Zr_5Gd_1$	Amorphous	1.5	340	335	110	0.76	83	This work
$Fe_{76}Cr_8B_{10}Zr_5Gd_1$	Amorphous	1.5	300	300	110	0.66	73	This work
$Fe_{75}Nb_{10}B_{15}$	Amorphous	1.5	250	N/A	190	0.60	115	[140]
$(Fe_{70}Ni_{30})_{89}Zr_7B_4$	Amorphous	1.5	342	N/A	N/A	0.70	N/A	[134]
$Fe_{64}Mn_{14}CoSi_{10}B_{11}$	Amorphous	1.5	457	N/A	N/A	0.83	N/A	[40]
$Fe_{72}Ni_{28}$	Amorphous	1.5	333	N/A	149	0.49	73	[142]
$(Fe_{85}Co_{15})_{75}Nb_{10}B_{15}$	Amorphous	1.5	440	N/A	124	0.82	102	[143]
$Gd_{55}Al_5Fe_{40}$	Amorphous	5.0	222	N/A	197	2.7	532	[100]
$Gd_{60}Fe_{20}Co_{10}Al_{10}$	Amorphous	5.0	222	N/A	167	4.4	736	[102]
$Gd_5Si_2Ge_2$	Crystalline	5.0	276	N/A	16.5	18.5	305	[17]

results in antiferromagnetic interactions. Therefore, the Curie temperature decreases. With regard to the refrigerant capacity of each metallic ribbon, it can be obtained from Eqs. (4.5) or (4.6). In this work, Eq.(4.6) was used to calculate the RC in order to make it more meaningful when compared with the results in the literature. The calculated RC results are listed in Table 5.1, together with the RC values of some other Fe-based materials as well as Gd-based metallic glasses reported in the literature. From the temperature dependence of the magnetic entropy change curves in Fig. 5.4, it is found that all the curves are relatively broad (large δT_{FWHM}), revealing that each ribbon has a wide working temperature range. This may compensate the effect of low peak magnetic entropy changes of Fe-based metallic glasses as compared to Gd-based materials when determining RC, as shown in Table 5.1. From Table 5.1, it can be seen that both the $\left|\Delta S_M^{peak}\right|$ and RC of the $Fe_{84-x}Cr_xB_{10}Zr_5Gd_1$ (x=2, 4, 6, 8) metallic ribbons are almost of the same order or even larger than the values of other reported Fe-based metallic alloys. Among the ribbons studied in this work, $Fe_{80}Cr_4B_{10}Zr_5Gd_1$ had the highest $\left|\Delta S_M^{peak}\right|$ (0.91 J/kgK) with a δT_{FWHM} value of 120 K and an RC value of 110 J/kg. Although both values of δT_{FWHM} and RC are of same order as those of other reported Fe-based metallic alloys, the $\left|\Delta S_M^{peak}\right|$ is 51.6% larger than that of $Fe_{75}Nb_{10}B_{15}$, 30.0% larger than that of $(Fe_{70}Ni_{30})_{89}Zr_7B_4$, 9.6% larger than that of $Fe_{64}Mn_{14}CoSi_{10}B_{11}$, 85.7% larger than that of $Fe_{72}Ni_{28}$ and 11.0% larger than that of $(Fe_{85}Co_{15})_{75}Nb_{10}B_{15}$. On the basis of the comparison of δT_{FWHM} , RC values as well as $\left|\Delta S_M^{peak}\right|$, it can be concluded that $Fe_{82}Cr_4B_{10}Zr_5Gd_1$ is a promising MCE material.

Since the RC is influenced by the maximum magnetic field, comparison of the RC should be carried out under the same maximum applied magnetic fields. In order to better compare the MCE with other reported results measured under different maximum applied magnetic fields, the following expression,

$$\left|\Delta S_M(T,H)\right| = c(T)H^n , \tag{5.1}$$

is applied, where *c(T)* is a constant [23, 135]. According to this equation and the data from the magnetization curves, the exponent, n , for the x=4 sample can be obtained from:

$$n = d\ln\left|\Delta S_M\right| / d\ln H . \tag{5.2}$$

Fig. 5.8 shows the temperature dependence of the exponent, n , for the x=4 sample under different applied fields, based on data collected under 0.5 T, 1 T and 1.5 T. The curves in Fig. 5.8 show that n is about 0.88 at T_C (360K). Based on Eq.(5.1)

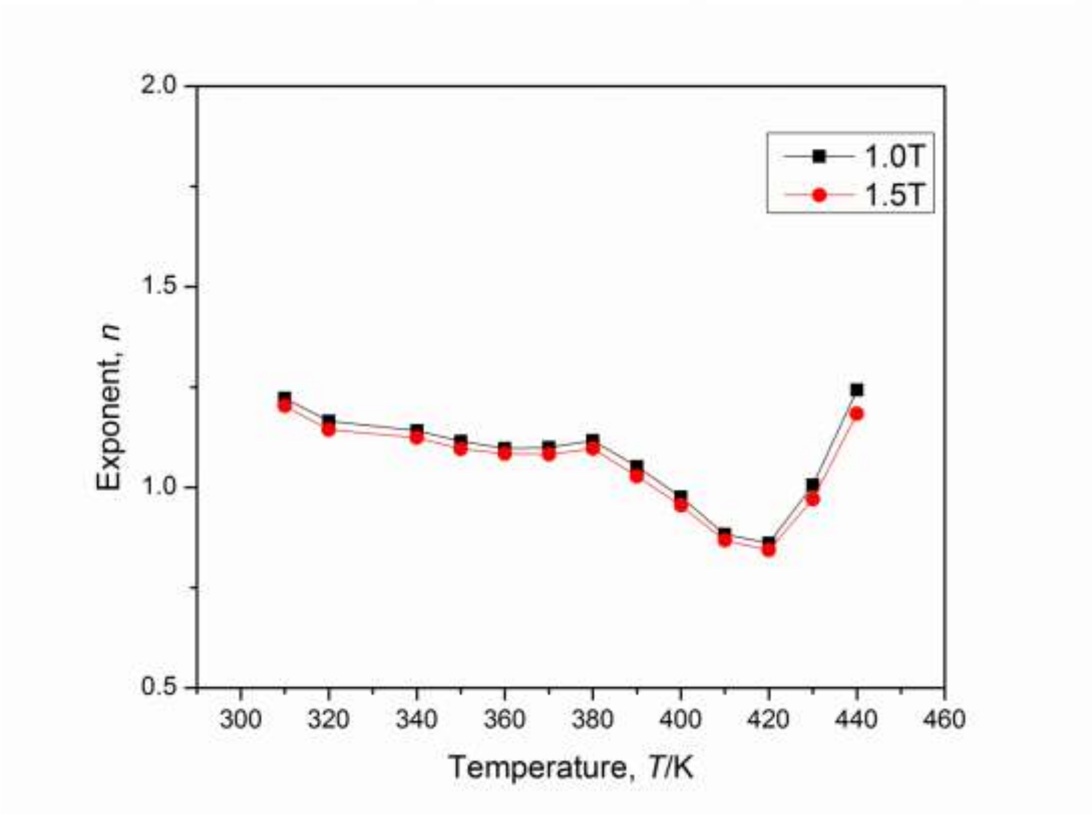

Figure 5. 8 Temperature dependence of the exponent for ribbon sample $Fe_{82}Cr_2B_{10}Zr_5Gd_1$ at two different maximum applied magnetic fields

and this n value, the $\left|\Delta S_M^{peak}\right|$ value of $Fe_{80}Cr_4B_{10}Zr_5Gd_1$ becomes 2.63 J/kgK, when the maximum applied magnetic field increases to 5 T. It is larger than that of both $Fe_{77}Gd_3Cr_8B_{12}$ (2.31 J/kgK) and $Fe_{75}Gd_5Cr_8B_{12}$ (2.34 J/kgK) under 5 T [103]. Based on this $\left|\Delta S_M^{peak}\right|$ value, the RC of $Fe_{80}Cr_4B_{10}Zr_5Gd_1$ becomes 315 J/kg if δT_{FWHM} is assumed to be the same as that at 1.5 T. It is worth mentioning that δT_{FWHM} will also increase when the maximum applied magnetic field increases. The RC of $Fe_{80}Cr_4B_{10}Zr_5Gd_1$, therefore, will be much larger than 315 J/kg when H increases from 1.5 T to 5 T. This is very attractive as the well-known magnetic material, $Gd_5Si_2Ge_2$ only has a refrigerant capacity of 305 J/kg under 5 T, as shown in Table 5.1 [17]. Although it can be seen in Table 5.1 that the $\left|\Delta S_M^{peak}\right|$ of Fe-based magnetic materials is smaller than that of Gd-based magnetic materials, the cost of Fe-based materials is much lower than that of Gd-based materials, which is of great importance for mass production. Besides, the large δT_{FWHM} makes the RC of the Fe-based magnetic materials comparable to that of the Gd-based ones, and the Curie temperatures of Fe-based materials are more suitable for room temperature applications. Moreover, the magnetocaloric effect of Fe-based materials can be optimized by adjusting the composition on the basis of this work.

5.1.3 Conclusions

In this study, new Fe-based amorphous ribbons $Fe_{84-x}Cr_xB_{10}Zr_5Gd_1$ (x=2, 4, 6, 8) were successfully fabricated and their magnetocaloric effect was investigated. The results show that a small addition of Cr can affect both the peak magnetic entropy change and the Curie temperature of the Fe-based metallic ribbons. With increasing amounts of Cr, the $\left|\Delta S_M^{peak}\right|$ can achieve a peak value and T_C decreases nearly linearly. The results show that the $Fe_{80}Cr_4B_{10}Zr_5Gd_1$ metallic glass achieves values of $\left|\Delta S_M^{peak}\right|$ 0.91 J/kgK and RC 110 J/kg at a T_C of 360 K. They are the highest $\left|\Delta S_M^{peak}\right|$ and the highest refrigeration capacity values near room temperature among all the Fe-based metallic glasses reported in the literature. Since both the peak magnetic entropy change and the Curie temperature are important factors for MCE materials, the $Fe_{80}Cr_4B_{10}Zr_5Gd_1$ metallic glass is shown to be a very promising MCE Fe-based material, and should be further investigated in regard to its MCE for wider commercial applications.

5.2 The effect of Other Elements Minor Addition on the MCE of FeZrB amorphous alloys

5.2.1 Introduction

In chapter 5.1, investigation has already revealed that the MCE of Fe-based amorphous ribbons can be enhanced by the addition of Cr, which provides a feasible method to optimize the MCE. On the basis of previous work, a more thorough investigation on the influence of the minor additions to the MCE of the FeZrB amorphous ribbon systems is discussed in this chapter.

5.2.2 Results and discussion

Based on the findings for FeZrB ternary alloys reported in the literature and from our previous work, $Fe_{88}Zr_8B_4$ (numbered as FZB001) amorphous alloy was selected as the master alloy composition for the subsequent minor additions due to its relatively large magnetic entropy change (0.884 J/kgK under 1.5 T), its Curie temperature close to room temperature (280 K) and its large refrigerant capacity (106.08 J/kg under 1.5 T). Ingots of FeZrB based alloys with different minor additions (Co, Er, Sm and Mn) were prepared from raw metallic materials with purity above 99.9% (at.%). The compositions are listed in Table 5.2.

Table 5. 2 The code numbers and their corresponding compositions used in the project

Number	Composition	Number	Composition

FZB001	$Fe_{88}Zr_8B_4$	FZB203	$Fe_{85}Zr_8B_4Er_3$
FZB101	$Fe_{87}Zr_8B_4Co_1$	FZB301	$Fe_{87}Zr_8B_4Sm_1$
FZB102	$Fe_{86}Zr_8B_4Co_2$	FZB302	$Fe_{86}Zr_8B_4Sm_2$
FZB103	$Fe_{88}Zr_7B_4Co_1$	FZB303	$Fe_{85}Zr_8B_4Sm_3$
FZB104	$Fe_{87}Zr_7B_4Co_2$	FZB401	$Fe_{87}Zr_8B_4Mn_1$
FZB105	$Fe_{88}Zr_8B_3Co_1$	FZB402	$Fe_{86}Zr_8B_4Mn_2$
FZB106	$Fe_{88}Zr_7B_3Co_2$	FZB403	$Fe_{85}Zr_8B_4Mn_3$
FZB107	$Fe_{87}Zr_7B_3Co_2$	FZB404	$Fe_{80}Zr_8B_4Mn_8$
FZB201	$Fe_{87}Zr_8B_4Er_1$	FZB405	$Fe_{78}Zr_8B_4Mn_{10}$
FZB202	$Fe_{86}Zr_8B_4Er_2$		

The ingots were repeatedly melted at least six times in an arc-melting machine under an argon atmosphere in order to ensure their homogeneity. A melt-spinning machine with single roller under an argon atmosphere was used to fabricate ribbons from the ingots. The dimensions of the as-spun ribbons were 0.05 mm in thickness and 1.5 mm in width. X-ray diffraction (XRD) measurement was performed using a Rigaku diffractometer with Cu-Kα radiation to check whether the as-spun ribbons were amorphous or not. In order to further confirm the microstructure of the specimens from the surface to the central region, a JEOL JEM-2010F high-resolution transmission electron microscope (HRTEM) was used. For HRTEM experiments, the samples were prepared by ion-polishing under a pure argon protection atmosphere with a GATAN 691 precision ion polishing system. The magnetic property related experiments were performed on a Quantum Design vibrating sample magnetometer (VSM). The magnetic hysteresis loops at different temperatures were obtained, with the measurements being conducted in a changing magnetic field between 0.7 T and -0.7 T, in steps of 0.007 T. The magnetization investigations were performed under temperatures from 150 K to 400 K in 10 K steps, and in a changing magnetic field increasing from 0 to 1.5 T in 0.005 T steps. The magnetocaloric effect (MCE) of the as-spun ribbons was obtained by calculating the working temperature range (ΔT) and the peak magnetic entropy change (ΔS_M^{peak}). The magnetic entropy change (ΔS_M)

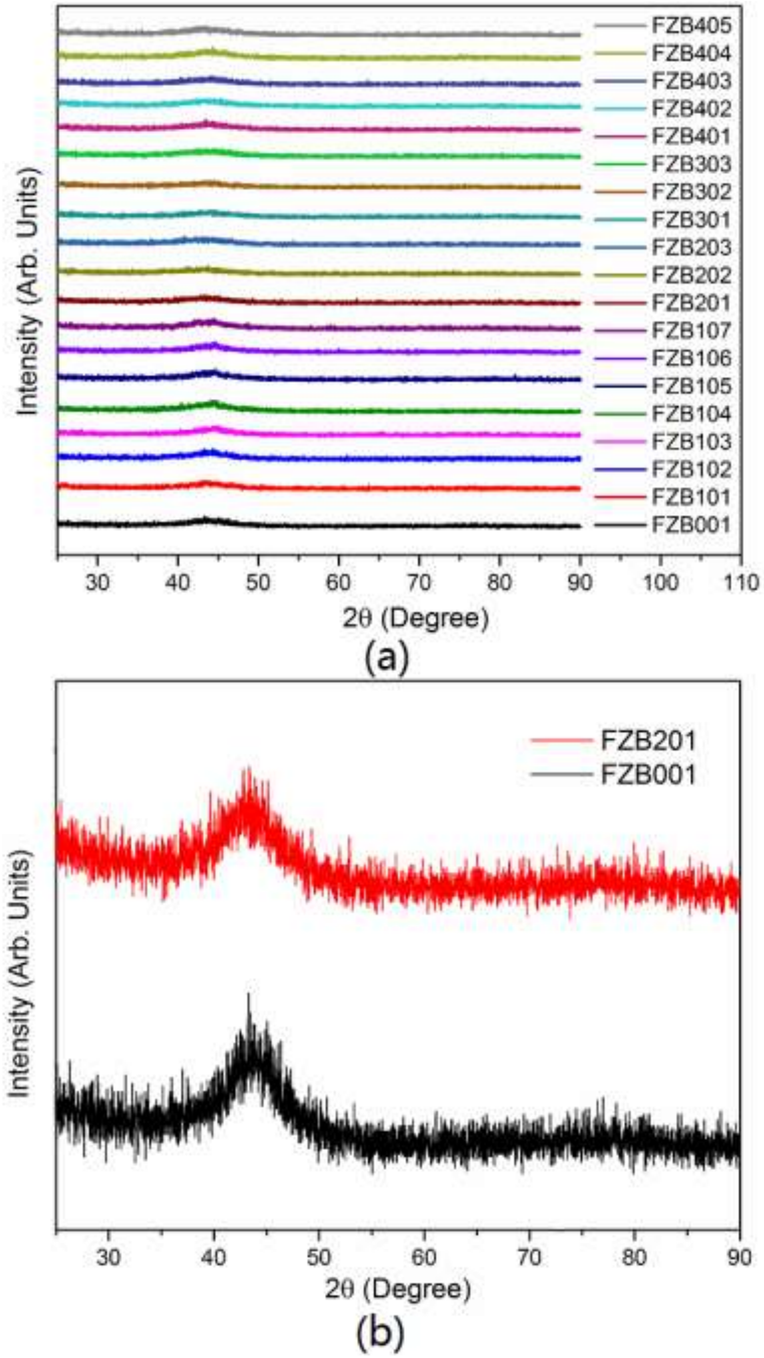

Figure 5. 9 (a) XRD results of all as-spun ribbons (b) XRD results of FZB001 and FZB201 ribbons

was then calculated from the results of the magnetization curves at different temperatures. The detailed procedures for calculating these parameters are given in [145].

Fig. 5.9a shows the XRD results of all the as-spun ribbons. All of the ribbons exhibit only a broad wave pack, around $2\theta = 45°$, with no sharp crystalline peaks, which indicates that all the as-spun ribbons are amorphous. The patterns in Fig. 5.9b are the magnified XRD results of FZB001 and FZB201.

In order to confirm the amorphous structure of the specimens, TEM investigations were carried out and the TEM result of FZB001 was shown in Fig. 5.10.

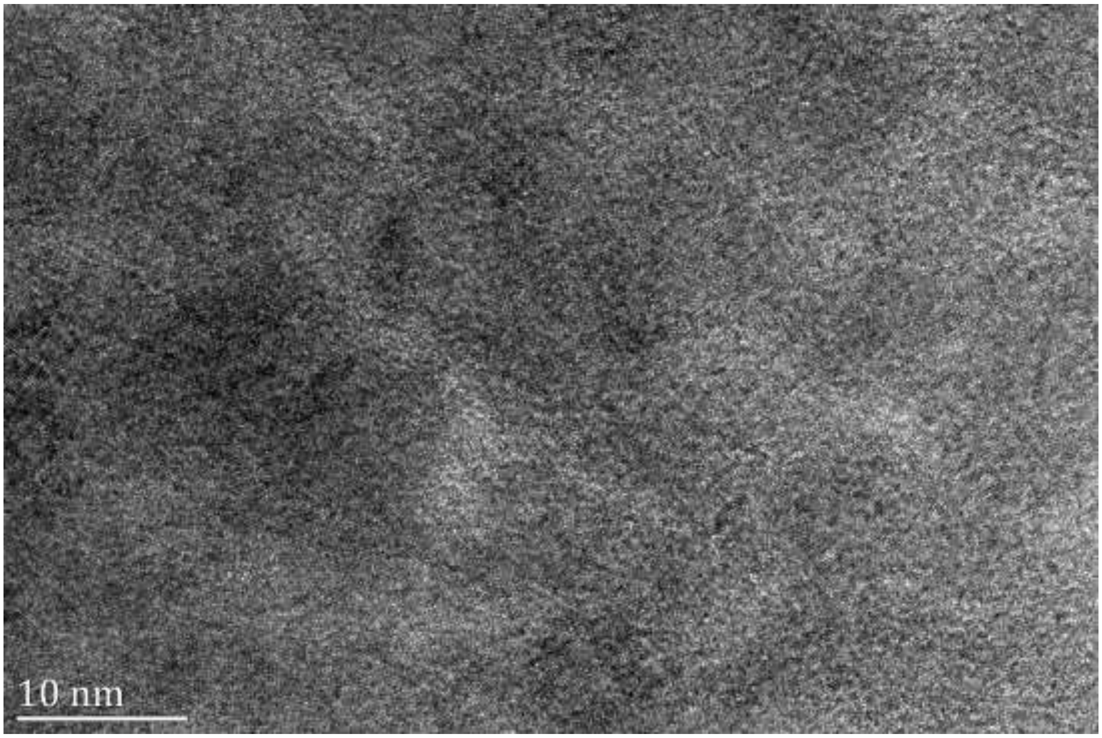

Figure 5. 10 TEM result of FZB001

The TEM result indicate that FZB001 is generally amorphous with a few short-

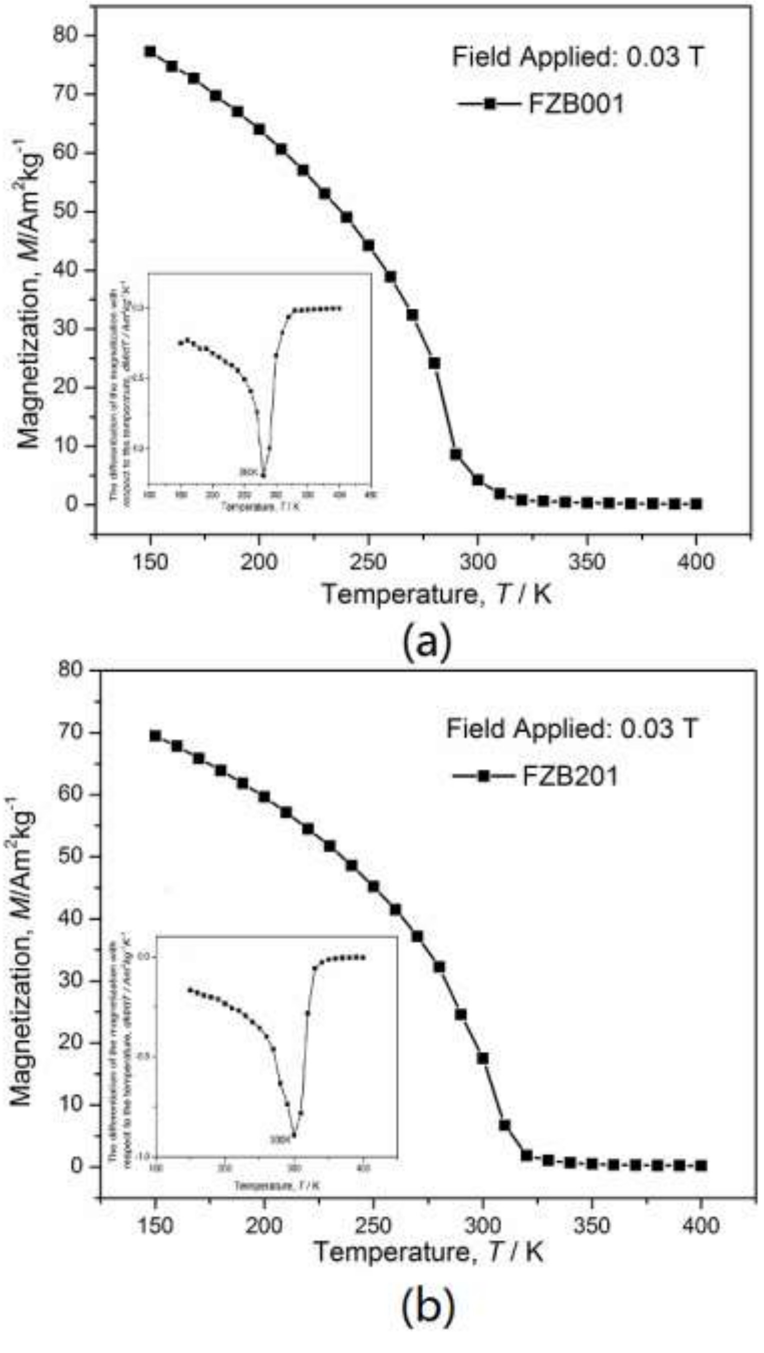

Figure 5. 11 Temperature-dependent magnetization curves of the as-spun ribbons (a) FZB001 and (b) FZB201 ribbons. The insets are the temperature-dependent differentiation of the magnetization with respect to the temperature

range order as well as medium-range order clusters.

Fig. 5.11 shows the temperature-dependent magnetization curves of the as-spun

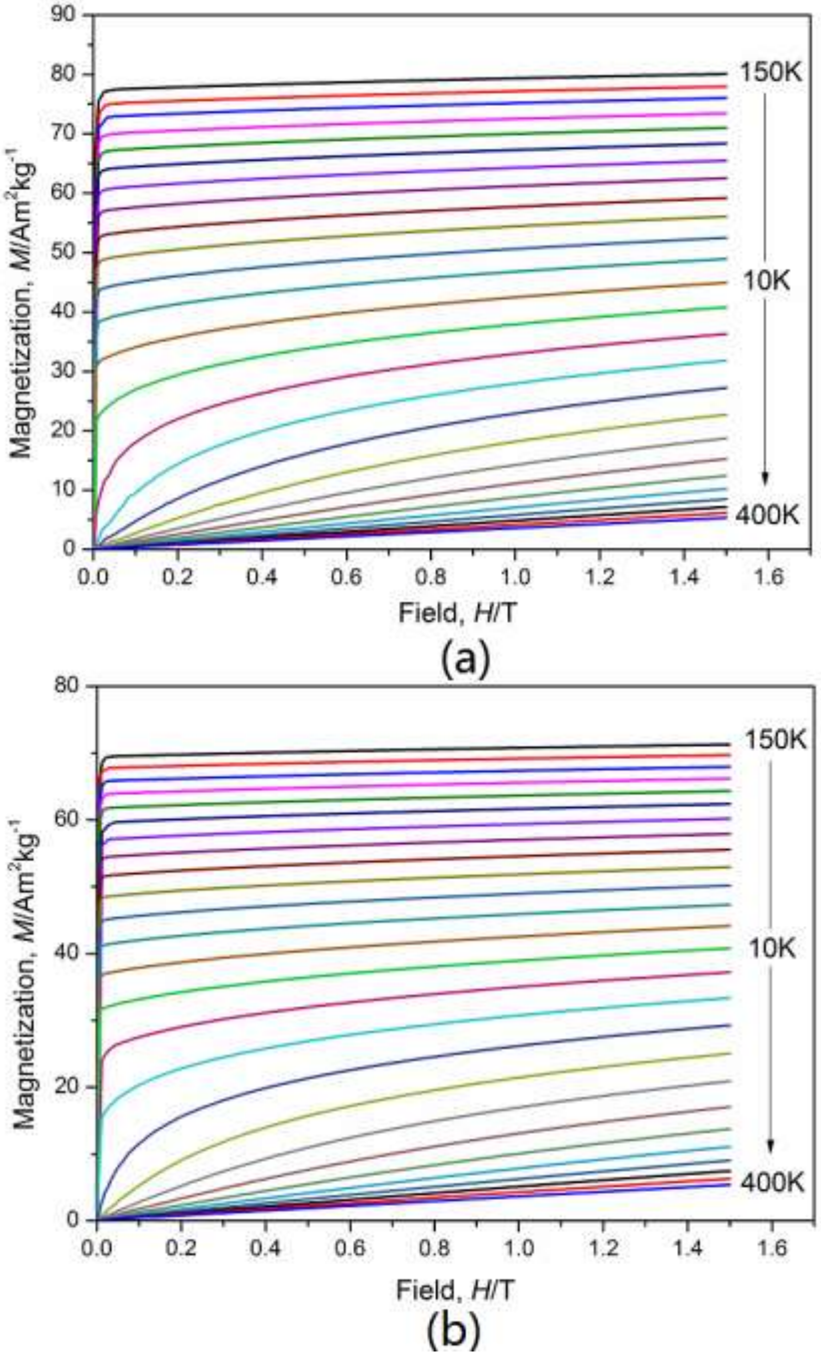

Figure 5. 12 Isothermal magnetization curves of the as-spun ribbons (a) FZB001 and (b) FZB201 ribbons

ribbons FZB001 and FZB201, for illustration. The curves were measured at different temperatures from 150 K to 400 K in 10 K steps. The applied magnetic field was 0.03 T. The inset curve is the temperature-dependent differentiation of the magnetization with respect to the temperature (dM/dT). The Curie temperature corresponded to the point where dM/dT reached its minimum value.

Molecular theory can be applied to explain the change of the Curie temperature in different compositions[136].

$$T_C = J(r) Z_T S(S+1)/3k_B \qquad (5.3)$$

where T_C corresponds to the Curie temperature, $J(r)$ to the distance dependent exchange between atoms, Z_T to the coordination number of the T (T=Fe) site, S to the spin quantum number and k_B to Boltzmann's constant. Among the four minor addition elements, the radii of the Er and Sm atoms are similar and both are much larger than that of the Fe atoms; the radius of the Mn atom is slightly larger than that of the Fe atom and the radius of the Co atom is slightly smaller than that of the Fe atom. As the amount of the substituted elements increases, the number of the alloying atoms surrounding the Fe atom site increases, which increases the value of Z_T. The variation of the distance (r) between the Fe atoms was investigated by simulation on the basis of a random model. For Fe atoms, $J'(r) > 0$. When Fe was substituted by 1 at.% Co, r increased from 3.49 Å to 3.59 Å. Both the increased $J(r)$ and increased Z_T work together to enlarge T_C. When Fe was substituted by 1 at.% Er or 1 at.% Mn, r decreased from 3.49 Å to 3.41 Å and 3.42 Å respectively. As the amount of Mn increased from 1 at.% to 10 at.%, r increases from 3.42 Å to 3.44 Å.

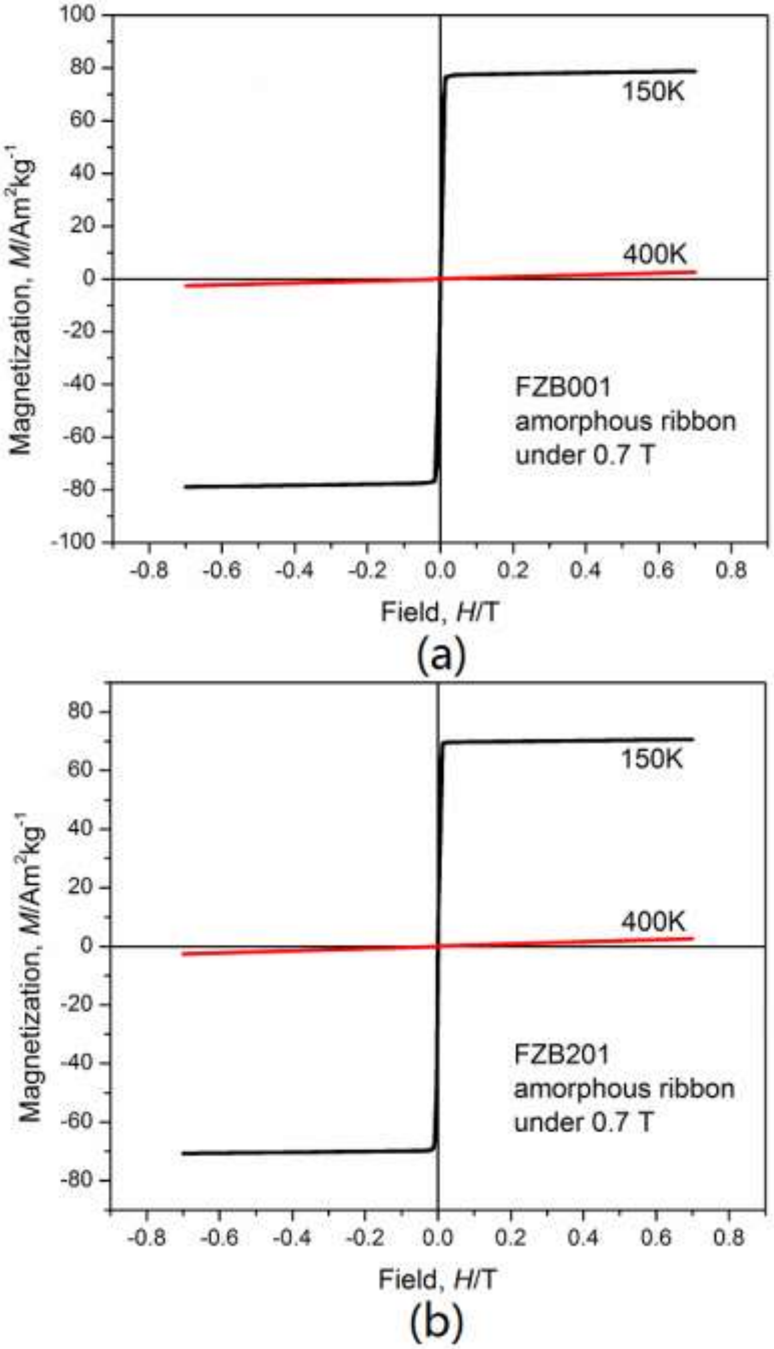

Figure 5. 13 Magnetic hysteresis loops of the as-spun ribbons (a) FZB001 and (b) FZB201 ribbons

When the additional amount was small, the effect of Z_T dominates T_C, consequently, T_C tends to increase. As the amount of Mn increased, the effect of $J(r)$ became dominate and T_C was suppressed due to the fact that more antiferromagnetic couplings emerged with more short Fe-Fe bonds.

The isothermal magnetization curves of the as-spun ribbons FZB001 and FZB201 are presented in Fig. 5.12. The saturation magnetization decreases as the temperature increases. Further, the curves in Fig. 5.12 indicate that the ribbons undergo a second order magnetic phase transition (SOMT).

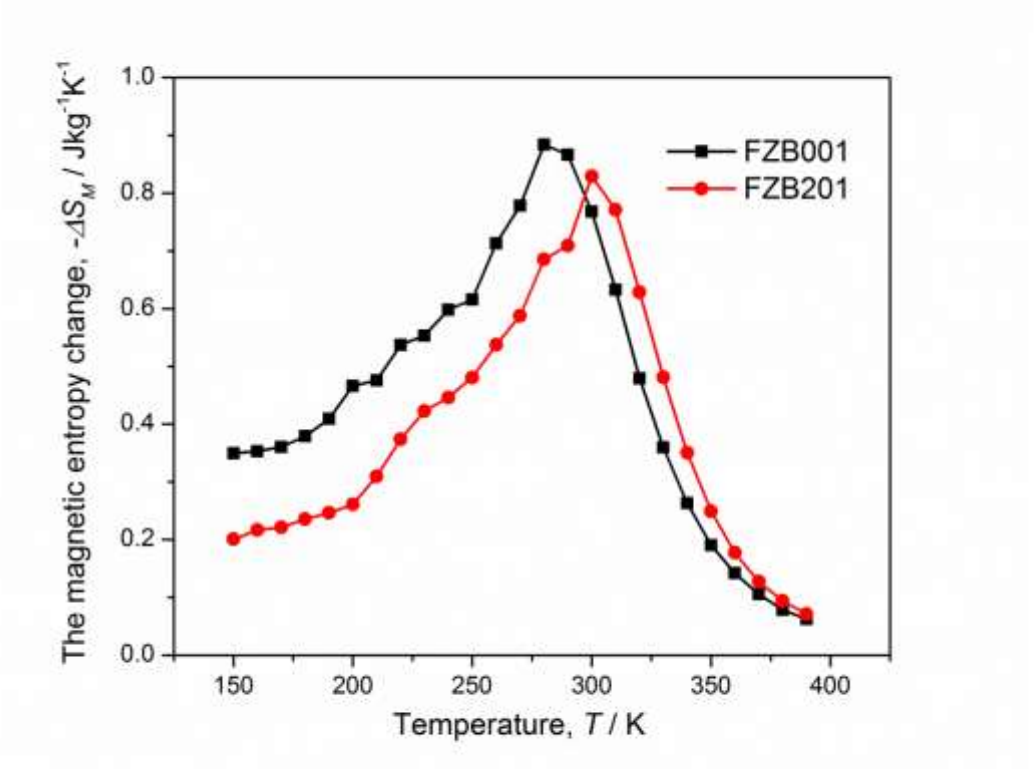

Figure 5. 14 Temperature dependent magnetic entropy change curves of FZB001 and FZB201 ribbons

Fig. 5.13 shows the magnetic hysteresis loops of the as-spun ribbons FZB001 and FZB201. For each ribbon, the hysteresis measurements were taken both at 150 K and 400K, corresponding to temperatures below and above the Curie temperature respectively. All the loops show almost zero coercivity and small hysteresis, which means all the ribbons exhibit excellent soft magnetic properties.

On the basis of the magnetization results, the magnetic entropy change (ΔS_M) at different temperatures can be obtained according to $\Delta S(T, \Delta H) = \int_{H_1}^{H_2} (\partial M(T, H)/\partial T)_H \, dH$, and the temperature dependent magnetic entropy change curves of FZB001 and FZB201 ribbons are shown in Fig. 5.14 The

shape of the curves also confirms that the ribbons undergo second order magnetic phase transition. The addition of Mn has a negative impact on the magnetic entropy change of the ribbons, while Co has a positive impact. In respect to the addition of Er and Sm, the impact is affected by the number of atoms of Er and Sm. The mechanism behind the change of ΔS_M is still under exploration, but is likely to be attributed to the complex inter-atomic coupling effect.

In order to make a better comparison with the results reported by other researchers, the equation $RC(\Delta H) = \left|\Delta S_M^{peak}\right| \times \delta T_{FWHM}$ was used to calculate the refrigerant capacity in this work. The magnetocaloric behavior of the as-spun ribbons including those investigated in this study as well as in the literature, is listed in Table 5.3. The MCE

Table 5. 3 The magnetocaloric effect of the magnetic materials studied in this work and reported in the literature

Nominal composition	Structure	Magnetic Field (T)	T_C (K)	δT_{FWHM} (K)	$\left\|\Delta S_M^{peak}\right\|$ (J kg^{-1}K^{-1})	RC (J kg^{-1})	Ref.
$Fe_{88}Zr_8B_4$	Amorphous	1.5	280	120	0.884	106.08	This work
$Fe_{87}Zr_8B_4Co_1$	Amorphous	1.5	320	110	0.715	78.65	This work
$Fe_{86}Zr_8B_4Co_2$	Amorphous	1.5	340	110	0.915	100.65	This work
$Fe_{88}Zr_7B_4Co_1$	Amorphous	1.5	300	130	0.672	87.36	This work
$Fe_{87}Zr_7B_4Co_2$	Amorphous	1.5	330	130	0.774	100.62	This work
$Fe_{88}Zr_8B_3Co_1$	Amorphous	1.5	300	130	0.799	103.87	This work
$Fe_{88}Zr_7B_3Co_2$	Amorphous	1.5	320	130	0.949	123.37	This work
$Fe_{87}Zr_8B_3Co_2$	Amorphous	1.5	330	140	0.945	132.6	This work
$Fe_{87}Zr_8B_4Er_1$	Amorphous	1.5	300	100	0.829	82.9	This work
$Fe_{86}Zr_8B_4Er_2$	Amorphous	1.5	300	100	0.607	60.7	This work
$Fe_{85}Zr_8B_4Er_3$	Amorphous	1.5	310	100	0.800	80	This work
$Fe_{87}Zr_8B_4Sm_1$	Amorphous	1.5	300	110	0.705	77.55	This work
$Fe_{86}Zr_8B_4Sm_2$	Amorphous	1.5	320	100	1.116	111.6	This work
$Fe_{85}Zr_8B_4Sm_3$	Amorphous	1.5	330	110	0.809	88.99	This work

$Fe_{87}Zr_8B_4Mn_1$	Amorphous	1.5	280	110	0.757	83.27	This work
$Fe_{86}Zr_8B_4Mn_2$	Amorphous	1.5	280	120	0.656	78.72	This work
$Fe_{85}Zr_8B_4Mn_3$	Amorphous	1.5	280	100	0.669	66.9	This work
$Fe_{80}Zr_8B_4Mn_8$	Amorphous	1.5	230	90	0.555	49.95	This work
$Fe_{78}Zr_8B_4Mn_{10}$	Amorphous	1.5	220	90	0.483	43.47	This work
$Fe_{86}Zr_9B_5$	Amorphous	1.5	330	120	1.13	135.6	[145]
$Fe_{80}Cr_4B_{10}Zr_5Gd_1$	Amorphous	1.5	360	120	0.91	110	[139]
$Fe_{75}Nb_{10}B_{15}$	Amorphous	1.5	250	190	0.60	115	[140]
$Fe_{79}Nb_7B_{14}$	Amorphous	1.5	372	N/A	1.07	N/A	[141]
$(Fe_{70}Ni_{30})_{89}Zr_7B_4$	Amorphous	1.5	342	N/A	0.70	N/A	[134]
$Fe_{64}Mn_{14}CoSi_{10}B_{11}$	Amorphous	1.5	457	N/A	0.83	N/A	[40]
$Fe_{72}Ni_{28}$	Amorphous	1.5	333	149	0.49	73	[142]
$(Fe_{85}Co_{15})_{75}Nb_{10}B_{15}$	Amorphous	1.5	440	124	0.82	102	[143]
$Gd_{55}Al_5Fe_{40}$	Amorphous	5.0	222	197	2.7	532	[100]
$Gd_{60}Fe_{20}Co_{10}Al_{10}$	Amorphous	5.0	222	167	4.4	736	[102]
$Gd_5Si_2Ge_2$	Crystalline	5.0	276	16.5	18.5	305	[17]

of ribbons in this work is generally better than that of Fe-based ribbons reported in the literature. Higher $\left|\Delta S_M^{peak}\right|$ was obtained with T_C closer to the room temperature, with these ribbons exhibiting relatively large RC.

The magnetocaloric effect obviously has a positive relation with the applied magnetic field. In order to make a comparison between the results calculated under different external magnetic fields, the relation between magnetocaloric effect and magnetic field was investigated[23]:

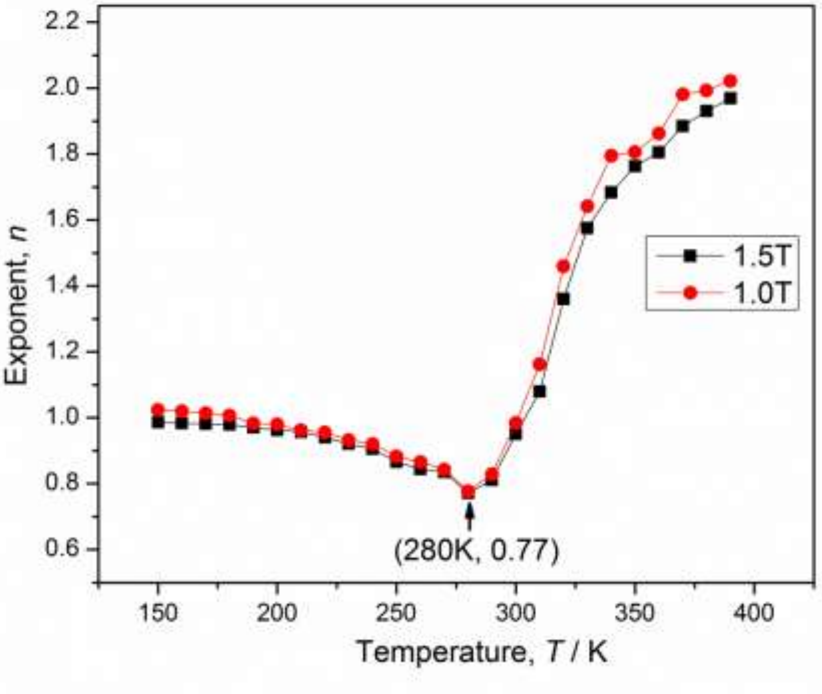

Figure 5. 15 Temperature dependent n value curves under different magnetic fields of the as-spun ribbon FZB001

$$|\Delta S_M(T,H)| \propto H^n \qquad (5.4)$$

where ΔS_M is the magnetic entropy change, H is the external magnetic field, T is the temperature and n is the critical exponent which is only affected by the intrinsic properties of the materials themselves. The temperature dependent n value curves of the as-spun ribbon FZB001 under different magnetic fields are shown in Fig. 5.15. The n values at different temperature points also confirm that the ribbons exhibit soft magnetic properties: $n \approx 0.77$ at T_C; n is close to 1 at temperatures far below T_C; n is close to 2 at temperatures far above T_C.

Similar to the magnetic entropy change, the refrigerant capacity is also related to the external magnetic fields, as given in the relation by Franco [106]:

$$RC \propto H^{1+1/\delta} \qquad (5.5)$$

Detailed calculation of δ is given in previous work[145]. The result of the FZB001 sample is: $RC \propto H^{1.1595}$. With the help of Eq.(5.4) and Eq.(5.5), when the external magnetic field changes from 1.5 T to 5.0 T, the peak magnetic entropy change of the FZB001 amorphous ribbon is 2.23 J/kgK at 280 K and the refrigerant capacity is 428.46 J/kg. Compared with the well-known $Gd_5Si_2Ge_2$ ($\left|\Delta S_M^{peak}\right|$=18.5 J/kgK, T_C=276 K and RC=305 J/kg under 5.0 T), although the $\left|\Delta S_M^{peak}\right|$ is not comparable, FZB001 exhibits almost 1.5 times the RC, and its T_C is closer to room temperature.

5.2.3 Conclusions

In this work, amorphous ribbons with different minor additions (Co, Er, Sm and Mn) in the master alloy $Fe_{88}Zr_8B_4$ were fabricated. The impact of different minor additions on the magnetocaloric effect was investigated. Among all the ribbons, the $Fe_{88}Zr_7B_3Co_2$ (FZB006) ribbon exhibited the largest RC (123.37 J/kg) and the $Fe_{86}Zr_8B_4Sm_2$ (FZB302) ribbon exhibited the largest $\left|\Delta S_M^{peak}\right|$(1.116 J/kgK). Both have a Curie temperature at about 320 K, which is close to room temperature. The relationship between the composition and the Curie temperature was investigated, and determined by both the inter-atomic distances and coordination numbers. The results gave solid experimental proof that the Curie temperature of Fe-based metallic glasses can be adjusted by alloying different elements. With proper amounts and appropriate elements, the Curie temperature can be tuned to a desired value. These amorphous ribbons are shown to have excellent potential for use as room temperature magnetic refrigerants. Although the relationship between the composition and the peak magnetic entropy changes is characterized in this work, its detailed mechanism is yet to be fully understood and is worth further study.

Chapter 6 Monte Carlo simulations on the MCE

Although much simulation work has been done on the MCE of the magnetic materials, there has been little work focus on amorphous materials. In this project, Monte Carlo simulation on the MCE of the metallic glass ribbons was undertaken. The method was derived from crystalline alloys by arranging the atoms in a random

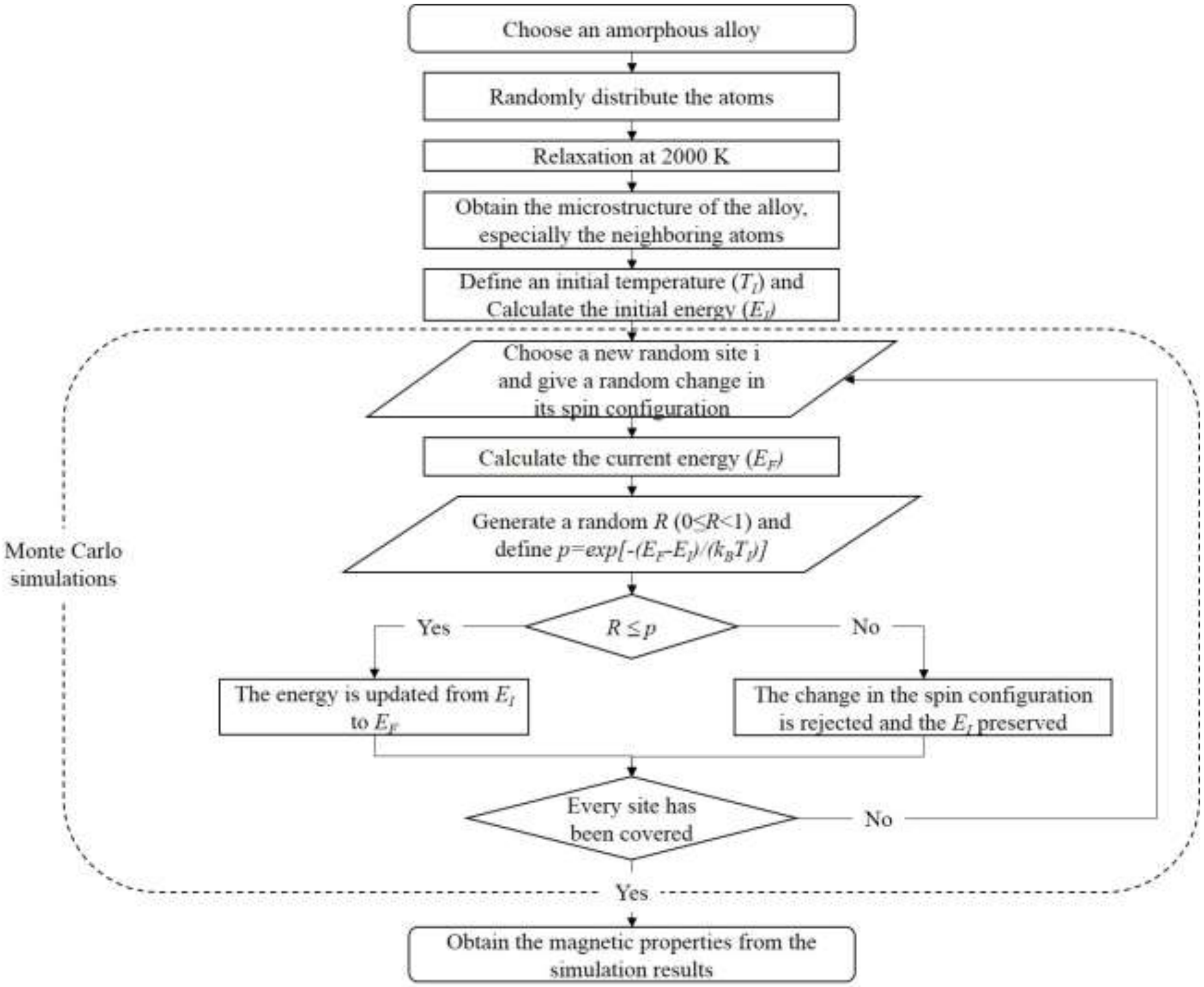

Figure 6. 1 The flow chart of the simulation work

way. For illustration purpose, the flow chart of the simulation work is shown in Fig. 6.1. After the composition of the alloy is determined, simulation on the random distribution of the atoms is carried out. A relaxation process is needed to eliminate the inner stress between atoms. Simulation of relaxation was performed using LAMMPS, with the temperature set at 2000 K. After that, the alloy could be considered as amorphous and the microstructure of the alloy determined. On the basis of the results, the neighboring atoms can be determined by the Voronoi calculations, and the Monte Carlo simulation method is then used to calculate the magnetic properties of the alloy. Approximations and assumptions were used during the simulation. Only the first neighboring atoms were considered when the coupling effect was calculated. It was also assumed that the simulated microstructure was almost the same as the real one. The random distribution of atoms and the relaxation of the alloy are common methods to simulate amorphous alloys, and there have already been programs to accomplish this effect. The main task of this project lays in the Monte Carlo simulation, due to the fact that there has been little research outcome on the simulation on the MCE of amorphous alloys. In the following part, the simulation work is introduced in detail.

6.1 Monte Carlo Simulation Algorithm

The critical factor in the simulation is to determine the total energy E of the alloy, because the following calculations on the magnetic properties are simulated on the basis of E. In the algorithm, E was calculated by the Hamiltonian which is dependent on the assumed coupling. In this project, the Hamiltonian was chosen as the simplest and most accepted form that included two terms:

(a) The coupling term: $-\sum_{ij}\lambda_{ij}\vec{S}_i\cdot\vec{S}_j$ represents the Hamiltonian two spin coupling where λ_{ij} is the exchange interaction parameter between site i and one of its neighboring sites j, $\vec{S}_i$ is the magnetic spin moment of site i

(b) The applied external magnetic field term: $\sum_i g\mu_B\vec{S}_i\cdot\vec{h}^{ext}$ where g is the Landè factor, μ_B is the Bohr magneton and $\vec{h}^{ext}$ is the external magnetic field.

Therefore, the general expression for the total energy used in the simulation is:

$$E = -\sum_{ij}\lambda_{ij}\vec{S}_i\cdot\vec{S}_j - \sum_i g\mu_B\vec{S}_i\cdot\vec{h}^{ext} \tag{6.1}$$

The ground state of the system can be obtained by minimizing the total energy E through adjusting $\vec{S}_i$.

The algorithm applied in the simulation of this project was on the basis of the importance sampling method reported by Metroplis et al. [146]:

(i) For each of magnetic spins in the system, randomly generate an initial configuration. An initial temperature (T_I) is also defined.

(ii) Calculate the initial energy (E_I) according to Eq. 6.1.

(iii) Choose a site i randomly, and a random change in its spin configuration is performed.

(iv) Calculate the current energy (E_F) according to Eq. 6.1.

(v) If $E_F < E_I$, the change in the spin configuration in step (iii) is accepted and the total energy is updated from E_I to E_F.

(vi) If $E_F > E_I$, a probability factor $p = exp[-(E_F - E_I)/(k_B T_I)]$ is introduced where k_B represents the Boltzmann constant.

(vii) Generate a random number R ($0 \leq R < 1$)

(viii) If $R \leq p$, the change in the spin configuration in step (iii) is accepted and the total energy is updated from E_I to E_F. Otherwise, the change in step (iii) is rejected and the previous spin configuration, as well as the total energy, are preserved.

(ix) Choose a new site and randomly change its spin configuration. Go to step (iv).

(x) Repeat the above steps until every site in the system is taken into account.

The whole process above forms just one Monte Carlo cycle. At the end of every Monte Carlo cycle, there is a total energy of the system E_i (where i is the number of a given Monte Carlo cycle). A large number of Monte Carlo cycles are necessary in the simulation, including thousands of cycles used to thermalize the system. To start the calculations from the simulation results, the mean energy $\langle E \rangle$ and the mean squared energy $\langle E^2 \rangle$ are obtained by the following equations:

$$\langle E\rangle = \frac{1}{N_M - N_T}\sum_{i>N_T}^{N_M} E_i \qquad (6.2)$$

$$\langle E^2\rangle = \frac{1}{N_M - N_T}\sum_{i>N_T}^{N_M} E_i^2 \qquad (6.3)$$

where N_M is the total number of Monte Carlo cycles in the simulation and N_T is the number of Monte Carlo cycles in the thermalization part. The magnetic part of the specific heat is obtained by:

$$C_{mag}(T,H) = \frac{\langle E^2\rangle - \langle E\rangle^2}{k_B T^2} \qquad (6.4)$$

Therefore, the magnetic part of the entropy can be calculated by:

$$S_{mag}(T,H) = \int_0^T \frac{C_{mag}(T,H)}{T}\,dT \qquad (6.5)$$

Both the specific heat and the entropy of the system have contributions from conduction electrons and lattice. In this simulation, a reasonable approximation was made that only the magnetic part of the specific heat and magnetic entropy depend on the external magnetic field.

6.2 Simulation results

The source code was written in FORTRAN language and is shown in Appendix II. The simulation was realized by Microsoft Visual Studio and started with binary $Gd_{50}Co_{50}$ and $Gd_{68}Ni_{32}$ amorphous alloys. The reason why these two Gd-based binary amorphous alloys were chosen includes: (1) The simulation of the MCE in amorphous alloys has not been undertaken by other researchers. In order to simplify the calculation, a binary system is preferred. (2) In this simulation, the interactions, especially the coupling effect between neighboring atoms, were considered to determine the energy of the alloy. Therefore, alloys consisting of only magnetic elements are preferred. (3) Fe-based binary amorphous alloys usually consist of Fe and another non-magnetic element, which makes the calculation rather complicated.

To simulate the amorphous state, the atoms of a magnetic metallic glass ribbon are randomly distributed in space. A 1 × 1 × 1 cell with 8000 atoms per cell was used in this project. During the simulation, only first neighbor interaction was considered. At

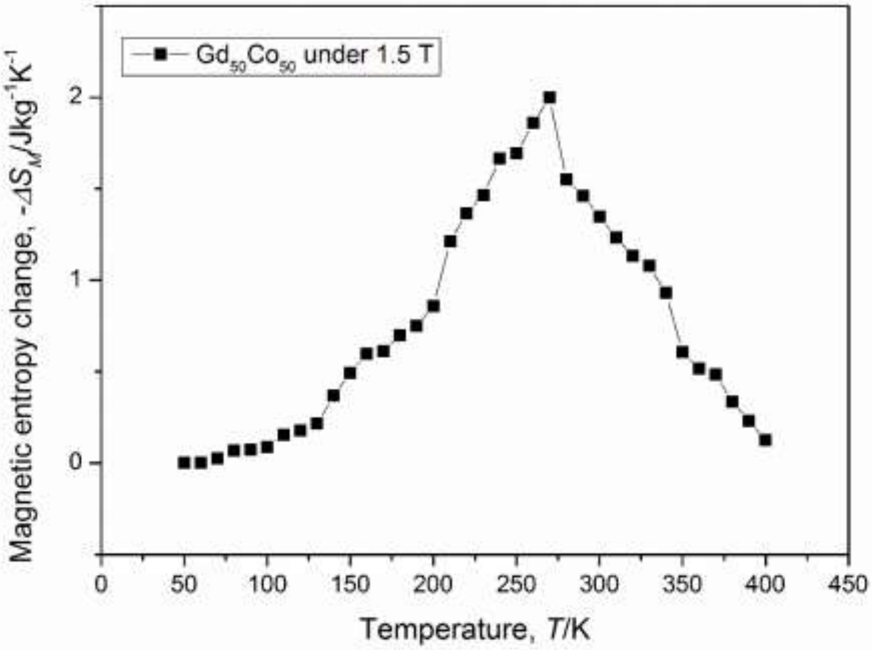

Figure 6. 2 The simulation result of the temperature dependent magnetic entropy change of $Gd_{50}Co_{50}$ amorphous materials

a given temperature, 60000 Monte Carlo cycles were executed in the simulation. The first 30000 cycles were used to thermalize the system and the last 30000 cycles were used to calculate the magnetic properties. The temperature in the simulation was set to decrease from 400 K to 50 K in 10 K steps. The external magnetic fields applied in the simulation were 1.5 T and 0 T. According to the methods described in Chapter 6.1, for each fixed magnetic field, the magnetic entropies were simulated under different temperatures. Consequently, the magnetic entropy change values under 1.5 T at different temperatures can be readily calculated. Fig. 6.2 shows the simulation results of the temperature dependence of the magnetic entropy change of $Gd_{50}Co_{50}$ amorphous materials. Investigations on the MCE of the $Gd_{50}Co_{50}$ amorphous ribbons have already been carried out [147], and the experimental results revealed that the Curie temperature for $Gd_{50}Co_{50}$ is 267.2 K and the absolute value of the peak magnetic entropy change under 1.5 T is about 1.87 J/kgK. In this project, the simulation result in Fig. 6.2 shows that the Curie temperature of $Gd_{50}Co_{50}$ is 270 K, only 1% higher than that of the experimental result. The absolute value of the peak magnetic entropy change obtained from the simulation is 2.00 J/kgK, which is about 7% larger than that of the experimental result. Fig. 6.3 shows the simulation results of the $Gd_{68}Ni_{32}$ amorphous materials. The MCE of the $Gd_{68}Ni_{32}$ amorphous ribbons was also given in the literature [148], with the experimental Curie temperature of the $Gd_{68}Ni_{32}$ amorphous ribbon at about 124 K and $\left|\Delta S_M^{peak}\right|$ at about 3.32 J/kgK under 1.5 T. According to our simulation result, the T_C of the $Gd_{68}Ni_{32}$ is 140 K and the $\left|\Delta S_M^{peak}\right|$ is 3.63 J/kgK. The T_C of the simulation result is 16 K higher than that of the published experimental result and the $\left|\Delta S_M^{peak}\right|$ of the simulation result is 0.31 J/kgK larger than that of the experimental results. Roughly speaking, the simulation results fitted the experimental results well, proving the simulation to be a valuable and reliable approach for verifying experimental results, as well as predicting the MCE of new magnetic materials. The difference in the Curie temperatures between the experimental results and the simulation results may be due to the different calculation methods. In the experiments, the Curie temperature was determined on the basis of the magnetization-temperature curves, and the T_C corresponds to the temperature where dM/dT is minimum. In the simulation, however, the T_C simply corresponds to the temperature where the magnetic entropy change reached its peak

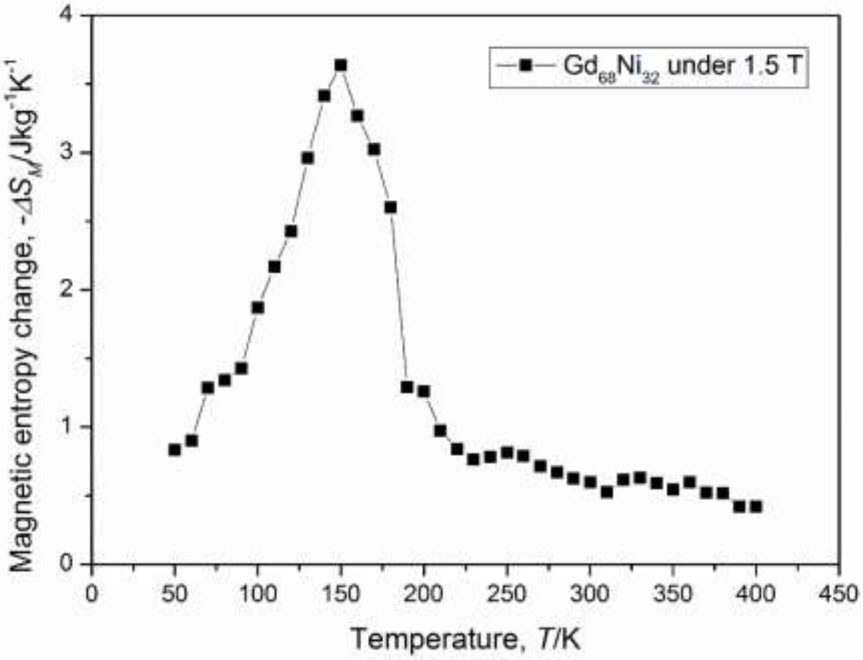

Figure 6. 3 The simulation result of the temperature dependent magnetic entropy change of $Gd_{50}Co_{50}$ amorphous materials

value. The difference in the $\left|\Delta S_M^{peak}\right|$ between the experimental results and the simulation results is caused by approximations in the algorithm. In order to make the simulation results fit perfectly with the experimental results, further optimization of the simulation is needed.

The results of the simulations on the Gd-based binary amorphous alloys prove the applicability of the method to predict and verify the MCE of the metallic glasses. Since the project is focused on the Fe-based metallic glasses, the simulation on the MCE of the Fe-based amorphous alloys is necessary. Given the fact that most of the Fe-based metallic glasses consist of at least one non-magnetic element, there is an assumption used in the simulation that only interactions between the magnetic elements would be considered. Composition of $Fe_{80}Mn_{10}Zr_{10}$ was chosen for investigation. The methods are similar to those used for the Gd-based binary alloys. In this FeMnZr alloy, only the interactions between Fe and Mn (Fe-Fe, Fe-Mn and Mn-Mn) were considered when determining the energy of the alloy. In order to make better comparison with the experimental results obtained by Min [149], the maximum external magnetic field was set to be 5 T. The simulation result was shown in Fig. 6.4. According to the simulation result, T_C of the $Fe_{80}Mn_{10}Zr_{10}$ is 170 K and $\left|\Delta S_M^{peak}\right|$ is 1.96 J/kgK under 5 T. In Min's work, the $Fe_{80}Mn_{10}Zr_{10}$ metallic ribbons exhibit a $\left|\Delta S_M^{peak}\right|$ of 2.33 J/kgK under 5 T and T_C is 195 K [149]. The difference between the simulation and experimental results could be caused by the assumption that only the interactions between the magnetic elements were taken into account.

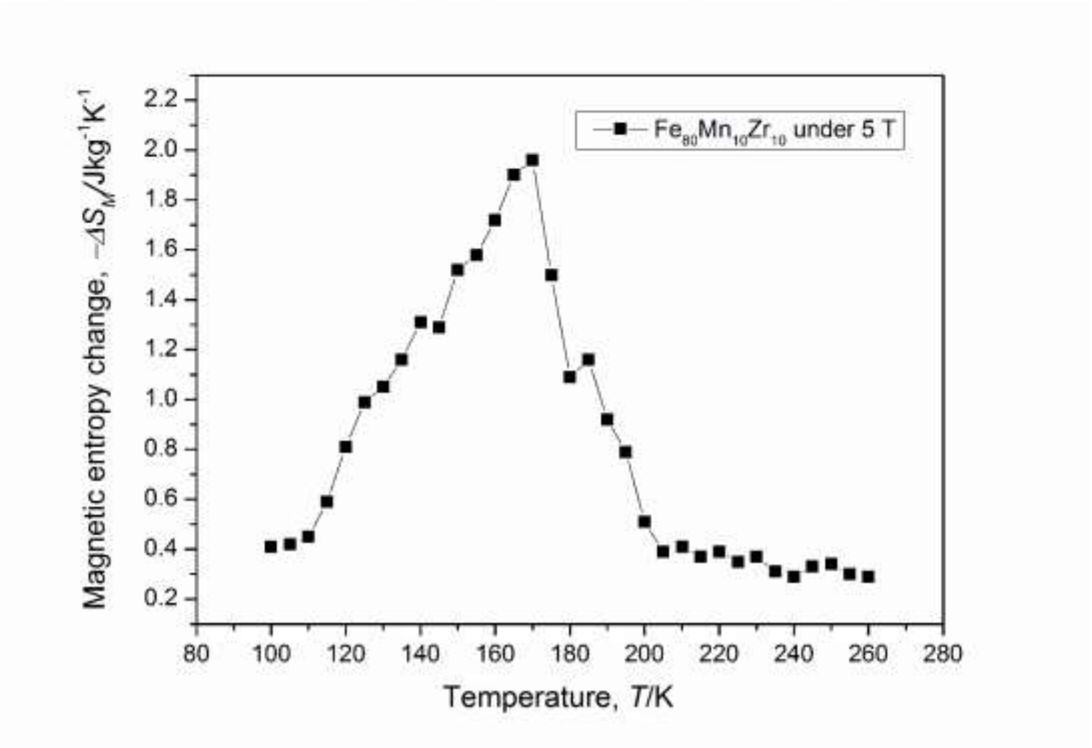

Figure 6. 4 The simulation result of the temperature dependent magnetic entropy change of $Fe_{80}Mn_{10}Zr_{10}$ amorphous materials

6.3 Conclusions

In this chapter, investigations on the MCE in the Gd-based as well as the Fe-based amorphous ribbons by Monte Carlo simulation were carried out. The results of the simulation on the Gd-based alloys fitted well with the experimental data. The results of the Fe-based alloys, however, differs from the experimental results. It can therefore be concluded that the Monte Carlo simulation provides a reliable alternative method to investigate the MCE in amorphous alloys consisting with all magnetic elements, and leads to a better understanding of the mechanism of the MCE. In order to better apply the simulation to the Fe-based metallic glasses, further improvement on the simulation is needed to eliminate or minimize the effect of ignoring the interactions between magnetic and non-magnetic elements. Except that, improvement should also made in the calculation method so that the interactions between the non-magnetic elements can also be considered.

Chapter 7 Overall conclusions

In last four chapters, I presented the work I have done in my study. The investigations on the MCE were carried out both in experiments and simulations. On the basis of the results presented above, the conclusions can be drawn in the following:

1. The MCE of FeZrB ternary amorphous ribbons was thoroughly investigated. Three new Fe-based series of glassy ribbons were designed and successfully fabricated. The magnetocaloric effect of those Fe-based amorphous ribbons was extensively studied. The results indicate that small replacement of boron with iron could obviously change both the Curie temperature and the peak magnetic entropy change. With increasing the amount of boron, all specimens in the three series of ribbons tend to exhibit larger peak magnetic entropy changes as well as Curie temperatures. $Fe_{86}Zr_9B_5$ exhibits a $\left|\Delta S_M^{peak}\right|$ value of 1.13 J/kgK at 330 K and a RC value of 135.6 J/kg. Although its $\left|\Delta S_M^{peak}\right|$ is not the largest among all the specimens, it is the most appropriate candidate for room temperature applications due to the fact that both its $\left|\Delta S_M^{peak}\right|$ and RC are relatively larger than those of other materials with its T_C is relatively closer to room temperature.

2. New Fe-based amorphous ribbons $Fe_{84-x}Cr_xB_{10}Zr_5Gd_1$ (x=2, 4, 6, 8) were successfully fabricated and their magnetocaloric effect was investigated. The results show that the minor addition of Cr can affect both the peak magnetic entropy change and the Curie temperature of the Fe-based metallic ribbons. With increasing amounts of Cr, the $\left|\Delta S_M^{peak}\right|$ can achieve a peak value and T_C decreases nearly linearly. The results show that the $Fe_{80}Cr_4B_{10}Zr_5Gd_1$ metallic glass achieves values of $\left|\Delta S_M^{peak}\right|$ 0.91 J/kgK and RC 110 J/kg at a T_C of 360K. They are the highest $\left|\Delta S_M^{peak}\right|$ and the highest refrigeration capacity values near room temperature among all the Fe-based metallic glasses reported in the literature. Since both the peak magnetic entropy change and the Curie temperature are important factors for MCE materials, the $Fe_{80}Cr_4B_{10}Zr_5Gd_1$ metallic glass is shown to be a very promising MCE Fe-based material, and should be further investigated in regard to its MCE for commercial applications.

3. Amorphous ribbons with different minor additions (Co, Er, Sm and Mn) in the master alloy $Fe_{88}Zr_8B_4$ were fabricated. The impact of different minor additions on the magnetocaloric effect was investigated. Among all the ribbons, the $Fe_{88}Zr_7B_3Co_2$ (FZB006) ribbon exhibited the largest RC (123.37 J/kg) and the $Fe_{86}Zr_8B_4Sm_2$ (FZB302) ribbon exhibited the largest $\left|\Delta S_M^{peak}\right|$(1.116 J/kgK). Both have a Curie temperature at about 320 K, which is close to room temperature. The relationship between the composition and the Curie temperature was investigated,

which was determined by both the inter-atomic distances and coordination numbers. The results give theoretical guidance in adjusting the Curie temperature of Fe-based alloys. These amorphous ribbons are shown to have excellent potential as room temperature magnetic refrigerants. Although the relationship between the composition and the peak magnetic entropy changes was characterized in this work, its detailed mechanism is yet to be fully understood and is worth further study.

4. Investigations on the MCE in the Gd-based as well as the Fe-based amorphous ribbons by Monte Carlo simulation were carried out. The results of the simulation on the Gd-based alloys agreed well with the experimental data. The results of the Fe-based alloys, however, differs from the experimental results. It can therefore be concluded that Monte Carlo simulation provides an alternative method to investigate the MCE in amorphous alloys consisting with all magnetic elements, and leads to a better understanding in the mechanism of the MCE.

Chapter 8 Future work

8.1 Develop composite materials with enhanced MCE

In this project, work has been done in the discovery of single amorphous materials with large MCE. In order to realize the magnetic refrigeration at room temperature, the working materials need to exhibit large $|\Delta S_M|$ in a wide temperature range covering the room temperature. The results, however, show that the materials with large $|\Delta S_M|$ usually have T_C either much larger or smaller than the room temperature. In the future, work will be done to develop materials with laminate structures. In each layer, there will be an amorphous material. All of the materials exhibit similar $\left|\Delta S_M^{peak}\right|$ but their T_C distributes evenly close to the room temperature. The laminate will be expected to exhibit a large $\left|\Delta S_M^{peak}\right|$ over a wide working temperature range, which is different from the single material that the $\left|\Delta S_M^{peak}\right|$ only exhibits at one temperature point. In such cases, the laminate material with enhanced MCE should be promising for the application of the magnetic refrigeration at room temperature.

8.2 Further improve the simulation on the MCE of the Fe-based amorphous materials

As mentioned before, in order to better apply the simulation to the Fe-based metallic glasses, further improvement is needed in two aspects. Firstly, improvement should be made on the assumption of the simulation. Solutions should be found that how to eliminate or minimize the effect of ignoring the interactions between magnetic and non-magnetic elements. Secondly, improvement should also be made on the calculation of the energy of the alloy. Better calculation method should be used so that the interactions between the non-magnetic elements can also be considered when the energy is calculated.

Appendix I The Regulations Regarding the Current Practice with Ozone Depletion and Greenhouse Effect

1. The Montreal Protocol on Substances that Deplete the Ozone Layer (Montreal Protocol 1987). To date, this Protocol has been signed and ratified by 197 countries.

2. In 1991, The Code of Practice for the Reduction of Chlorofluorocarbon (CFC) Emissions from Refrigeration and Air Conditioning Systems was carried out in Canada.

3. In 1998, Ozone-depleting Substances Regulations were effective in Canada.

4. In 2003, the Canadian federal government enacted the Federal Halocarbon Regulations.

5. In 1993, China has enacted the national plan about phasing out the ozone depleting substances.

6. In the United States of America, Environmental Protection Agency (EPA) regulates the phaseout under Title VI of the Clean Air Act.

Appendix II Main Source Code of the Monte Carlo Simulation

```
SUBROUTINE READ_FILE
   INCLUDE 'MCMAG.INC'


   REAL*8, DIMENSION(3)::JOUR
   REAL*8, DIMENSION(2)::HEURE
   INTEGER, DIMENSION(NAMAX)::NAT_READ,NVS_READ
   REAL*8, DIMENSION(NAMAX,NNMAX)::AJJX_READ,AJJY_READ,AJJZ_READ,AJXY_READ,AJXZ_READ,AJYX_READ,AJYZ_READ,AJZX_READ,AJZY_READ
   REAL*8 TCOJX_READ,TCOJY_READ,TCOJZ_READ,TCOJXY_READ,TCOJXZ_READ,TCOJYZ_READ,TCOJYX_READ,TCOJZX_READ,TCOJZY_READ
   REAL*8, DIMENSION(NAMAX)::AMPS_READ,D0_READ,DX_READ,DY_READ,DZ_READ,D_READ,DDIX_READ,DDIY_READ,DDIZ_READ
   INTEGER, DIMENSION(NAMAX,NNMAX)::NAV_READ
```

```
   INTEGER, DIMENSION(NAMAX,NNMAX,3)::M_READ

   INTEGER NIN,NFI,NA_READ,JCOD_READ,IANI_READ,NMOT_READ

   CHARACTER NFILA*10,TITL1_READ*80,TITL2_READ*80,NFIL_READ*6



   COMMON /READ2/TITL1_READ,TITL2_READ,NFIL_READ,      &

        /COM4/M_READ,                    &

        /COM2/NA_READ,IANI_READ,               &

         /COM8/NVS_READ,                 &


/TEST/AJJX_READ,AJJY_READ,AJJZ_READ,AJXY_READ,AJXZ_READ,AJY
Z_READ,AJYX_READ,AJZX_READ,AJZY_READ,    &

         /TEST20/NAV_READ,               &

         /TEST5/NAT_READ,                &

         /TEST2/JCOD_READ,               &

         /READ4/D_READ,DX_READ,DY_READ,DZ_READ,          &

         /READ5/DDIX_READ,DDIY_READ,DDIZ_READ,D0_READ,    &

         /READ1/NMOT_READ,               &
```

```
     /COM5/AMPS_READ

CALL DATE(JOUR)
CALL TIME(HEURE)
WRITE(LPT,1300)JOUR(1),JOUR(2),JOUR(3),HEURE(1),HEURE(2)
WRITE(LPT,3990)
WRITE(LPT,2233)
WRITE(LPT,3990)
WRITE(LPT,2011)NFIL_READ
WRITE(LPT,25)TITL1_READ
WRITE(LPT,25)TITL2_READ
WRITE(LPT,1290)
NFILA = NFIL_READ//'.DAT'
READ(I01,*)NA_READ,JCOD_READ,NMOT_READ
```

```
      IF
(((JCOD_READ.NE.0).AND.(JCOD_READ.NE.1).AND.(JCOD_READ.NE.2)).OR
.(NA_READ.EQ.0).OR.(NMOT_READ.LT.1)) THEN

 1121   WRITE (ITTO,1122)NFILA

        WRITE (ITTO,1123)

        STOP

      END IF



      IANI_READ=1



      IF (NA_READ<0) THEN

        IANI_READ=-1

        NA_READ=-NA_READ

      END IF




      DO I=1,NA_READ
```

```
      IF (IANI_READ==1) READ(I01,*)NAT_READ(I),NVS_READ(NAT_READ(I)),D_READ(NAT_READ(I)),DDIX_READ(NAT_READ(I)),DDIY_READ(NAT_READ(I)),DDIZ_READ(NAT_READ(I))

      IF (IANI_READ==-1) READ(I01,*)NAT_READ(I),NVS_READ(NAT_READ(I))

       IF ((NAT_READ(I).LT.1).OR.(NVS_READ(NAT_READ(I)).LT.1).OR.(NAT_READ(I).GT.NA_READ)) THEN

 1124     WRITE (ITTO,1122)NFILA

        WRITE (ITTO,1125)

        STOP

      END IF



WRITE(LPT,24)NAT_READ(I),D_READ(NAT_READ(I)),DDIX_READ(NAT_READ(I)),DDIY_READ(NAT_READ(I)),DDIZ_READ(NAT_READ(I)),NVS_READ(NAT_READ(I))
```

```
      IF (JCOD_READ.EQ.0) THEN
        DO J=1,NVS_READ(NAT_READ(I))

READ(I01,*)NAV_READ(NAT_READ(I),J),(M_READ(NAT_READ(I),J,K),K=1,
3),AJJX_READ(NAT_READ(I),J)
          IF
((NAV_READ(NAT_READ(I),J).LT.1).OR.(NAV_READ(NAT_READ(I),J).GT.N
A_READ)) THEN
 1126        WRITE (ITTO,1122)NFILA
            WRITE (ITTO,1127)
            STOP
          END IF

WRITE(LPT,17)NAV_READ(NAT_READ(I),J),(M_READ(NAT_READ(I),J,K),K
=1,3),NAT_READ(I),NAV_READ(NAT_READ(I),J),AJJX_READ(NAT_READ(I)
,J)
          AJJY_READ(NAT_READ(I),J)=AJJX_READ(NAT_READ(I),J)
```

```
      AJJZ_READ(NAT_READ(I),J)=AJJX_READ(NAT_READ(I),J)

     END DO



    ELSE IF (JCOD_READ.EQ.1) THEN

     DO J=1,NVS_READ(NAT_READ(I))


READ(I01,*)NAV_READ(NAT_READ(I),J),(M_READ(NAT_READ(I),J,K),K=1,
3),AJJX_READ(NAT_READ(I),J),AJJY_READ(NAT_READ(I),J),AJJZ_READ(N
AT_READ(I),J)

      IF (NAV_READ(NAT_READ(I),J).LT.1) THEN

1128         WRITE (ITTO,1122)NFILA

       WRITE (ITTO,1127)

       STOP

      END IF


WRITE(LPT,92)NAV_READ(NAT_READ(I),J),(M_READ(NAT_READ(I),J,K),K
```

```
=1,3),NAT_READ(I),NAV_READ(NAT_READ(I),J),AJJX_READ(NAT_READ(I)
,J),AJJY_READ(NAT_READ(I),J),AJJZ_READ(NAT_READ(I),J)
          END DO



        ELSE IF (JCOD_READ.EQ.2) THEN
          DO J=1,NVS_READ(NAT_READ(I))

READ(I01,*)NAV_READ(NAT_READ(I),J),(M_READ(NAT_READ(I),J,K),K=1,
3),&

AJJX_READ(NAT_READ(I),J),AJJY_READ(NAT_READ(I),J),AJJZ_READ(NA
T_READ(I),J),&

AJXY_READ(NAT_READ(I),J),AJXZ_READ(NAT_READ(I),J),AJYZ_READ(N
AT_READ(I),J),&

AJYX_READ(NAT_READ(I),J),AJZX_READ(NAT_READ(I),J),AJZY_READ(N
AT_READ(I),J)
```

```
        IF (NAV_READ(NAT_READ(I),J).LT.1) THEN
 1129       WRITE (ITTO,1122)NFILA
          WRITE (ITTO,1127)
          STOP
        END IF

WRITE(LPT,192)NAV_READ(NAT_READ(I),J),(M_READ(NAT_READ(I),J,K),
K=1,3),&
                 NAT_READ(I),NAV_READ(NAT_READ(I),J),&

AJJX_READ(NAT_READ(I),J),AJXY_READ(NAT_READ(I),J),AJXZ_READ(N
AT_READ(I),J),&

AJYX_READ(NAT_READ(I),J),AJJY_READ(NAT_READ(I),J),AJYZ_READ(N
AT_READ(I),J),&

AJZX_READ(NAT_READ(I),J),AJZY_READ(NAT_READ(I),J),AJJZ_READ(NA
T_READ(I),J)
       END DO
```

```
      END IF

     END DO

     WRITE(LPT,6951)
     NACO=0

  27 READ(I01,*)NIN,NFI,SMO

     NACO = NACO+NFI-NIN+1

     DO I=NIN,NFI
      AMPS_READ(I)=SMO
      WRITE(LPT,9878)I,AMPS_READ(I)
     END DO
```

```
      IF (NACO.NE.NA_READ) GO TO 27

      DO I=1,NA_READ

D0_READ(I)=SQRT(DDIX_READ(I)*DDIX_READ(I)+DDIY_READ(I)*DDIY_
READ(I)+DDIZ_READ(I)*DDIZ_READ(I))
        IF(D0_READ(I).NE.0) THEN
          DX_READ(I)=DDIX_READ(I)/D0_READ(I)
          DY_READ(I)=DDIY_READ(I)/D0_READ(I)
          DZ_READ(I)=DDIZ_READ(I)/D0_READ(I)
        END IF
      END DO

      WRITE(ITTO,5995)
```

```
  1300 FORMAT(/,29X,3A4,2X,2A4//)

 1122 FORMAT(/,1X,' VERIFY YOUR INPUT FILE ',A10,/,&

          '        POSSIBLE ERRORS :')

 1123 FORMAT(1X,' NA and NMOT must be integers and at least equal to 1'&

          ,/,1X,' JCOD must be equal to 0, 1 or 2')

 1125 FORMAT(1X,' NAT must be an integer between 1 and NA'&

          ,/, 1X,' NV must be an integer at least equal to 1')

 1127 FORMAT(1X,' NAV must be an integer between 1 and NA'&

          ,/,1X,' Cell indices must be integers')

 1131 FORMAT(1X,' NI and NF must be integers and at least equal to 1'&

          ,/,1X,' NF must always be larger than or equal to NI'&

          ,/,1X,' The largest NF must be equal to NAT'&

          ,/,1X,' A spin amplitude must be attributed to any site'&

          ,/,1X,' Spin amplitudes must be positive or equal to 0')

 2233   FORMAT(/,31X,'   PROGRAM   MCMAG',/,12X,'SIMULATION   OF
MAGNETIC'&

          ' STRUCTURE BY A MONTE-CARLO METHOD',/,26X,&
```

```
          'VAX-FORTRAN VERSION 8801',//,&
          10X,' ENERGY CALCULATED ACCORDING TO THE FOLLOWING'&
          ' EXPRESSION :',/,14X,&
          'E = - 0.5*(Si`[Jij]Sj) + ((Di`Si)**2)/|Di| - H`Si',/)
2011 FORMAT(//,1X,' Input file : ',A6,'.DAT  contains the '&
          'following data : ',//)
  1290 FORMAT(/)
  25 FORMAT(1X,A80)
  17 FORMAT(9X,'Site ',I5,'  in cell (',I2,',',I2,',',I2,')',&
          '  with J(',I5,',',I5,') =',D12.4,' K')
  24 FORMAT(/,1X,'SITE ',I5,' [ D = ',F8.3,' along the direction ',&
          3(F6.3,2X),']',/,9X,'with ',I2,' neighbours :')
  92 FORMAT(9X,'Site ',I5,'  in cell (',I2,',',I2,',',I2,')',&
          '  with coupling (',I5,',',I5,') :',/,15X,&
          'Jx = ',F8.3,' K , Jy = ',F8.3,' K , Jz = ',F8.3,' K')
9878 FORMAT(22X,' Spin amplitude ( ',I5,' ) = ',F5.3)
 192 FORMAT(9X,'Site ',I5,'  in cell (',I2,',',I2,',',I2,')',/,&
```

```
            15X,'with J tensor (',I5,',',I5,') =   ',3(F8.3,X),/,&
            41X,3(F8.3,X),/,41X,3(F8.3,X))
 9876 FORMAT(1X,'D(',I2,') = ',F8.3,2X,'( direction ',3(F6.3,2X),&
             ')')
 3990 FORMAT(1X,' ------------------------------------------'&
            '-----------------------------------')
  6951 FORMAT(//)
5995   FORMAT(1X)


      RETURN
END SUBROUTINE READ_FILE


SUBROUTINE MC_CYCLE
      INCLUDE 'MCMAG.INC'
      INTEGER NA_CYC,U,V,W,K,N,IT_CYC,NOM_CYC,COUNT,IRAN_CYC
      INTEGER
I1,I2,LU_CYC,LV_CYC,LW_CYC,NPAJ_CYC,NFIP_CYC,NMULT_CYC
```

```
  REAL*8, DIMENSION(NAMAX,NUMAX+1,NVMAX+1,NWMAX+1)::&

   SX_CYC,SY_CYC,SZ_CYC,COMX_CYC,SOMY_CYC,SOMZ_CYC

  REAL*8, DIMENSION(NAMAX,NUMAX,NVMAX,NWMAX)::&

   SOMX_CYC,SOMX2_CYC,SOMY2_CYC,SOMZ2_CYC



  REAL*8 ENMIN,EX,EN_CYC,RAN,RAN_NUMBER,&


OMX,OMY,OMZ,DELTA_CYC,X_CYC,Y_CYC,Z_CYC,T_CYC,SNOM_CYC,E
NM_CYC,EN2M_CYC,MAG2_CYC,k_B,S,SM_CYC



  COMMON /PALL/LU_CYC,LV_CYC,LW_CYC,IRAN_CYC,          &

      /COM2/NA_CYC,                          &

      /CYC8/DELTA_CYC,X_CYC,Y_CYC,Z_CYC,NFIP_CYC,NMULT_CYC
&

      /CYC9/SOMX_CYC,                          &

      /CYC10/IT_CYC,NOM_CYC,                          &

      /SOMM2/COMX_CYC,                          &
```

```
      /COM6/NPAJ_CYC,                    &
      /CYC3/SX_CYC,SY_CYC,SZ_CYC,  &
      /CYC4/SOMY_CYC,SOMZ_CYC,                     &
      /CYC5/SOMX2_CYC,SOMY2_CYC,SOMZ2_CYC,            &
      /COM1/T_CYC,                          &
      /RES2/SNOM_CYC,                      &
      /CYC6/EN_CYC,                          &
      /CYC7/ENM_CYC,EN2M_CYC,MAG2_CYC,          &
      /SPIN/SM_CYC



k_B=1.3806D-23
DO W=1,LW_CYC
  DO V=1,LV_CYC
    DO U=1,LU_CYC
      DO K=1,NA_CYC
```

```
        SOMX_CYC(K,U,V,W)=0.

        SOMY_CYC(K,U,V,W)=0.

        SOMZ_CYC(K,U,V,W)=0.

        SOMX2_CYC(K,U,V,W)=0.

        SOMY2_CYC(K,U,V,W)=0.

        SOMZ2_CYC(K,U,V,W)=0.

      END DO

    END DO

  END DO

END DO

COUNT=0

NPAJ_CYC=0

ENM_CYC=0.

EN2M_CYC=0.

EN_CYC=0

SM_CYC=0.

MAG2_CYC=0.
```

```
      OMX=0.

      OMY=0.

      OMZ=0.




      IF (IRAN_CYC.EQ.1) THEN          ! ISING SPINS


!C

!C***** MONTE CARLO LOOPS FOR ISING SPINS *****

!C


       CALL RANDOM_SEED()

       DO 102 ITIME=1,IT_CYC


        DO W=1,LW_CYC

         DO V=1,LV_CYC

          DO U=1,LU_CYC
```

```
      DO N=1,NA_CYC


        CALL EN1_CALC(N,U,V,W)


        ASUP=-DELTA_CYC/T_CYC-88.029

        IF(ASUP.GT.0) GO TO 500

        AINF=-DELTA_CYC/T_CYC+89.415

        IF(AINF.LT.0) GO TO 10

        EX=EXP(-DELTA_CYC/(k_B*T_CYC))

        CALL RANDOM_NUMBER(RAN_NUMBER)

        RAN=RAN_NUMBER

        IF(EX-RAN)10,500,500


500          EN_CYC=EN_CYC+DELTA_CYC

        SX_CYC(N,U,V,W)=X_CYC

        SY_CYC(N,U,V,W)=Y_CYC

        SZ_CYC(N,U,V,W)=Z_CYC
```

```
              IF (ITIME.GT.NOM_CYC) NPAJ_CYC=NPAJ_CYC+1
  10          END DO
            END DO
           END DO
          END DO
!C
!C * * * MEAN VALUES AND VARIANCE OF MAGNETIC MOMENTS AND ENERGY * * *
!C FIRST PART OF CALCULATION: SOMMATION OVER THE SNOM_CYC=IT_CYC-NOM_CYC LAST CYCLES
!C
          IF(ITIME-NOM_CYC)102,102,103
  103     COUNT=COUNT+1
          DO W=1,LW_CYC
           DO V=1,LV_CYC
            DO U=1,LU_CYC
             DO K=1,NA_CYC
```

```
                OMX=OMX+SX_CYC(K,U,V,W)

                OMY=OMY+SY_CYC(K,U,V,W)

                OMZ=OMZ+SZ_CYC(K,U,V,W)

                SOMX_CYC(K,U,V,W)=SOMX_CYC(K,U,V,W)+SX_CYC(K,U,V,W)

                SOMY_CYC(K,U,V,W)=SOMY_CYC(K,U,V,W)+SY_CYC(K,U,V,W)

                SOMZ_CYC(K,U,V,W)=SOMZ_CYC(K,U,V,W)+SZ_CYC(K,U,V,W)


SOMX2_CYC(K,U,V,W)=SOMX2_CYC(K,U,V,W)+SX_CYC(K,U,V,W)**2


SOMY2_CYC(K,U,V,W)=SOMY2_CYC(K,U,V,W)+SY_CYC(K,U,V,W)**2


SOMZ2_CYC(K,U,V,W)=SOMZ2_CYC(K,U,V,W)+SZ_CYC(K,U,V,W)**2

               END DO

              END DO

             END DO

            END DO

            ENM_CYC=ENM_CYC+EN_CYC
```

```
          EN2M_CYC=EN2M_CYC+EN_CYC*EN_CYC

          MAG2_CYC=MAG2_CYC+OMX**2+OMY**2+OMZ**2

          OMX=0.

          OMY=0.

          OMZ=0.

  102   END DO

!C

!C***** END OF MONTE CARLO LOOPS FOR ISING SPINS *****

!C



      ELSE IF (IRAN_CYC.EQ.2) THEN     ! XY SPINS



!C

!C***** MONTE CARLO LOOPS FOR XY SPINS *****

!C



        CALL RANDOM_SEED()
```

```
DO 202 ITIME=1,IT_CYC


 DO W=1,LW_CYC

  DO V=1,LV_CYC

   DO U=1,LU_CYC

    DO N=1,NA_CYC


     CALL EN2_CALC(N,U,V,W)


     ASUP=-DELTA_CYC/T_CYC-88.029

     IF(ASUP.GT.0) GO TO 502

     AINF=-DELTA_CYC/T_CYC+89.415

     IF(AINF.LT.0) GO TO 1291

     EX=EXP(-DELTA_CYC/(k_B*T_CYC))

     CALL RANDOM_NUMBER(RAN_NUMBER)

     RAN=RAN_NUMBER

     IF(EX-RAN)1291,502,502
```

```
          502       EN_CYC=EN_CYC+DELTA_CYC
                     SX_CYC(N,U,V,W)=X_CYC
                     SY_CYC(N,U,V,W)=Y_CYC
                     IF (ITIME.GT.NOM_CYC) NPAJ_CYC=NPAJ_CYC+1
  1291         END DO
              END DO
            END DO
          END DO
!C
!C * * * MEAN VALUES AND VARIANCE OF MAGNETIC MOMENTS AND
ENERGY * * *
!C FIRST PART OF CALCULATION: SOMMATION OVER THE
SNOM_CYC=IT_CYC-NOM_CYC LAST CYCLES
!C
          IF(ITIME-NOM_CYC)202,202,203
  203     COUNT=COUNT+1
          DO W=1,LW_CYC
```

```
      DO V=1,LV_CYC
        DO U=1,LU_CYC
          DO K=1,NA_CYC
            OMX=OMX+SX_CYC(K,U,V,W)
            OMY=OMY+SY_CYC(K,U,V,W)
            SOMX_CYC(K,U,V,W)=SOMX_CYC(K,U,V,W)+SX_CYC(K,U,V,W)
            SOMY_CYC(K,U,V,W)=SOMY_CYC(K,U,V,W)+SY_CYC(K,U,V,W)

SOMX2_CYC(K,U,V,W)=SOMX2_CYC(K,U,V,W)+SX_CYC(K,U,V,W)**2

SOMY2_CYC(K,U,V,W)=SOMY2_CYC(K,U,V,W)+SY_CYC(K,U,V,W)**2
          END DO
        END DO
      END DO
    END DO
    ENM_CYC=ENM_CYC+EN_CYC
    EN2M_CYC=EN2M_CYC+EN_CYC*EN_CYC
```

```
          MAG2_CYC=MAG2_CYC+OMX**2+OMY**2
          OMX=0.
          OMY=0.
  202   END DO
!C
!C***** END OF MONTE CARLO LOOPS FOR XY SPINS *****
!C

      ELSE IF (IRAN_CYC.EQ.3) THEN     ! HEISENBERG SPINS


!C
!C***** MONTE CARLO LOOPS FOR HEISENBERG SPINS *****
!C

        DO ITIME=1,IT_CYC

          DO W=1,LW_CYC
```

```
     DO V=1,LV_CYC

      DO U=1,LU_CYC

       DO N=1,NA_CYC



        CALL EN3_CALC(N,U,V,W)



        IF (DELTA_CYC.GT.0) THEN

         GO TO 5030

        ELSE

        EX=EXP(DELTA_CYC/(k_B*T_CYC))

        CALL RANDOM_NUMBER(RAN_NUMBER)

        RAN=RAN_NUMBER

        IF(EX-RAN)1301,5030,5030

5030         EN_CYC=EN_CYC-DELTA_CYC

        SX_CYC(N,U,V,W)=X_CYC

        SY_CYC(N,U,V,W)=Y_CYC

        SZ_CYC(N,U,V,W)=Z_CYC
```

```
                END IF

                IF (ITIME.GT.NOM_CYC) NPAJ_CYC=NPAJ_CYC+1

   1301            END DO

            END DO

          END DO

        END DO

        S=0.

         DO W=1,LW_CYC

          DO V=1,LV_CYC

            DO U=1,LU_CYC

              DO N=1,NA_CYC


S=S+(SX_CYC(N,U,V,W)**2+SY_CYC(N,U,V,W)**2+SZ_CYC(N,U,V,W)**2)*
*0.5

              END DO

            END DO

          END DO
```

```
     END DO
     S=S/NAMAX
!C
!C * * * MEAN VALUES AND VARIANCE OF MAGNETIC MOMENTS AND ENERGY * * *
!C FIRST PART OF CALCULATION: SOMMATION OVER THE SNOM_CYC=IT_CYC-NOM_CYC LAST CYCLES
!C
     IF(ITIME-NOM_CYC)302,302,303
 303  COUNT=COUNT+1
     DO W=1,LW_CYC
      DO V=1,LV_CYC
       DO U=1,LU_CYC
        DO K=1,NA_CYC
         OMX=OMX+SX_CYC(K,U,V,W)
         OMY=OMY+SY_CYC(K,U,V,W)
         OMZ=OMZ+SZ_CYC(K,U,V,W)
```

```
        SOMX_CYC(K,U,V,W)=SOMX_CYC(K,U,V,W)+SX_CYC(K,U,V,W)

        SOMY_CYC(K,U,V,W)=SOMY_CYC(K,U,V,W)+SY_CYC(K,U,V,W)

        SOMZ_CYC(K,U,V,W)=SOMZ_CYC(K,U,V,W)+SZ_CYC(K,U,V,W)


SOMX2_CYC(K,U,V,W)=SOMX2_CYC(K,U,V,W)+SX_CYC(K,U,V,W)**2


SOMY2_CYC(K,U,V,W)=SOMY2_CYC(K,U,V,W)+SY_CYC(K,U,V,W)**2


SOMZ2_CYC(K,U,V,W)=SOMZ2_CYC(K,U,V,W)+SZ_CYC(K,U,V,W)**2

       END DO

      END DO

     END DO

    END DO

    ENM_CYC=ENM_CYC+EN_CYC

    EN2M_CYC=EN2M_CYC+EN_CYC*EN_CYC

    MAG2_CYC=MAG2_CYC+OMX**2+OMY**2+OMZ**2

    SM_CYC=SM_CYC+S
```

```
          OMX=0.
          OMY=0.
          OMZ=0.
  302   END DO

!C
!C***** END OF MONTE CARLO LOOPS FOR HEISENBERG SPINS *****
!C

      ELSE IF (IRAN_CYC.EQ.4) THEN     ! q-STATE POTTS PLANAR SPINS

!C
!C***** MONTE CARLO LOOPS FOR q-STATE PLANAR POTTS SPINS *****
!C

        CALL RANDOM_SEED()
        DO 402 ITIME=1,IT_CYC
```

```
      DO W=1,LW_CYC

       DO V=1,LV_CYC

        DO U=1,LU_CYC

         DO N=1,NA_CYC



          CALL ENq_CALC(N,U,V,W)



          ASUP=-DELTA_CYC/T_CYC-88.029

          IF(ASUP.GT.0) GO TO 522

          AINF=-DELTA_CYC/T_CYC+89.415

          IF(AINF.LT.0) GO TO 22

          EX=EXP(-DELTA_CYC/(k_B*T_CYC))

          CALL RANDOM_NUMBER(RAN_NUMBER)

          RAN=RAN_NUMBER

          IF(EX-RAN)22,522,522

522            EN_CYC=EN_CYC+DELTA_CYC
```

```
         SX_CYC(N,U,V,W)=X_CYC
         SY_CYC(N,U,V,W)=Y_CYC
         IF (ITIME.GT.NOM_CYC) NPAJ_CYC=NPAJ_CYC+1
 22      END DO
       END DO
      END DO
     END DO
!C
!C * * * MEAN VALUES AND VARIANCE OF MAGNETIC MOMENTS AND ENERGY * * *
!C FIRST PART OF CALCULATION: SOMMATION OVER THE SNOM_CYC=IT_CYC-NOM_CYC LAST CYCLES
!C
     IF(ITIME-NOM_CYC)402,402,403
 403  COUNT=COUNT+1
     DO W=1,LW_CYC
      DO V=1,LV_CYC
```

```
          DO U=1,LU_CYC
            DO K=1,NA_CYC
              OMX=OMX+SX_CYC(K,U,V,W)
              OMY=OMY+SY_CYC(K,U,V,W)
              SOMX_CYC(K,U,V,W)=SOMX_CYC(K,U,V,W)+SX_CYC(K,U,V,W)

SOMX2_CYC(K,U,V,W)=SOMX2_CYC(K,U,V,W)+SX_CYC(K,U,V,W)**2

SOMY2_CYC(K,U,V,W)=SOMY2_CYC(K,U,V,W)+SY_CYC(K,U,V,W)**2
            END DO
          END DO
        END DO
      END DO
      ENM_CYC=ENM_CYC+EN_CYC
      EN2M_CYC=EN2M_CYC+EN_CYC*EN_CYC
      MAG2_CYC=MAG2_CYC+OMX**2+OMY**2
```

```
          OMX=0.

          OMY=0.

  402   END DO


!C

!C***** END OF MONTE CARLO LOOPS FOR q-STATE POTTS SPINS *****

!C


      END IF


      DO W=1,LW_CYC

        DO V=1,LV_CYC

          DO U=1,LU_CYC

            DO K=1,NA_CYC

              SOMX_CYC(K,U,V,W)=SOMX_CYC(K,U,V,W)/SNOM_CYC

              COMX_CYC(K,U,V,W)=SOMX_CYC(K,U,V,W)

              SOMY_CYC(K,U,V,W)=SOMY_CYC(K,U,V,W)/SNOM_CYC
```

```
        SOMZ_CYC(K,U,V,W)=SOMZ_CYC(K,U,V,W)/SNOM_CYC

        SOMX2_CYC(K,U,V,W)=SOMX2_CYC(K,U,V,W)/SNOM_CYC

        SOMY2_CYC(K,U,V,W)=SOMY2_CYC(K,U,V,W)/SNOM_CYC

        SOMZ2_CYC(K,U,V,W)=SOMZ2_CYC(K,U,V,W)/SNOM_CYC

        AX=SOMX2_CYC(K,U,V,W)-SOMX_CYC(K,U,V,W)**2

        IF(AX.LT.0) AX=0

        AY=SOMY2_CYC(K,U,V,W)-SOMY_CYC(K,U,V,W)**2

        IF(AY.LT.0) AY=0

        AZ=SOMZ2_CYC(K,U,V,W)-SOMZ_CYC(K,U,V,W)**2

        IF(AZ.LT.0) AZ=0

        SOMX2_CYC(K,U,V,W)=SQRT(AX)

        SOMY2_CYC(K,U,V,W)=SQRT(AY)

        SOMZ2_CYC(K,U,V,W)=SQRT(AZ)

      END DO

    END DO

  END DO

END DO
```

```
   RETURN

  END SUBROUTINE MC_CYCLE

 SUBROUTINE RAN3D(RADIUS,X1,Y1,Z1)
      REAL*8
RADIUS,RADIUS_R3,R1,R2,R3,X_sub,Y_sub,Z_sub,RR,SCALE,X1,Y1,Z1
     COMMON /RAN/RADIUS_R3
 1080    CALL RANDOM_NUMBER(R1)
     CALL RANDOM_NUMBER(R2)
     CALL RANDOM_NUMBER(R3)
     RADIUS=RADIUS_R3
     X_sub  =  2.*R1 - 1.
     Y_sub  =  2.*R2 - 1.
     Z_sub  =  2.*R3 - 1.
     RR =  X_sub*X_sub + Y_sub*Y_sub + Z_sub*Z_sub
```

```
          IF(RR .GT. 1.)  GOTO 1080

          SCALE  =  RADIUS / SQRT(RR)

          X1  =  X_sub * SCALE

          Y1  =  Y_sub * SCALE

          Z1  =  Z_sub * SCALE

          RETURN

END SUBROUTINE RAN3D



SUBROUTINE EN3_CALC(N_EN3,U_EN3,V_EN3,W_EN3)

          INCLUDE 'MCMAG.INC'



          INTEGER
N_EN3,U_EN3,V_EN3,W_EN3,K,I,IM_EN3,NFIP_EN3,NMULT_EN3

          REAL*8
DELTA_EN3,X_EN3,Y_EN3,Z_EN3,TCOJX_EN3,TCOJY_EN3,TCOJZ_EN3,TC
OJXY_EN3,TCOJXZ_EN3,TCOJYZ_EN3,TCOJYX_EN3,TCOJZX_EN3,TCOJZY
_EN3,&

                 HX_EN3,HY_EN3,HZ_EN3,X,Y,Z,RADIUS_EN3,G,U_B
```

```
        REAL*8,
DIMENSION(NAMAX)::AMPS_EN3,AMPS2_EN3,AJSX_EN3,AJSY_EN3,AJSZ
_EN3,D_EN3,DX_EN3,DY_EN3,DZ_EN3

        REAL*8,
DIMENSION(NAMAX,NNMAX)::AJXX_EN3,AJYY_EN3,AJZZ_EN3,AJJX_EN
3,AJJY_EN3,AJJZ_EN3,AJXY_EN3,AJXZ_EN3,AJYZ_EN3,AJYX_EN3,AJZX_E
N3,AJZY_EN3

        INTEGER, DIMENSION(NAMAX,NNMAX)::NAV_EN3

        REAL*8,
DIMENSION(NAMAX,NUMAX+1,NVMAX+1,NWMAX+1)::SX_EN3,SY_EN3,
SZ_EN3

        REAL*8,
DIMENSION(NAMAX,NUMAX,NVMAX,NWMAX)::SOMX_EN3

        INTEGER, DIMENSION(NAMAX)::NVS_EN3

        INTEGER, DIMENSION(NNMAX)::NU_EN3,NV_EN3,NW_EN3

        REAL*8,
DIMENSION(NMOMAX)::IUM_EN3,IVM_EN3,IWM_EN3,NUMB_EN3,AJMO
D_EN3

        INTEGER, DIMENSION(NMOMAX)::NM_EN3
```

```
       CHARACTER*1 ANSMOD_EN3
   COMMON /FIELD/HX_EN3,HY_EN3,HZ_EN3,&
           /COM8/NVS_EN3,              &
           /CONDL/NU_EN3,NV_EN3,NW_EN3,          &
/TEST/AJJX_EN3,AJJY_EN3,AJJZ_EN3,AJXY_EN3,AJXZ_EN3,AJYZ_EN3,AJYX_EN3,AJZX_EN3,AJZY_EN3, &
           /TEST20/NAV_EN3,    &
           /READ4/D_EN3,DX_EN3,DY_EN3,DZ_EN3,          &
           /CYC1/AJXX_EN3,AJYY_EN3,AJZZ_EN3,        &
/CYC2/AJMOD_EN3,IUM_EN3,IVM_EN3,IWM_EN3,NUMB_EN3,NM_EN3,IM_EN3, &
           /CYC9/SOMX_EN3,AJSX_EN3,AJSY_EN3,AJSZ_EN3,    &
           /CYC3/SX_EN3,SY_EN3,SZ_EN3,&
           /COM5/AMPS_EN3,AMPS2_EN3,
           /MOD1/ANSMOD_EN3,            &
```

```
/CYC8/DELTA_EN3,X_EN3,Y_EN3,Z_EN3,NFIP_EN3,NMULT_EN3,&

        /RAN/RADIUS_EN3

     G=2.0

     U_B=9.274099D-24



     AJSX_EN3(N_EN3)=0

     AJSY_EN3(N_EN3)=0

     AJSZ_EN3(N_EN3)=0



     DO K=1,NVS_EN3(N_EN3)

      AJXX_EN3(N_EN3,K)=AJJX_EN3(N_EN3,K)

      AJYY_EN3(N_EN3,K)=AJJY_EN3(N_EN3,K)

      AJZZ_EN3(N_EN3,K)=AJJZ_EN3(N_EN3,K)



  !C

  !C*****    LOCAL MODIFICATION OF COUPLING (IF ANY)    ******
```

```
!C



        IF ((ANSMOD_EN3.EQ.'Y').OR.(ANSMOD_EN3.EQ.'y')) THEN

          DO I=1,IM_EN3

            IF
((W_EN3.EQ.IWM_EN3(I)).AND.(V_EN3.EQ.IVM_EN3(I)).AND.(U_EN3.EQ.IU
M_EN3(I))&

                .AND.(N_EN3.EQ.NM_EN3(I)).AND.(K.EQ.NUMB_EN3(I)) ) THEN

              AJXX_EN3(N_EN3,K)=AJMOD_EN3(I)

              AJYY_EN3(N_EN3,K)=AJMOD_EN3(I)

              AJZZ_EN3(N_EN3,K)=AJMOD_EN3(I)

            END IF

          END DO


!C

!C*****    END OF MODIFICATION    *****

!C
```

```
        END IF


        CALL BOUND_COND(N_EN3,K,U_EN3,V_EN3,W_EN3)


   !C
   !C*****    COMPUTE DELTA    *****
   !C
        IF
(  (NAV_EN3(N_EN3,K).NE.N_EN3).OR.(NU_EN3(K).NE.U_EN3).OR.(NV_EN3
(K).NE.V_EN3)&
            .OR.(NW_EN3(K).NE.W_EN3) ) THEN


AJSX_EN3(N_EN3)=AJSX_EN3(N_EN3)+AJXX_EN3(N_EN3,K)*SX_EN3(NAV
_EN3(N_EN3,K),NU_EN3(K),NV_EN3(K),NW_EN3(K))&


+AJXY_EN3(N_EN3,K)*SY_EN3(NAV_EN3(N_EN3,K),NU_EN3(K),NV_EN3(
K),NW_EN3(K))&
```

```
+AJXZ_EN3(N_EN3,K)*SZ_EN3(NAV_EN3(N_EN3,K),NU_EN3(K),NV_EN3(K
),NW_EN3(K))

AJSY_EN3(N_EN3)=AJSY_EN3(N_EN3)+AJYY_EN3(N_EN3,K)*SY_EN3(NAV
_EN3(N_EN3,K),NU_EN3(K),NV_EN3(K),NW_EN3(K))&

+AJYX_EN3(N_EN3,K)*SX_EN3(NAV_EN3(N_EN3,K),NU_EN3(K),NV_EN3(
K),NW_EN3(K))&

+AJYZ_EN3(N_EN3,K)*SZ_EN3(NAV_EN3(N_EN3,K),NU_EN3(K),NV_EN3(K
),NW_EN3(K))

AJSZ_EN3(N_EN3)=AJSZ_EN3(N_EN3)+AJZZ_EN3(N_EN3,K)*SZ_EN3(NAV_
EN3(N_EN3,K),NU_EN3(K),NV_EN3(K),NW_EN3(K))&

+AJZX_EN3(N_EN3,K)*SX_EN3(NAV_EN3(N_EN3,K),NU_EN3(K),NV_EN3(K
),NW_EN3(K))&
```

```
+AJZY_EN3(N_EN3,K)*SY_EN3(NAV_EN3(N_EN3,K),NU_EN3(K),NV_EN3(K
),NW_EN3(K))
          END IF
        END DO
   IF (NFIP_EN3.NE.0) THEN
          RADIUS_EN3=AMPS2_EN3(N_EN3)
          CALL RAN3D(RADIUS_EN3,X_EN3,Y_EN3,Z_EN3)
        END IF
   DELTA_EN3 = -((SX_EN3(N_EN3,U_EN3,V_EN3,W_EN3)-
X_EN3)*(0.5*AJSX_EN3(N_EN3)+(G*U_B*HX_EN3))&
             +(SY_EN3(N_EN3,U_EN3,V_EN3,W_EN3)-
Y_EN3)*(0.5*AJSY_EN3(N_EN3)+(G*U_B*HY_EN3))&
             +(SZ_EN3(N_EN3,U_EN3,V_EN3,W_EN3)-
Z_EN3)*(0.5*AJSZ_EN3(N_EN3)+(G*U_B*HZ_EN3)))
   RETURN
END SUBROUTINE EN3_CALC
```

References

[1] J. W. Klement, R. H. Willens, and P. Duwez, "Non-crystalline structure in solidified gold–silicon alloys," *Nature,* vol. 187, pp. 869-870, 1960.

[2] H. W. Kui, A. L. Greer, and D. Turnbull, "Formation of bulk metallic glass by fluxing," *Applied Physics Letters,* vol. 45, p. 615, 1984.

[3] C. Suryanarayana and A. Inoue, *Bulk Metallic Glasses*. Boca Raton: CRC Press, 2010.

[4] A. Inoue, N. Nishiyama, and H. Kimura, "Preparation and thermal stability of bulk amorphous $Pd_{40}Cu_{30}Ni_{10}P_{20}$ alloy cylinder of 72 mm in diameter," *Materials Transactions Jim,* vol. 38, pp. 179-183, Feb 1997.

[5] A. Inoue, K. Kita, T. Zhang, and T. Masumoto, "An Amorphous $La_{55}AI_{25}Ni_{20}$ Alloy Prepared by Water Quenching," *Materials Transactions Jim,* vol. 30, pp. 722-725, 1989.

[6] S. Li, D. Q. Zhao, M. X. Pan, and W. H. Wang, "A bulk metallic glass based on heavy rare earth gadolinium," *Journal of Non-Crystalline Solids,* vol. 351, pp. 2568-2571, Sep 2005.

[7] T. D. Shen, U. Harms, and R. B. Schwarz, "Bulk Fe-Based Metallic Glass with Extremely Soft Ferromagnetic Properties," *Materials Science Forum,* vol. 386-388, pp. 441-446, 2002.

[8] A. Inoue, "Recent progress of Zr-based bulk amorphous alloys," *Science Reports of the Research Institutes Tohoku University Series a-Physics Chemistry and Metallurgy,* vol. 42, pp. 1-11, Mar 1996.

[9] A. Inoue, "Bulk amorphous alloys with soft and hard magnetic properties," *Materials Science and Engineering a-Structural Materials Properties Microstructure and Processing*, vol. 226, pp. 357-363, Jun 1997.

[10] I. W. Donald and H. A. Davies, "Prediction of glass-forming ability for metallic systems," *Journal of Non-Crystalline Solids,* vol. 30, pp. 77-85, 1978.

[11] A. Hrubý, "Evaluation of glass-forming tendency by means of DTA," *Czechoslovak Journal of Physics,* vol. 22, pp. 1187-1193, 1972.

[12] Y. Li, S. C. Ng, C. K. Ong, H. H. Hng, and T. T. Goh, "Glass forming ability of bulk glass forming alloys," *Scripta Materialia,* vol. 36, pp. 783-787, 1997.

[13] Z. P. Lu and C. T. Liu, "A new glass-forming ability criterion for bulk metallic glasses," *Acta Materialia,* vol. 50, pp. 3501-3512, 2002.

[14] W. Thomson, "II. On the thermoelastic, thermomagnetic, and pyroelectric properties of matter," *Philosophical Magazine Series 5,* vol. 5, pp. 4-27, 1878/01/01 1878.

[15] E. Warburg, "Magnetische Untersuchungen," *Annalen der Physik,* vol. 249, pp. 141-164, 1881.

[16] K. A. GschneidnerJr, V. K. Pecharsky, and A. O. Tsokol, "Recent developments in magnetocaloric materials," *Reports on Progress in Physics,* vol. 68, pp. 1479-1539, 2005.

[17] V. K. Pecharsky and J. K. A. Gschneidner, "Giant Magnetocaloric Effect in $Gd_5(Si_2Ge_2)$," *Physical Review Letters*, vol. 78, pp. 4494-4497, 1997.

[18] L. Xia, K. C. Chan, and M. B. Tang, "Enhanced glass forming ability and refrigerant capacity of a $Gd_{55}Ni_{22}Mn_3Al_{20}$ bulk metallic glass," *Journal of Alloys and Compounds*, vol. 509, pp. 6640-6643, 2011.

[19] S. Lu, M. B. Tang, and L. Xia, "Excellent magnetocaloric effect of a $Gd_{55}Al_{20}Co_{25}$ bulk metallic glass," *Physica B: Condensed Matter*, vol. 406, pp. 3398-3401, 2011.

[20] H. Fu and M. Zou, "Magnetic and magnetocaloric properties of ternary Gd–Co–Al bulk metallic glasses," *Journal of Alloys and Compounds*, vol. 509, pp. 4613-4616, 2011.

[21] Z. Zheng, X. Zhong, K. Su, H. Yu, Z. Liu, and D. Zeng, "Magnetic properties and large magnetocaloric effects in amorphous Gd-Al-Fe alloys for magnetic refrigeration," *Science China Physics, Mechanics and Astronomy*, vol. 54, pp. 1267-1270, 2011.

[22] H. Fu, M. Zou, Q. Cao, V. K. Pecharsky, K. A. Gschneidner, and L. S. Chumbley, "Microstructure and magnetocaloric effects in partially amorphous $Gd_{55}Co_{15}Al_{30-x}Si_x$ alloys," *Materials Science and Engineering: A*, vol. 528, pp. 5219-5222, 2011.

[23] V. Franco, A. Conde, J. M. Romero-Enrique, and J. S. Blázquez, "A universal curve for the magnetocaloric effect: an analysis based on scaling relations," *Journal of Physics: Condensed Matter*, vol. 20, p. 285207, 2008.

[24] P. Duwez, "Amorphous Ferromagnetic Phase in Iron-Carbon-Phosphorus Alloys," *Journal of Applied Physics*, vol. 38, p. 4096, 1967.

[25] F. Johnson and R. D. Shull, "Amorphous-FeCoCrZrB ferromagnets for use as high-temperature magnetic refrigerants," *Journal of Applied Physics,* vol. 99, p. 08K909, 2006.

[26] H. Hiroyoshi, "Arrott-Noakes plots near the Curie temperature of Fe_3Pt: Ordered and disordered alloys in high magnetic fields," *Journal of Applied Physics,* vol. 53, p. 2453, 1982.

[27] I. Kucuk, M. Aykol, O. Uzun, M. Yildirim, M. Kabaer, N. Duman, F. Yilmaz, K. Erturk, M. V. Akdeniz, and A. O. Mekhrabov, "Effect of (Mo, W) substitution for Nb on glass forming ability and magnetic properties of Fe–Co-based bulk amorphous alloys fabricated by centrifugal casting," *Journal of Alloys and Compounds,* vol. 509, pp. 2334-2337, 2011.

[28] P. Álvarez, J. L. Sánchez Llamazares, P. Gorria, and J. s. A. Blanco, "Enhanced refrigerant capacity and magnetic entropy flattening using a two-amorphous FeZrB(Cu) composite," *Applied Physics Letters,* vol. 99, p. 232501, 2011.

[29] F. J. Liu, K. F. Yao, and H. Y. Ding, "Fe-based glassy alloys with high iron content and high saturation magnetization," *Intermetallics,* vol. 19, pp. 1674-1677, 2011.

[30] A. Makino, T. Kubota, C. Chang, M. Makabe, and A. Inoue, "FeSiBP Bulk Metallic Glasses with Unusual Combination of High Magnetization and High Glass-Forming Ability," *Materials Transactions,* vol. 48, pp. 3024-3027, 2007.

[31] V. Franco, J. S. Blázquez, and A. Conde, "Field dependence of the magnetocaloric effect in materials with a second order phase transition: A master curve for the magnetic entropy change," *Applied Physics Letters*, vol. 89, p. 222512, 2006.

[32] J. Y. Law, V. Franco, and R. V. Ramanujan, "Influence of La and Ce additions on the magnetocaloric effect of Fe–B–Cr-based amorphous alloys," *Applied Physics Letters,* vol. 98, p. 192503, 2011.

[33] H. Oesterreicher and F. T. Parker, "Magnetic cooling near Curie temperatures above 300 K," *Journal of Applied Physics,* vol. 55, p. 4334, 1984.

[34] B. Schwarz, N. Mattern, Q. Luo, and J. Eckert, "Magnetic properties and magnetocaloric effect of rapidly quenched Gd–Co–Fe–Al alloys," *Journal of Magnetism and Magnetic Materials,* vol. 324, pp. 1581-1587, 2012.

[35] K. A. Gschneidner and V. K. Pecharsky, "Magnetic refrigeration materials (invited)," *Journal of Applied Physics*, vol. 85, p. 5365, 1999.

[36] J. Gondro, J. Świerczek, J. Olszewski, J. Zbroszczyk, K. Sobczyk, W. H. Ciurzyńska, J. Rzącki, and M. NabiaŁek, "Magnetization behavior and magnetocaloric effect in bulk amorphous $Fe_{60}Co_5Zr_8Mo_5W_2B_{20}$ alloy," *Journal of Magnetism and Magnetic Materials,* vol. 324, pp. 1360-1364, 2012.

[37] P. Álvarez, J. S. Marcos, P. Gorria, L. F. Barqu ń, and J. A. Blanco, "Magneto-caloric effect in FeZrB amorphous alloys near room temperature," *Journal of Alloys and Compounds,* vol. 504, pp. S150-S154, 2010.

[38] Y. K. Fang, C. C. Yeh, C. C. Hsieh, C. W. Chang, H. W. Chang, W. C. Chang, X. M. Li, and W. Li, "Magnetocaloric effect in Fe–Zr–B–M (M=Mn, Cr, and Co) amorphous systems," *Journal of Applied Physics*, vol. 105, p. 07A910, 2009.

[39] S. Gorsse, C. Mayer, and B. Chevalier, "Magnetocaloric effect in $Tb_{60}Ni_{30}Al_{10}$ glass: A material that can either heat or cool upon magnetization," *Journal of Applied Physics,* vol. 109, p. 033914, 2011.

[40] J. H. Lee, S. J. Lee, W. B. Han, H. H. An, and C. S. Yoon, "Magnetocaloric effect of $Fe_{64}Mn_{15-x}Co_xSi_{10}B_{11}$ amorphous alloys," *Journal of Alloys and Compounds,* vol. 509, pp. 7764-7767, 2011.

[41] V. Franco, A. Conde, and L. F. Kiss, "Magnetocaloric response of FeCrB amorphous alloys: Predicting the magnetic entropy change from the Arrott–Noakes equation of state," *Journal of Applied Physics,* vol. 104, p. 033903, 2008.

[42] J. Gao, H. U. I. Cao, Y. Zhang, and Z. Dong, "PHASE RELATIONS AND MICROSTRUCTURE OF La-Fe-Si ALLOYS UNDER DIFFERENT SOLIDIFICATION CONDITIONS," *International Journal of Modern Physics B,* vol. 25, p. 4277, 2011.

[43] B. F. Yu, Q. Gao, B. Zhang, X. Z. Meng, and Z. Chen, "Review on research of room temperature magnetic refrigeration," *International Journal of Refrigeration,* vol. 26, pp. 622-636, 2003.

[44] C.-Y. Lin, H.-Y. Tien, and T.-S. Chin, "Soft magnetic ternary iron-boron-based bulk metallic glasses," *Applied Physics Letters,* vol. 86, p. 162501, 2005.

[45] V. K. Pecharsky and K. A. Gschneidner, "Some common misconceptions concerning magnetic refrigerant materials," *Journal of Applied Physics,* vol. 90, p. 4614, 2001.

[46] J. Wang, R. Li, N. Hua, L. Huang, and T. Zhang, "Ternary Fe–P–C bulk metallic glass with good soft-magnetic and mechanical properties," *Scripta Materialia,* vol. 65, pp. 536-539, 2011.

[47] V. Franco, J. S. Blázquez, M. Millán, J. M. Borrego, C. F. Conde, and A. Conde, "The magnetocaloric effect in soft magnetic amorphous alloys," *Journal of Applied Physics,* vol. 101, p. 09C503, 2007.

[48] Y. Wang and X. Bi, "The role of Zr and B in room temperature magnetic entropy change of FeZrB amorphous alloys," *Applied Physics Letters,* vol. 95, p. 262501, 2009.

[49] N. A. de Oliveira and P. J. von Ranke, "Theoretical aspects of the magnetocaloric effect," *Physics Reports,* vol. 489, pp. 89-159, 2010.

[50] I. Skorvanek and J. Kovac, "Magnetocaloric behaviour in amorphous and nanocrystalline FeNbB soft magnetic alloys," *Czechoslovak Journal of Physics,* vol. 54, pp. D189-D192, 2004.

[51] V. K. Pecharsky and K. A. Gschneidner, "Magnetocaloric effect and magnetic refrigeration," *Journal of Magnetism and Magnetic Materials,* vol. 200, pp. 44-56, Oct 1999.

[52] J. M. Barandiarán and J. Colmenero, "Continuous cooling approximation for the formation of a glass," *Journal of Non-Crystalline Solids,* vol. 46, pp. 277-287, 1981.

[53] H. Men and D. H. Kim, "Fabrication of ternary Mg–Cu–Gd bulk metallic glass with high glass-forming ability under air atmosphere," *Journal of Materials Research,* vol. 18, pp. 1502-1504, 2003.

[54] X. H. Lin and W. L. Johnson, "Formation of Ti–Zr–Cu–Ni bulk metallic glasses," *Journal of Applied Physics,* vol. 78, pp. 6514-6519, 1995.

[55] Z. P. Lu, Y. Li, and S. C. Ng, "Reduced glass transition temperature and glass forming ability of bulk glass forming alloys," *Journal of Non-Crystalline Solids,* vol. 270, pp. 103-114, 2000.

[56] B. Cantor, U. o. S. M. S. Group, and M. Society, *Rapidly quenched metals III: proceedings of the Third International Conference on Rapidly Quenched Metals, organised jointly by the Materials Science Group of the University of Sussex and the Metals Society, London, and held at the University of Sussex, Brighton, on 3-7 July, 1978*: Metals Society, 1978.

[57] A. Inoue, T. Zhang, A. Takeuchi, and W. Zhang, "Hard magnetic bulk amorphous Nd-Fe-Al alloys of 12 mm in diameter made by suction casting," *Materials Transaction, JIM,* vol. 37, pp. 636-640, 1996.

[58] W. L. Johnson, "Bulk Glass-Forming Metallic Alloys: Science and Technology [1998 Mrs Medal Award Lecture, Presented at Symposium Mm]," *MRS Proceedings,* vol. 554, 2011.

[59] T. Egami, "The atomic structure of aluminum based metallic glasses and universal criterion for glass formation," *Journal of Non-Crystalline Solids,* vol. 205–207, Part 2, pp. 575-582, 1996.

[60] T. Egami and Y. Waseda, "Atomic size effect on the formability of metallic glasses," *Journal of Non-Crystalline Solids*, vol. 64, pp. 113-134, 1984.

[61] A. Inoue, "Recent Progress of Zr-Based Bulk Amorphous Alloys," *Science reports of the Research Institutes, Tohoku University. Ser. A, Physics, chemistry and metallurgy*, vol. 42, pp. 1-11, 1996/03/28 1996.

[62] I. Akihisa, "Stabilization of Supercooled Liquid and Opening-up of Bulk Glassy Alloys," *Proceedings of the Japan Academy. Ser. B: Physical and Biological Sciences*, vol. 73, pp. 19-24, 1997 1997.

[63] D. Xu, B. Lohwongwatana, G. Duan, W. L. Johnson, and C. Garland, "Bulk metallic glass formation in binary Cu-rich alloy series – Cu100−xZrx (x=34, 36, 38.2, 40 at.%) and mechanical properties of bulk Cu64Zr36 glass," *Acta Materialia*, vol. 52, pp. 2621-2624, 2004.

[64] K.-F. Yao and F. Ruan, "Pd--Si Binary Bulk Metallic Glass Prepared at Low Cooling Rate," *Chinese Physics Letters*, vol. 22, pp. 1481-1483, 2005.

[65] L. Xia, W. H. Li, S. S. Fang, B. C. Wei, and Y. D. Dong, "Binary Ni–Nb bulk metallic glasses," *Journal of Applied Physics*, vol. 99, p. 026103, 2006.

[66] R. Schulz, K. Samwer, and W. L. Johnson, "Kinetics of phase separation in Cu50Zr50 metallic glasses," *Journal of Non-Crystalline Solids*, vol. 61–62, Part 2, pp. 997-1002, 1984.

[67] K. V. Rao, R. Malmhall, G. Backstrom, and S. M. Bhagat, "Hall effect in amorphous magentic materials-Metglas 2826 and 2826B," *Solic State Communications*, vol. 19, pp. 193-195, 1976.

[68] E. Figueroa, L. Lundgren, O. Beckman, and S. M. Bhagat, "The anomalous magnetisation of amorphous Metglas 2826-A," *Solid State Communications*, vol. 20, pp. 961-964, 1976.

[69] R. Malmhall, G. Backstrom, K. V. Rao, S. M. Bhagat, M. Meichle, and M. B. Salamon, "Metglas 2826B-transport, magnetic and thermal properties," *Journal of Applied Physics*, vol. 49, pp. 1727-1729, 1978.

[70] W. H. Wang, C. Dong, and C. H. Shek, "Bulk metallic glass," *Materials Science Engineering R*, vol. 44, pp. 45-89, 2004.

[71] Available: www.liquidmetals.com

[72] A. M. Tishin and Y. I. Spichkin, *The magnetocaloric effect and its applications*: Institute of Physics Publishing, 2003.

[73] A. M. Tishin, "Magnetocaloric effect in strong magnetic fields," *Cryogenics*, vol. 30, pp. 127-136, 1990.

[74] E. S. R. Gopal, *Specific heats at low temperatures*: Plenum Press, 1966.

[75] W. J. Moore, "Thermodynamics of solids (Swalin, Richard A.)," *Journal of Chemical Education*, vol. 39, p. 488, 1962/09/01 1962.

[76] A. M. Tishin, J. K.A. Gschneidner, and V. K. Pecharsky, "Magnetocaloric effect and heat capacity in the phase-transition region," *Physical Review B*, vol. 59, pp. 503-511, 1999.

[77] B. Yu, M. Liu, P. W. Egolf, and A. Kitanovski, "A review of magnetic refrigerator and heat pump prototypes built before the year 2010," *International Journal of Refrigeration,* vol. 33, pp. 1029-1060, 2010.

[78] W. A. Steyert, "Stirling-cycle rotating magnetic refrigerators and heat engines for use near room temperature," *Journal of Applied Physics,* vol. 49, p. 1216, 1978.

[79] L. D. Kirol and M. W. Dacus, "Rotary recuperative magnetic heat pump," 1988, pp. 757-765.

[80] C. Zimm, A. Jastrab, A. Sternberg, V. Pecharsky, K. Gschneidner Jr, M. Osborne, and I. Anderson, "Description and performance of a near-room temperature magnetic refrigerator," *Advances in cryogenic engineering,* vol. 43, pp. 1759-1766, 1998.

[81] Z. Yan and J. Chen, "The effect of field dependent heat capacity on the characteristics of the ferromagnetic Ericsson refrigeration cycle," *Journal of Applied Physics,* vol. 72, pp. 1-5, 1992.

[82] J. Chen and Z. Yan, "The effect of field - dependent heat capacity on regeneration in magnetic Ericsson cycles," *Journal of Applied Physics,* vol. 69, p. 6245, 1991.

[83] W. Dai, "Regenerative balance in magnetic Ericsson refrigeration cycles," *Journal of Applied Physics,* vol. 71, pp. 5272-5274, 1992.

[84] R. Caballero-Flores, V. Franco, A. Conde, K. Knipling, and M. Willard, "Optimization of the refrigerant capacity in multiphase magnetocaloric materials," *Applied Physics Letters*, vol. 98, p. 102505, 2011.

[85] K. Gschneidner Jr and V. Pecharsky, "Magnetocaloric materials," *Annual review of materials science*, vol. 30, pp. 387-429, 2000.

[86] A. M. Tishin, "Chapter 4 Magnetocaloric effect in the vicinity of phase transitions," in *Handbook of Magnetic Materials*. vol. Volume 12, K. H. J. Buschow, Ed., ed: Elsevier, 1999, pp. 395-524.

[87] K. A. Gschneidner and V. K. Pecharsky, "Magnetic Refrigeration," in *Intermetallic Compounds - Principles and Practice*, ed: John Wiley & Sons, Ltd, 2002, pp. 519-539.

[88] B. Ekkes, "Developments in magnetocaloric refrigeration," *Journal of Physics D: Applied Physics*, vol. 38, p. R381, 2005.

[89] L. Morellon, P. A. Algarabel, M. R. Ibarra, J. Blasco, B. García-Landa, Z. Arnold, and F. Albertini, "Magnetic-field-induced structural phase transition in $Gd_5(Si_{1.8}Ge_{2.2})$," *Physical Review B*, vol. 58, pp. R14721-R14724, 1998.

[90] W. Choe, V. K. Pecharsky, A. O. Pecharsky, K. A. Gschneidner, Jr., V. G. Young, Jr., and G. J. Miller, "Making and Breaking Covalent Bonds across the Magnetic Transition in the Giant Magnetocaloric Material $Gd_5(Si_2Ge_2)$," *Physical Review Letters*, vol. 84, pp. 4617-4620, 2000.

[91] A. Fujita, K. Fukamichi, K. Koyama, and K. Watanabe, "X-ray diffraction study in high magnetic fields of magnetovolume effect in itinerant-electron

metamagnetic La$(Fe_{0.88}Si_{0.12})_{13}$ compound," *Journal of Applied Physics,* vol. 95, pp. 6687-6689, 2004.

[92] V. Provenzano, A. J. Shapiro, and R. D. Shull, "Reduction of hysteresis losses in the magnetic refrigerant Gd5Ge2Si2 by the addition of iron," *Nature,* vol. 429, pp. 853-857, 2004.

[93] K. A. Gschneidner, Jr., V. K. Pecharsky, E. Brück, H. G. M. Duijn, and E. M. Levin, "Comment on “Direct Measurement of the `Giant' Adiabatic Temperature Change in $Gd_5Si_2Ge_2$”," *Physical Review Letters,* vol. 85, pp. 4190-4190, 2000.

[94] W. F. Giauque and D. P. MacDougall, "Attainment of Temperatures Below 1 ° Absolute by Demagnetization of Gd_{2}(SO_{4})_{3} ·8H_{2}O," *Physical Review,* vol. 43, pp. 768-768, 1933.

[95] B. Schwarz, N. Mattern, J. Moore, K. Skokov, O. Gutfleisch, and J. Eckert, "Influence of sample geometry on determination of magnetocaloric effect for Gd60Co30Al10 glassy ribbons using direct and indirect methods," *Journal of Magnetism and Magnetic Materials,* 2011.

[96] T. V. Jayaraman, M. A. Koten, and J. E. Shield, "Near room temperature magnetocaloric properties of melt-spun Gd100-xBx (x= 0, 5, 10, 15, & 20 at.%) alloys," *Journal of Magnetism and Magnetic Materials,* 2011.

[97] X. Zhong, P. Tang, Z. Liu, D. Zeng, Z. Zheng, H. Yu, W. Qiu, and M. Zou, "Magnetic properties and large magnetocaloric effect in Gd-Ni amorphous ribbons for magnetic refrigeration applications in intermediate temperature range," *Journal of Alloys and Compounds,* 2011.

[98] N. S. Bingham, H. Wang, F. Qin, H. X. Peng, J. F. Sun, V. Franco, H. Srikanth, and M. H. Phan, "Excellent magnetocaloric properties of melt-extracted Gd-based amorphous microwires," *Applied Physics Letters,* vol. 101, p. 102407, 2012.

[99] Q. Luo, D. Q. Zhao, M. X. Pan, and W. H. Wang, "Magnetocaloric effect in Gd-based bulk metallic glasses," *Applied Physics Letters,* vol. 89, p. 081914, 2006.

[100] Q. Dong, B. Shen, J. Chen, J. Shen, F. Wang, H. Zhang, and J. Sun, "Large magnetic refrigerant capacity in Gd71Fe3Al26 and Gd65Fe20Al15 amorphous alloys," *Journal of Applied Physics*, vol. 105, pp. 053908-053908-4, 2009.

[101] Q. Y. Dong, B. G. Shen, J. Chen, J. Shen, H. W. Zhang, and J. R. Sun, "Magnetic entropy change and refrigerant capacity in GdFeAl compound," *Journal Of Applied Physics,* vol. 105, pp. 07A305-07A305-3, Apr 1 2009.

[102] B. Schwarz, B. Podmilsak, N. Mattern, and J. Eckert, "Magnetocaloric effect in Gd-based Gd60FexCo30-xAl10 metallic glasses," *Journal of Magnetism and Magnetic Materials,* vol. 322, pp. 2298-2303, 2010.

[103] J. Law, R. Ramanujan, and V. Franco, "Tunable Curie temperatures in Gd alloyed Fe-B-Cr magnetocaloric materials," *Journal of Alloys and Compounds,* vol. 508, pp. 14-19, 2010.

[104] M. Phejar, V. Paul-Boncour, and L. Bessais, "Structural and magnetic properties of magnetocaloric LaFe13-xSix compounds synthesized by high energy ball-milling," *Intermetallics,* vol. 18, pp. 2301-2307, 2010.

[105] K. A. Gschneidner and V. K. Pecharsky, "Thirty years of near room temperature magnetic cooling: Where we are today and future prospects," *International Journal of Refrigeration,* vol. 31, pp. 945-961, 2008.

[106] V. Franco and A. Conde, "Scaling laws for the magnetocaloric effect in second order phase transitions: From physics to applications for the characterization of materials," *International Journal of Refrigeration,* vol. 33, pp. 465-473, 2010.

[107] A. Arrott and J. E. Noakes, "Approximate Equation of State For Nickel Near its Critical Temperature," *Physical Review Letters,* vol. 19, pp. 786-789, 1967.

[108] N. Metropolis and S. Ulam, "The Monte Carlo Method," *Journal of the American Statistical Association,* vol. 44, pp. 335-341, 1949.

[109] D. P. Landau and K. Binder, *A guide to monte carlo simulations in statistical physics - 3rd Edition*. New York: Cambridge University Press, 2009.

[110] P. Lacorre and J. Pannetier, "MCMAG: A computer program to simulate magnetic structures," *Journal of Magnetism and Magnetic Materials,* vol. 71, pp. 63-82, 1987.

[111] L. H. Bennett, R. D. McMichael, H. C. Tang, and R. E. Watson, "Monte Carlo simulations of the magnetocaloric effect in superferromagnetic clusters having uniaxial magnetic anisotropy," *Journal Of Applied Physics,* vol. 75, pp. 5493-5495, 1994.

[112] E. P. Nóbrega, N. A. d. Oliveira, P. J. v. Ranke, and A. Troper, "The magnetocaloric effect in R5Si4 (R = Gd, Tb): a Monte Carlo calculation," *Journal of Physics: Condensed Matter,* vol. 18, pp. 1275-1283, 2006.

[113] E. P. Nóbrega, N. A. de Oliveira, P. J. von Ranke, and A. Troper, "Monte Carlo calculations of the magnetocaloric effect in RAl2 (R=Dy,Er)," *Journal Of Applied Physics,* vol. 99, p. 08Q103, 2006.

[114] E. P. Nóbrega, N. A. de Oliveira, P. J. von Ranke, and A. Troper, "Monte Carlo calculations of the magnetocaloric effect inGd5(SixGe1−x)4compounds," *Physical Review B,* vol. 72, 2005.

[115] E. P. Nobrega, N. A. de Oliveira, P. J. von Ranke, and A. Troper, "Monte Carlo calculations of the magnetocaloric effect in gadolinium," *Journal Of Magnetism And Magnetic Materials,* vol. 320, pp. e147-e149, 2008.

[116] P. Weiss and A. Piccard, "Le phénomène magnétocalorique," *Journal de Physique Théorique et Appliquée,* vol. 7, pp. 103-109, 1917.

[117] P. Debye, "Einige Bemerkungen zur Magnetisierung bei tiefer Temperatur," *Annalen der Physik,* vol. 386, pp. 1154-1160, 1926.

[118] W. F. Giauque, "A THERMODYNAMIC TREATMENT OF CERTAIN MAGNETIC EFFECTS. A PROPOSED METHOD OF PRODUCING TEMPERATURES CONSIDERABLY BELOW 1 ° ABSOLUTE," *Journal of the American Chemical Society,* vol. 49, pp. 1864-1870, 1927.

[119] W. F. Giauque and D. P. MacDougall, "Attainment of Temperatures Below 1deg Absolute by Demagnetization of $Gd_2(SO_4)_3 \cdot 8H_2O$," *Physical Review,* vol. 43, p. 768, 1933.

[120] C. Zimm, A. Jastrab, A. Sternberg, V. Pecharsky, K. Gschneidner, M. Osborne, and I. Anderson, "Description and Performance of a Near-Room

Temperature Magnetic Refrigerator," in *Advances in Cryogenic Engineering*, P. Kittel, Ed., ed Boston, MA: Springer US, 1998, pp. 1759-1766.

[121] O. Tegus, E. Bruck, K. H. J. Buschow, and F. R. de Boer, "Transition-metal-based magnetic refrigerants for room-temperature applications," *Nature*, vol. 415, pp. 150-152, 2002.

[122] S. J. Lee, J. M. Kenkel, V. K. Pecharsky, and D. C. Jiles, "Permanent magnet array for the magnetic refrigerator," *Journal Of Applied Physics*, vol. 91, p. 8894, 2002.

[123] N. Hirano, S. Nagaya, M. Takahashi, T. Kuriyama, K. Ito, S. Nomura, M. Adams, M. DiPirro, S. Breon, D. Glaister, J. R. Hull, P. Kittel, V. Pecharsky, R. Radebaugh, J. Theilacker, S. Van Sciver, J. G. Weisend Ii, and A. Zeller, "Development of magnetic refrigerator for room temperature application," *AIP Conference Proceedings,* vol. 613, pp. 1027-1034, 2002.

[124] M. A. Richard, A. M. Rowe, and R. Chahine, "Magnetic refrigeration: Single and multimaterial active magnetic regenerator experiments," *Journal Of Applied Physics,* vol. 95, pp. 2146-2150, 2004.

[125] C. Zimm, "Development of a magnetic refrigeration prototype for operation at ambient temperatures," presented at the APS March Meeting 2003, Austin, TX, 2003.

[126] W. Wu, "Room temperature magnetic refrigeration using a 1.4 Tesla permanent magnet field source," presented at the APS March Meeting 2003, Austin, TX, 2003.

[127] H. N., "Room Temperature Magnetic Refrigerator Using Permanent Magnets," presented at the APS March Meeting 2003, Austin, TX, 2003.

[128] P. Clot, D. Viallet, F. Allab, A. Kedous-Lebouc, J. M. Fournier, and J. P. Yonnet, "A magnet-based device for active magnetic regenerative refrigeration," *IEEE Transactions on Magnetics,* vol. 39, pp. 3349-3351, 2003.

[129] F. Shir, C. Mavriplis, L. H. Bennett, and E. D. Torre, "Analysis of room temperature magnetic regenerative refrigeration," *International Journal of Refrigeration,* vol. 28, pp. 616-627, 2005.

[130] A. Rowe and A. Tura, "Experimental investigation of a three-material layered active magnetic regenerator," *International Journal of Refrigeration,* vol. 29, pp. 1286-1293, 2006.

[131] C. Aprea, A. Greco, A. Maiorino, and C. Masselli, "The energy performances of a rotary permanent magnet magnetic refrigerator," *International Journal of Refrigeration,* vol. 61, pp. 1-11, 2016.

[132] Available: www.cooltech-applications.com

[133] A. Waske, B. Schwarz, N. Mattern, and J. Eckert, "Magnetocaloric (Fe–B)-based amorphous alloys," *Journal of Magnetism and Magnetic Materials,* vol. 329, pp. 101-104, 2013.

[134] J. J. Ipus, H. Ucar, and M. E. McHenry, "Near Room Temperature Magnetocaloric Response of an (FeNi)ZrB Alloy," *Magnetics, IEEE Transactions on,* vol. 47, pp. 2494-2497, 2011.

[135] R. Caballero-Flores, V. Franco, A. Conde, K. E. Knipling, and M. A. Willard, "Influence of Co and Ni addition on the magnetocaloric effect in $Fe_{88-2x}Co_xNi_xZr_7B_4Cu_1$ soft magnetic amorphous alloys," *Applied Physics Letters,* vol. 96, pp. 182506-3, 2010.

[136] R. C. O’Handley, "Physics of ferromagnetic amorphous alloys," *Journal Of Applied Physics,* vol. 62, pp. R15-R49, 1987.

[137] Q. Yu, X. D. Wang, H. B. Lou, Q. P. Cao, and J. Z. Jiang, "Atomic packing in Fe-based metallic glasses," *Acta Materialia,* vol. 102, pp. 116-124, 2016.

[138] L. F. Kiss, T. Kemény, V. Franco, and A. Conde, "Enhancement of magnetocaloric effect in B-rich FeZrBCu amorphous alloys," *Journal Of Alloys And Compounds,* vol. 622, pp. 756-760, 2015.

[139] D. Guo, K. C. Chan, and L. Xia, "Influence of Minor Addition of Cr on the Magnetocaloric Effect in Fe-Based Metallic Ribbons," *Materials Transactions*, vol. 57, pp. 9-14, 2016.

[140] J. J. Ipus, J. S. Blazquez, V. Franco, A. Conde, and L. F. Kiss, "Magnetocaloric response of $Fe_{75}Nb_{10}B_{15}$ powders partially amorphized by ball milling," *Journal of Applied Physics,* vol. 105, pp. 123922-6, 2009.

[141] S.-G. Min, K.-S. Kim, S.-C. Yu, and K.-W. Lee, "The magnetization behavior and magnetocaloric effect in amorphous Fe–Nb–B ribbons," *Materials Science & Engineering A,* vol. 449-451, pp. 423-425, 2007.

[142] H. Ucar, J. J. Ipus, V. Franco, M. E. McHenry, and D. E. Laughlin, "Overview of Amorphous and Nanocrystalline Magnetocaloric Materials Operating Near Room Temperature," *Jom,* vol. 64, pp. 782-788, 2012.

[143] J. J. Ipus, J. S. Blázquez, V. Franco, and A. Conde, "Influence of Co addition on the magnetic properties and magnetocaloric effect of Nanoperm (Fe1−XCoX)75Nb10B15 type alloys prepared by mechanical alloying," *Journal of Alloys and Compounds,* vol. 496, pp. 7-12, 2010.

[144] D. Martínez-Blanco, P. Gorria, A. Fernández-Martínez, M. J. Pérez, G. J. Cuello, and J. A. Blanco, "Spin-glass-like behaviour in ball milled Fe30Cr70 alloy studied by ac magnetic susceptibility," *Journal of Alloys and Compounds,* vol. 509, pp. S397-S399, 2011.

[145] D. Q. Guo, K. C. Chan, L. Xia, and P. Yu, "Magneto-caloric effect of FexZryB100−x−y metallic ribbons for room temperature magnetic refrigeration," *Journal Of Magnetism And Magnetic Materials,* vol. 423, pp. 379-385, 2017.

[146] N. Metropolis, A. W. Rosenbluth, M. N. Rosenbluth, A. H. Teller, and E. Teller, "Equation of State Calculations by Fast Computing Machines," *The Journal of Chemical Physics,* vol. 21, pp. 1087-1092, 1953.

[147] L. Xia, C. Wu, S. H. Chen, and K. C. Chan, "Magneto-caloric effect of a Gd50Co50 amorphous alloy near the freezing point of water," *AIP Advances,* vol. 5, p. 097122, 2015.

[148] X. C. Zhong, P. F. Tang, Z. W. Liu, D. C. Zeng, Z. G. Zheng, H. Y. Yu, W. Q. Qiu, and M. Zou, "Magnetic properties and large magnetocaloric effect in Gd–Ni amorphous ribbons for magnetic refrigeration applications in intermediate temperature range," *Journal Of Alloys And Compounds,* vol. 509, pp. 6889-6892, 2011.

[149] S. G. Min, K. S. Kim, S. C. Yu, H. S. Suh, and S. W. Lee, "Analysis of magnetization and magnetocaloric effect in amorphous FeZrMn ribbons," *Journal Of Applied Physics*, vol. 97, p. 10M310, 2005.